IDENTIFICATION OF NEW PREDICTIVE BIOMARKERS AND CHARACTERIZATION OF MOLECULAR MECHANISMS OF DRUG-RESISTANCE IN CHRONIC MYELOID LEUKEMIA

by

Ryan Yen

B.Sc., The University of British Columbia, 2015

A DISSERTATION SUBMITTED IN PARTIAL FULFILLMENT OF

THE REQUIREMENTS FOR THE DEGREE OF

DOCTOR OF PHILOSOPHY

in

THE FACULTY OF GRADUATE AND POSTDOCTORAL STUDIES

(Experimental Medicine)

THE UNIVERSITY OF BRITISH COLUMBIA

(Vancouver)

August 2022

The following individuals certify that they have read, and recommend to the Faculty of Graduate and Postdoctoral Studies for acceptance, the dissertation entitled:

Identification of New Predictive Biomarkers and Characterization of Molecular Mechanisms of Drug-Resistance in Chronic Myeloid Leukemia

submitted by Ryan Yen in partial fulfilment of the requirements for

the degree of Doctor of Philosophy

in Experimental Medicine

Examining Committee:

Dr. Xiaoyan Jiang, Distinguished Scientist, Department of Medical Genetics, UBC
Supervisor

Dr. Gregg Morin, Senior Scientist, Department of Medical Genetics, UBC
Supervisory Committee Member

Dr. Steven Pelech, Professor, Department of Medicine, UBC
Supervisory Committee Member

Dr. Alice Mui, Associate Professor, Departments of Surgery and Biochemistry & Molecular Biology, UBC
University Examiner

Dr. Wan Lam, Distinguished Scientist, Department of Pathology and Laboratory Medicine, UBC
University Examiner

Dr. Shaoguang Li, Professor, Department of Medicine, UMass Chan Medical School
External University Examiner

Additional Supervisory Committee Members:

Dr. Catherine Pallen, Associate Member, Department of Pathology and Laboratory Medicine, UBC
Supervisory Committee Member

Abstract

Treatment of BCR-ABL1$^+$ human leukemia, especially for early phase chronic myeloid leukemia (CML) patients, has been greatly improved by ABL tyrosine kinase inhibitor (TKI) therapies. However, early relapses and acquired drug resistance remain problems. Thus, identification of new biomarkers and therapeutic targets are needed to predict patients' responses for providing alternative treatment strategy and to overcome drug resistance by developing more effective therapies in CML.

To identify new biomarkers that can predict a patient's response to TKI therapies in CML, the expression of 47 microRNAs (miRNAs) that were differentially expressed between normal bone marrow and CML or in Imatinib (IM)-responders versus nonresponders was evaluated in CD34$^+$ CML cells pre- and post-nilotinib (NL) therapy from a cohort of 58 patients enrolled in a clinical trial. Using Cox Proportional Hazard analysis and machine learning algorithms, miR-145 and miR-708 were identified as predictors for NL nonresponse in treatment-naïve cells, while miR-150 and miR-185 were predictors at 1-month and 3-month post-NL treatment. Interestingly, incorporation of *in vitro* colony formation data into either panel improved the predictive power at each time point. Thus, this new predictive model may be developed into a prognostic tool for use in the clinic.

To investigate the molecular functions of the Ahi-1 oncogene and its SH3 domain in regulation of TKI resistance, a high-content antibody microarray was performed in BCR-ABL1$^+$ cells expressing different constructs of Ahi-1. This analysis uncovered that the eIF4F complex, the key regulator of the mRNA-ribosome recruitment phase of translation initiation, was differentially expressed in wildtype Ahi-1 and IM-resistant cells. Interestingly, increased expression of several eIF4F complex members was demonstrated in CD34$^+$ CML patient cells

compared to normal bone marrow, particularly eIF4G1, the scaffolding protein of the complex. Strikingly, inhibition of eIF4G1 by shRNA or a selective inhibitor, SBI-756 impaired survival, increased IM sensitivity and reduced eIF4F complex activity significantly in IM-resistant cells. Additionally, inhibition of eIF4G1 resulted in a significant reduction of BCR-ABL1 protein expression in resistant cells, which may provide a novel strategy of targeting BCR-ABL1. Thus, understanding the mechanism of drug resistance mediated by eIF4G1 could lead to novel strategies to overcome these challenges.

Lay Summary

Chronic myeloid leukemia (CML) can be managed by drugs that act against the disease-specific fusion protein, BCR-ABL1, which drives the disease. Even though these therapies are effective, they are not curative, and relapses occur due to the survival of drug-resistant cells. Thus, it is necessary to find markers that can predict resistance to adapt therapies or use alternative combination strategies when treatments are no longer effective. Small pieces of genetic materials called microRNAs were found to have predictive abilities for patients' drug responses. Furthermore, a protein called eIF4G1 involved in the process of protein production was detected in greater amounts in drug resistant CML cells. Suppression of eIF4G1, by an inhibitor or genetic knockdown, resulted in an impairment of CML cell survival and increased their sensitivity to BCR-ABL1 inhibitors. These treatments resulted in a reduction of BCR-ABL1 protein levels and may offer alternative strategies to drug inhibition of BCR-ABL1's effects.

Preface

I, Ryan Yen, performed all the experiments except for the parts stated below. In this dissertation, I designed and conducted the experiments, analyzed and interpreted the data, and wrote the dissertation, under the supervision of Dr. Xiaoyan Jiang at the Terry Fox Laboratory, BC Cancer Research Institute. Dr. Xiaoyan Jiang also contributed to all the experimental designs, data interpretation, and dissertation editing.

The contents of Chapter 3 and sections of Chapter 2 have been published as a first-author publication. **Yen R**, Grasedieck S, Wu A, Lin H, Su J, Rothe K, Nakamoto H, Forrest DL, Eaves CJ, and Jiang X. (2022). Identification of key microRNAs as predictive biomarkers of Nilotinib response in chronic myeloid leukemia: a sub-analysis of the ENESTxtnd clinical trial. *Leukemia*. Published online August 23, 2022. doi:10.1038/s41375-022-01680-4 The studies include collaborations with Drs. Connie Eaves, Donna L. Forrest, Sarah Grasedieck, Hanyang Lin, Jiechuang Su, Katharina Rothe, and Andrew Wu. Dr. Sarah Grasedieck provided expertise in complex statistical and data analyses. Drs. Hanyang Lin, Jiechuang Su, and Katharina Rothe and Andrew Wu performed the q-RT-PCR, CFC experiments and initial data analyses. Dr. Donna L. Forrest provided the clinical data and insightful discussion. I contributed to 70% of the work in this chapter, as I performed all the bioinformatic and statistical analyses, analyzed the data, and generated the Figures and Tables.

In Chapter 4, the studies include collaborations with Drs. Steven Pelech, Lambert Yue, and Christopher Hughes. Drs. Steven Pelech and Lambert Yue designed and performed the antibody microarray analysis and quantified the antibody signals. Dr. Christopher Hughes helped for performing the polysome fractionation experiments. I contributed to 90% of the work in this

chapter, as I designed and performed vast majority of the experiments, analyzed the data, and generated the Figures and Tables.

All experiments that involved primary CML samples or healthy donors were approved by the University of British Columbia Clinical Research Ethics Board under the certification number H20-00421.

Table of Contents

List of Tables

List of Figures

List of Abbreviations

4E-BP = eIF4E Binding Protein
5-HT_{2C}R = Serotonin Receptor 2C
ABL1 = Abelson Murine Leukemia Viral Oncogene Homolog 1
AGO = Argonaute
AHI-1 = Abelson Helper Integration Site-1
Ahi-1 $SH3^{\Delta}$ = BCR-ABL1-Transduced BaF3 Cells Co-Expressing SH3 Domain-Deleted Ahi-1
AKT = Protein Kinase B
ALL = Acute Lymphoid Leukemia
ALOX5 = Arachidonate 5-Lipoxygenase
AML = Acute Myeloid Leukemia
A-MuLV = Abelson Murine Leukemia Virus
ANOVA = Analysis of Variance
AP = Accelerated Phase
APC = Allophycocyanin
ASO = Antisense Oligonucleotide
ATP = Adenosine Triphosphate
AUC = Area Under the Curve
B/A only = BCR-ABL1-Transduced BaF3 Cells
BC = Blast Crisis
BCL2 = B-Cell Lymphoma 2
Bcl-XL = B-Cell Lymphoma-Extra Large
BCR = Breakpoint Cluster Region
BIN1 = Bridging Integrator 1
BL = Baseline
BLK = B Lymphoid Tyrosine Kinase
BM = Bone Marrow
BOS = Bosutinib
BP = Blastic Phase
CCN3 = Cellular Communication Network Factor 3
CCND3 = Cyclin D3
CD = Cluster of Differentiation
cDNA = Complementary DNA
CFC = Colony-Forming Cell
CHX = Cycloheximide
CI = Confidence Interval
C_i = Concordance Index
CLL = Chronic Lymphoid Leukemia

CLP = Common Lymphoid Progenitor
CML = Chronic Myeloid Leukemia
CMP = Common Myeloid Progenitor
CoxPH = Cox Proportional Hazard
CP = Chronic Phase
CST = Cell Signaling Technology
Ct = Cycle Threshold
CTCL = Cutaneous T-Cell Lymphoma
DA = Dasatinib
DAPI = 4',6-Diamidino-2-Phenylindole
DGCR8 = DiGeorge Syndrome Critical Region 8
DICER1 = Double-Stranded RNA-Specific Endoribonuclease
DMEM = Dulbecco's Modified Eagle Medium
DNA = Deoxyribonucleic Acid
DNM2 = Dynamin 2
eIF = Eukaryotic Initiation Factor
ELN = European Leukemia Network
EMS = Electron Microscopy Sciences
ETR = Early Treatment Response
FBS = Fetal Bovine Serum
FIJI = FIJI is Just ImageJ
GMP = Granulocyte/Macrophage Progenitor
GRB2 = Growth Factor Receptor-Bound Protein 2
HINT = Histidine Triad Nucleotide Binding Protein
HR = Hazard Ratio
HSC = Hematopoietic Stem Cell
HSP90 = Heat Shock Protein 90
IC_{50} = Half Maximal Inhibitory Concentration
IFNγ = Inerferon-Gamma
ILK = Integrin Linked Kinase
IM = Imatinib Mesylate
IRES = Internal Ribosome Entry Site
IRIS = International Randomized Study of Interferon and Cytarabine Versus STI751
JAK = Janus Kinase
JS = Joubert Syndrome
JSRD = Joubert Syndrome Related Disorders
K562R = Imatinib Resistant K562
Lin = Lineage
LSC = Leukemic Stem Cell

M1 = Month 1
M3 = Month 3
MAPK = Mitogen-Activated Protein Kinase
MDM2 = Mouse Double Minute 2 Homolog
MEK = Mitogen-Activated Protein Kinase Kinase
MEP = Megakaryocyte/Erythrocyte Progenitor
mg = Milligrams
miRNA = microRNA
mL = Millilitres
mM = Millimolar
MMP3 = Matrix Metalloproteinase-3
MMR = Major Molecular Response
MNK = MAP Kinase-Interacting Kinase 1
MSR1 = Macrophage Scavenger Receptor 1
MTOR = Mammalian Target of Rapamycin
NB = Naïve Bayes
NF1 = Neurofibromin 1
NL = Nilotinib
nM = Nanomolar
NR = Nonresponder
NSCLC = Non-Small Cell Lung Cancer
NTCB = 2-Nitro-5-Thiocyanatobenzoic Acid
OncomiR = Oncogenic MicroRNA
OPP = O-Propargyl-Puromycin
OXPHOS = Oxidative Phosphorylation
p70S6K1 = p70 Ribosomal S6 Kinase
PAK6 = p21-Activated Kinase 6
Pat A = Pateamine
PB = Peripheral Blood
PBS = Phosphate-Buffered Saline
PDCD4 = Programmed Cell Death Protein 4
PDGFRA = Platelet Derived Growth Factor Receptor Alpha
PEI = Polyethylenimine
Ph Chr = Philadelphia Chromosome
PI = Propidium Iodide
PI3K = Phospho-Inositide-3-Kinase
PIC = Preinitiation Complex
PLA = Proximity Ligation Assay
PP2A = Protein Phosphatase 2

PR = Precision Recall
PRAME = Nuclear Receptor Transcriptional Regulator
PTEN = Phosphatase and Tensin Homolog
PTK2 = Protein Tyrosine Kinase 2
PVDF = Polyvinylidene Difluoride
qPCR = Quantitative Polymerase Chain Reaction
qRT-PCR = Quantitative Real-Time Polymerase Chain Reaction
R = Responder
RAF = Rapidly Accelerated Fibrosarcoma
RB = Retinoblastoma Protein
RF = Random Forest
rIFN-α = Recombinant Human Interferon-Alpha
RISC = RNA-Induced Silencing Complex
RNA = Ribonucleic Acid
RNU48 = Small Nucleolar RNA 48
ROC = Receiver Operating Characteristic
ROS = Reactive Oxygen Species
RPMI = Roswell Park Memorial Institute
RPS6K = Ribosomal S6 Kinase
RPTOR = Regulatory-Associated Protein of mTOR
rRNA = Ribosomal RNA
RSK = p90 Ribosomal S6 Kinase
RT = Reverse Transcriptase
SCT = Stem Cell Transplantation
SDS = Sodium Dodecyl-Sulfate
SDS-PAGE = Sodium Dodecyl-Sulfate Polyacrylamide Gel Electrophoresis
SH3 = Src Homology 3
shRNA = Short Hairpin RNA
STAT = Signal Transducer and Activator of Transcription
TBST = Tris-Buffered Saline Tween 20
TC = Ternary Complex
TCGA = The Cancer Genome Atlas
TFR = Treatment-Free Remission
TGF-β = Transforming Growth Factor Beta
TKI = Tyrosine Kinase Inhibitor
tRNA = Transfer RNA
U = Units
UMAP = Uniform Manifold Approximation and Projection
UTR = Untranslated Region

VEGF = Vascular Endothelial Growth Factor
VSV-G = Vesicular Stomatitis Virus Glycoprotein
WT Ahi-1 = BCR-ABL1-Transduced BaF3 Cells Co-Expressing Wildtype Ahi-1
β2M = Beta-2 Microglobulin
μg = Microgram
μL = Microlitre
μM = Micromolar

Amino Acids

E = Glutamic Acid = Glu
H = Histidine = His
I = Isoleucine = Ile
L = Leucine = Leu
M = Methionine = Met
Q = Glutamine = Glu
S = Serine = Ser
T = Threonine = Thr
Y = Tyrosine = Tyr

Acknowledgements

I am most thankful to my supervisor Dr. Xiaoyan Jiang, for accepting me as her graduate student, supporting and guiding me throughout my studies, and working through my inadequacies. Thank you for always believing in me and challenging me through this entire process. Not only have you provided me with scientific mentorship, but I have also learned many valuable life lessons along the way. I have matured to become a better person while working with you, and I appreciate the invaluable opportunities that you have provided to allow me to improve upon myself every step of the way.

I would also like to express my gratitude to my Supervisory Committee Members, Drs. Gregg Morin, Catherine Pallen, and Steven Pelech for overseeing the progress of my project. I am grateful for all the insights and advice you have provided during all my committee meetings.

I am extremely fortunate to have undergone this journey with the support of my fellow lab members, past and present. Thank you, Will, for training and guiding me when I first joined the lab to allow me to find my footing. Andrew, I appreciate everything you have helped me with and how great we work as a team, and I will never forget the times we have spent together in and outside the lab. Thank you, Min, for the insightful discussions we have and your support for any uncertainties I had. Thank you to my other lab members Josephine, Katharina, Leon, Sujie, Vanessa, Kelly, Jennifer, Young, Yehyeon, Athena, Sammy, Heather, and Tom for creating a positive working environment to ensure that research is an enjoyable experience.

I thank my colleagues in the Terry Fox Laboratory and the BC Cancer Research Institute who have all contributed to providing a supportive setting for science. In particular, I would like to acknowledge the staff at the Stem Cell Assay Lab and Flow Core facilities.

I would also like to acknowledge the Collings Stevens Chronic Leukemia Research Fund, CIHR, CCS, LLSC, and Novartis for funding my work; Experimental Medicine Program, UBC, and CIHR for funding my tuition and fellowship, and ASH and ESH for funding my conference travels.

Finally, my deepest gratitude goes towards my wife, Helen, and my family for their love and support throughout this entire process. I could not have been able to reach my goals and achievements without their support and encouragement.

To my loving and supportive wife,

and my caring family.

Chapter 1: Introduction

1.1 Chronic Myeloid Leukemia

1.1.1 Introduction to CML

Chronic myeloid leukemia (CML) is a clonal myeloproliferative disease characterized by the uncontrolled growth of myeloid cells. This disease develops in 1-2 people per 100,000 people every year and accounts for 15% of all newly diagnosed adult leukemia cases.[1] The median age of patients with CML diagnosis is 50-60 years with a slight skew towards males than females.[2] The defining feature of CML is the Philadelphia (Ph) chromosome, an abnormally small chromosome first discovered by Peter Nowell and David Hungerford in 1959.[3] Later in 1973, the Ph chromosome was described as a reciprocal translocation between the long arms of chromosome 9 and 22 by Janet D. Rowley.[4] Even though most CML patients have the Ph chromosome, a small proportion of patients that are Ph negative have other translocations that result in a disease resembling CML.[5]

CML is a triphasic disease and is caused by the acquisition of the *BCR-ABL1* fusion gene in a hematopoietic stem cell (HSC), which transforms it into a leukemic stem cell (LSC) (Figure 1.1). The LSC population expands due to self-renewal properties and gives rise to a progeny of cells with oncogenic properties, overtaking normal cells with BCR-ABL1^{+} cells.[6] This results in an elevated white cell counts and CML patients most often are diagnosed at this point with chronic phase (CP) CML. As the untreated disease progresses due to an accumulation of mutations, CML patients advance to an accelerated phase (AP) in 3-5 years. Eventually, these patients progress to a blastic phase (BP) or blast crisis (BC), which is the most aggressive and final stage of CML.[7] BP is characterized by an accumulation of undifferentiated blast cells in the blood and the bone marrow (BM) resembling a more deadly acute leukemia. There are twice as

many CML-BP cases with elevated levels of myeloid blast cells than lymphoid blast cells.[2] Patients in AP are diagnosed with a presence of 15-29% blasts in the blood or BM, while patients with ≥30% blasts are diagnosed with BP as defined by the European Leukemia Network (ELN).[8,9]

CML is driven by the gene product of the Ph chromosome. This chromosomal abnormality fuses the Abelson murine leukemia viral oncogene homolog 1 (*ABL1*) and the breakpoint cluster region (*BCR*) gene to create a fusion oncoprotein BCR-ABL1 with constitutive protein tyrosine kinase activity.[10] ABL1 is a non-receptor protein tyrosine kinase that shuttles between the cytoplasm and nucleus to transduce signaling pathways initiated from the cell surface by growth factors and adhesion receptors.[11] Normally, the ABL1 phosphotransferase activity is auto-inhibited by the myristoyl group at the N-terminus.[12] However, when fused to BCR, this auto-inhibitory structure is lost and results in a constitutively active kinase that is confined to the cytoplasm.[13] Additionally, the coiled-coil domain of BCR aids in the dimerization and constitutive activation of the ABL1 kinase domain to phosphorylate many substrates on tyrosine (Tyr) residues in multiple signaling pathways such as MAPK, PI3K/AKT, and JAK/STAT pathways.[14–18] This is aided by the phosphorylation of Tyr-177 by ABL1, allowing for the binding of GRB2, which is an adaptor protein to transduce epidermal growth factor signals to activate MAPK and PI3K pathways.[19,20] Hence, BCR-ABL1 drives the pathogenesis of CML by activating these signaling pathways to provide growth advantages and resist apoptosis, which leads to a massive accumulation of myeloid cells in CML patients.

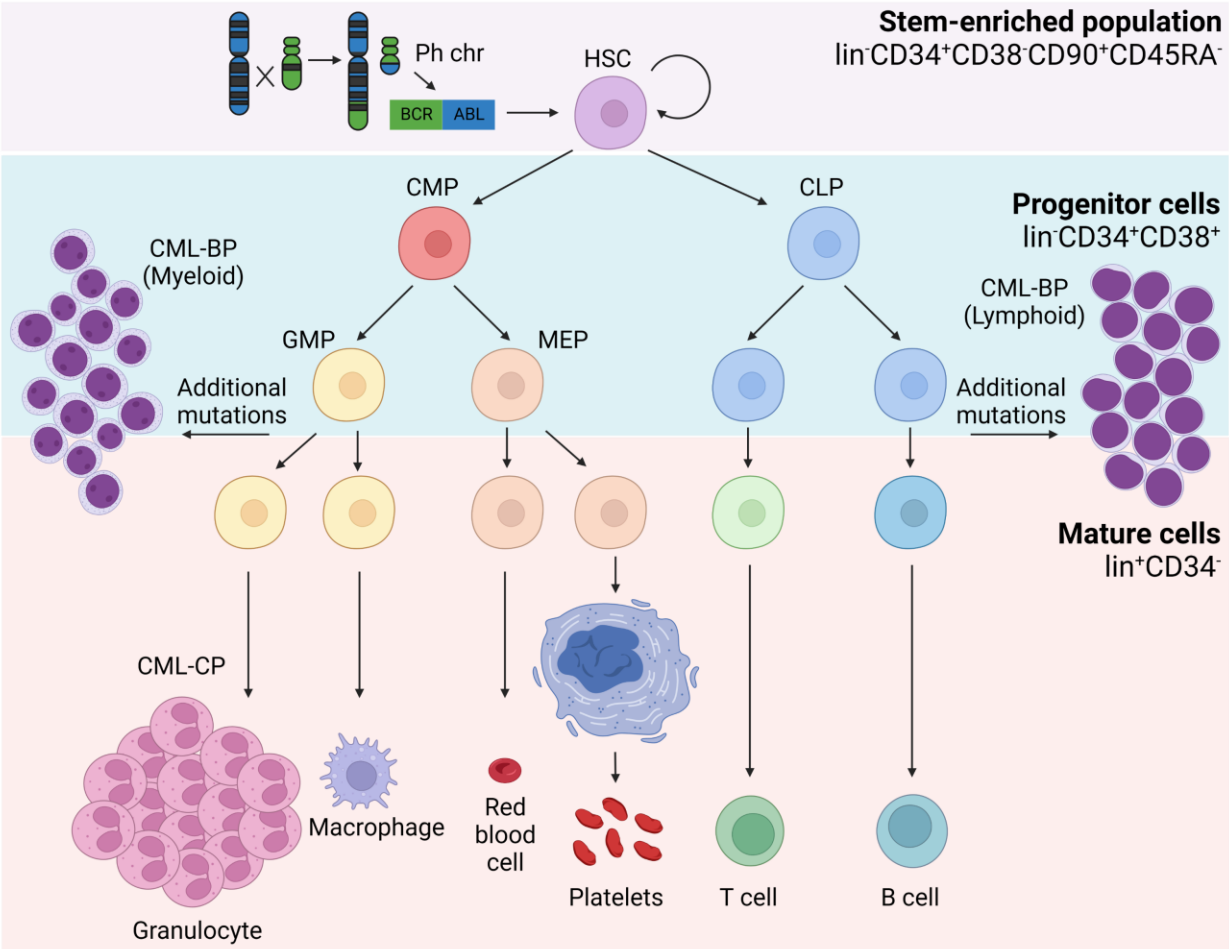

Figure 1.1: Hematopoiesis and Development of Chronic Myeloid Leukemia. The hematopoietic stem cell (HSC) gives rise to two types of progenitors: common myeloid progenitor (CMP) and common lymphoid progenitor (CLP). CMPs will then give rise to granulocyte/macrophage progenitors (GMPs) and megakaryocyte/erythrocyte progenitors (MEPs). These progenitor cells then differentiate into their respective mature blood cells. The CLP will go through phases of cell differentiation and result in mature T and B cells. CML is a clonal disease which begins with the acquisition of the Philadelphia chromosome (Ph chr) in a (HSC) turning it into a leukemic stem cell (LSC). BCR-ABL1-driven LSCs given rise to an excessive number of granulocytes, which is defined as the chronic phase of CML (CML-CP). As mutations accumulate through CML progression to the blast phase (CML-BP), differentiation is blocked and LSCs can give rise to both the myeloid and lymphoid blast cells. Created with BioRender.com

BCR-ABL1 fusion genes can exist as three different molecule weights depending on the breakpoints of the *BCR* gene: P190, P210, and P230 BCR-ABL1. The variations in the breakpoints lead to differing lengths of the *BCR* gene, while the *ABL1* gene remains consistent

for all three forms of BCR-ABL1.[21] The most common form of BCR-ABL1 in CML-CP patients is P210, but it can also be found in acute myeloid leukemia (AML) and acute lymphoid leukemia (ALL) patients that progressed from CML-BP.[5,22] The P190 form is found more commonly in patients with primary Ph^+ B-cell ALL and occasionally in primary AML patients that did not progress from CML-BP.[23] The P230 form is found in neutrophilic-chronic myeloid leukemia, which is a more benign version of CML that seldom progress to BP.[24]

1.1.2 Early CML Therapies and Discovery of Imatinib Mesylate

CML was a difficult disease to treat without the current knowledge and technology in our present society. The earliest documented treatment for CML was the use of arsenic-containing compounds in 1865, which later during beginning of the 20th century, radiotherapy was adopted as the standard therapy.[25] Radiotherapy was then replaced by alkylating agents, such as busulfan and hydroxyurea in the 1960s, which were able to reduce white blood cell counts and minimize symptoms.[25,26] Unfortunately, alkylating agents did not stop CML disease progression due to persistence of Ph-positive cells; hence, alternative therapies were necessary to target these cells.[25,26] The next development of CML therapy was allogenic stem cell transplantation (allo-SCT) and helped prolong the survival of patients, with some achieving complete and permanent cytogenic remission.[27,28] Although allo-SCT was the only curative therapy during this period, it limited patients by forcing them to find suitable donors and carries a significant risk of graft-versus-host disease and infections.[29] Patients without suitable donors for allo-SCT required an alternative therapy and were treated with recombinant human interferon-alpha (rIFN-α). Although rIFN-α increased median survival of patients with cytogenetic response compared to

past treatments, there were many adverse side effects such as hair loss, vomiting, and muscle pain.[30,31]

In the 1990's, CML therapy dramatically advanced with the idea to use an ABL1-specific kinase inhibitor to target ABL-associated leukemias and, several protein-tyrosine kinase blockers were able to reduce the activity of BCR-ABL1.[32] Continuing with this study, Druker *et al.* demonstrated the use of CGP57148 or STI571, which now is referred to as imatinib mesylate (IM), to inhibit cellular proliferation, colony formation, and leukemia development in mice transplanted with BCR-ABL1-expressing cells.[33] IM selectively inhibits the ABL1 kinase by blocking the binding site of adenosine triphosphate (ATP), preventing the downstream phosphorylation of targets that activate growth pathways to drive leukemogenesis.[25] A phase I clinical trial tested the use of IM in CML-CP patients with previous rIFN-α treatment failure and demonstrated that 98% of patients achieved a complete hematological response with daily doses of >300 mg IM, which is defined as a white blood cell count of $<10\times10^9$/L, basophils <5%, platelet count $<450\times10^9$/L with no detection of myelocytes or myeloblasts.[34,35] Furthermore, 54% of these patients reached major or minor cytogenetic responses (1-35% or 36%-65% Ph-positive metaphases, respectively) and 13% of patients had complete cytogenetic remission (≤1% Ph-positive metaphase).[34,35] Following this, a phase III randomized clinical trial, IRIS (International Randomized Study of Interferon and Cytarabine versus STI751), was conducted to compare the efficacy and toxicity of rIFN-α and IM in 1,106 newly diagnosed CML-CP patients. At a median follow-up of 18 months, 76% of patients that received IM reached complete cytogenetic remission compared to only 34.7% of patients that received rIFN-α and cytarabine.[36] After 8 years of follow-up, patients with IM had an event-free survival rate of 81% and a progression-free survival rate of 92%.[37]

1.1.3 Protein-Tyrosine Kinase Inhibitor Resistance in CML

Although IM is still recommended as a front-line therapy today, it is not curative as some AP and BC CML patients are less responsive to treatments and cases of resistance are apparent in 20-30% of patients.[38–40] With the advancement of technology, *BCR-ABL1* transcript levels measured by quantitative reverse transcriptase polymerase chain reaction (qRT-PCR) is the preferred method of monitoring disease due to its simplicity and requiring only a blood draw versus a bone marrow biopsy for cytogenetics. Failure to respond is defined by having >10% *BCR-ABL1* transcript (1-log reduction) by 6 months of treatment and >1% (2-log reduction) at 12 months, while the optimal response is ≤0.1% (3-log reduction) at 12 months.[9] A major molecular response (MMR) is defined by a 3-log reduction in *BCR-ABL1* transcript levels compared to pre-treatment levels and a loss of this response after 12 months is also considered a failure to respond, which may be a consequence of resistance.[9,35] Drug resistance can be divided into primary resistance, a lack of efficacy, or acquired resistance, a loss of a prior response. Due to the selective nature of targeted therapies, like IM, resistant cells can arise due to the eradication the responsive population and allowing less responsive cells to accumulate mutations to eventually become resistant to IM treatment. Due to the oncogenic nature of BCR-ABL1 causing genetic instability, these cells can develop BCR-ABL1-dependent or independent resistant mechanisms.[41,42]

1.1.3.1 BCR-ABL1-dependent Resistance Mechanisms and Current TKIs

BCR-ABL1-dependent resistance arise most often due to point mutations that prevent drug binding but can also involve *BCR-ABL1* gene amplification. X-ray crystallographic studies

revealed that IM binds to the inactive conformation of BCR-ABL1 and Y253, E225, and T315 are important residues that when mutated can prevent IM binding.[43,44] To overcome these mutations, second-generation tyrosine kinase inhibitors (TKIs) were developed such as nilotinib (NL), an improved version of IM, as well as dasatinib (DA) and bosutinib (BOS), which are both dual Src/ABL1 inhibitors. NL is similar in structure to IM, but it is more potent and can bind to the inactive form of BCR-ABL1 with 10-50-fold greater affinity.[45] DA was found to be bound to multiple conformation states of BCR-ABL1, which explains its greater potency over IM.[46] BOS can bind to both the active and inactive conformations of BCR-ABL1 and still be active in BCR-ABL1 mutants with Q252H and L384M point mutations, which are insensitive to both NL and DA.[47,48] Unfortunately, these TKIs are still insensitive to BCR-ABL1 having the "gatekeeper" mutation T315I, which hinders the formation of a critical hydrogen bond necessary to bind the ATP-binding site.[49] Only ponatinib, a third-generation TKI designed to overcome the "gatekeeper" mutation, can inhibit the BCR-ABL1 T315I mutant, but was shown to have significant risk of adverse events in patients during a phase II clinical trial compared to previous TKIs.[49,50] Another third-generation TKI, Asciminib, was designed to bind to the myristoyl pocket making it the first allosteric inhibitor of BCR-ABL1 and can inhibit multiple BCR-ABL1 mutants including T315I.[51] Currently, four TKIs are approved as front-line treatments for CML-CP: imatinib, nilotinib, dasatinib, and bosutinib.[1] However, resistance mechanisms can arise independent of BCR-ABL1.

1.1.3.2 BCR-ABL1-independent Resistance Mechanisms

Cases of BCR-ABL1-independent resistance are mostly observed in patients who progressed to CML-AP or BC and/or relapsed. TKIs generally target proliferative CML cells but

fail to eliminate quiescent LSCs.[52–54] LSCs are phenotypically similar to HSCs with both having cell surface antigens of $Lin^{-}CD34^{+}CD38^{-}CD90^{+}CD45RA^{-}$ but it has been reported that LSCs also express additional markers such as CD25, CD26, CD33, CD123, and IL1RAP.[55–62] Although CML LSCs also have increased level of BCR-ABL1 expression and kinase activity, LSCs do not completely rely on BCR-ABL1 transforming activity for survival. Hence, TKIs do not effectively eliminate this population.[63,64] Finding mechanisms for LSC survival and TKI resistance can uncover alternative treatment strategies to target this population for a more curative treatment.

Genome instability is a hallmark of cancer and BCR-ABL1 activity enables this phenotype in CML patients.[65] This is supported by the observation of CML patients in BC having a higher frequency of copy number alterations and cytogenetic abnormalities compared to patients in CP.[66] BCR-ABL1 contributes to genomic instability through generation of reactive oxygen species leading to higher rates of mutation and disruption of the DNA damage response resulting in error prone DNA repair, and several other mechanisms.[42,67,68] Accumulation of mutations can result in the activation of alternative signaling pathways to promote survival and proliferation (JAK/STAT, Src, RAF/MEK/ERK), bone marrow microenvironment interactions (ILK, Notch), stem cell maintenance (PI3K/AKT, Alox5, AHI-1-BCR-ABL1-JAK2-PP2A, Msr1, Blk) and self-renewal (Hedgehog, WNT/β-catenin), and pro-survival pathways including autophagy.[69–80] Additionally, BCR-ABL1-independent resistance mechanisms include deregulation of drug transporters by decreasing influx or increasing efflux of IM.[63,81] Since TKI monotherapies are not curative due to a wide range of resistance mechanisms, it is imperative to be able to predict drug resistance to overcome primary resistance and acquired resistance by developing more effective combination therapies for improved treatment and care.

1.2 Biomarkers and Predictive Models in CML

1.2.1 Identification of Molecular and Genetic Signatures as Biomarkers in CML

Biomarkers are clinical and diagnostic tools with predictive powers for treatment selection to identify patients who are likely to benefit from a particular therapy or alternative therapies are needed. Measurements for biomarkers are evaluated to indicate normal biological processes, pathogenic processes, or responses treatments.[82] Interestingly, studies have demonstrated that molecular and genetic signatures in CML could serve as important biomarkers of disease progression and drug resistance. Such markers include gene mutation signatures, gene and protein expression patterns, and cell surface markers. The most well-known biomarker in CML is BCR-ABL1. Its expression, copy number and mutational status are useful indicators of TKI response and offers utility in the clinic. For example, screening for point mutations in BCR-ABL1 kinase domain, like the T315I gatekeeper mutation, prior to treatment would allow clinicians to devise a treatment regimen for patients that targets resistant cells immediately and bypass early generation TKIs which would be ineffective.[83] Expression profiling of CML-CP patients at diagnosis and post-treatment can be used to identify of molecular markers of progression. A 75 mRNA transcript signature, comprised of 50 upregulated and 25 downregulated genes, in treatment-naïve patient cells was able to predict major cytogenetic response in 12 months with an accuracy of 87%.[84] Another study explored the changes in gene expression of CML patients that progressed from CP to advanced CML (AP/BC) and found 3,000 genes to be significantly associated with CML disease progression.[85] Components of the WNT/β-catenin pathway and alternative kinase signaling regulation, decreased expression of transcription factors (Jun B, Fos), and increased expression of PRAME were associated with

advanced CML.[85] Building off the data generated from the previous study, another group used an algorithm that integrated expression data with predicted protein functional relationships and CML progression associated genes to develop a 6-gene panel from CML-CP patients that predicted relapse after bone marrow transplantation.[86] Expression profiles are not limited to analyzing gene expression but can also be expanded to analyze protein expression and cell surface markers. Proteomic analysis has also been used to identify overexpressed proteins like HSP90, RB, BCL2, and PP2A in CML-BC patient cells compared to those in CP.[87] Another study used high-resolution label-free mass spectrometry to compare bone marrow plasma from IM-resistant and IM-sensitive patients and identified altered lipid metabolism and WNT signaling in resistant patients.[88] Furthermore, cell surface marker analysis coupled with single-cell transcriptomics determined that the most TKI-insensitive LSC population is $Lin^{-}CD34^{+}CD38^{-}CD45RA^{-}cKIT^{-}CD26^{+}$, which expressed a primitive, quiescent molecular expression signature.[89] These studies demonstrate the differences found in each stage of CML progression or in TKI-resistant and TKI-sensitive patients that can be used as a foundation for biomarkers for predictive studies.

1.2.2 Biological Functions of MicroRNAs and their Predictive Roles as Biomarkers in CML

Another class of biomarkers are microRNAs (miRNAs), which are small pieces of noncoding RNA (18-25 nucleotides long) that are highly conserved across many species and can act as a tumour suppressor or oncogene in regulating gene expression post-transcriptionally.[90] In the nucleolus, miRNAs are transcribed by RNA polymerase II as primary miRNAs. The Drosha-DGCR8 complex then process the primary miRNAs into hairpin intermediate pre-miRNAs.[90]

Pre-miRNAs are exported to the cytoplasm and meet the DICER1 enzyme to be further processed into mature miRNAs. Finally, mature miRNAs are loaded onto the RNA-induced silencing complex (RISC), which can degrade specific mRNA transcripts dependent on the sequence of the miRNA or repress translation by binding to the 3'-untranslated region (3'-UTR).[90] The miRNA loaded RISC complex recruits Argonaute (AGO) proteins such as AGO-2, to specific sequences via base-pairing interactions.[91] This binding is dependent on a short span of the miRNA sequence of 7 nucleotides long called the seed.[91] The complementary pairing between the seed and its target is considered the minimum element required to engage the target mRNA.[91] After the seed binds to its target, a partial duplex is formed, which disrupts the endonuclease activity of AGO-2 and only complementary binding of the full miRNA sequence can allow for mRNA cleavage by AGO-2.[91,92] However, regulation of target expression by miRNA relies on AGO cofactors through translational suppression and mRNA destabilization.[91] The first report of differential miRNA expression linked to human malignancies described miR-15a and miR-16-1 expression was consistently reduced in approximately 68% cases of chronic lymphoid leukemia (CLL).[93] Currently, many studies demonstrate that deregulation of miRNAs can lead to aberrant expression of their downstream target genes in numerous solid tumours and hematopoietic malignancies.[94–99]

Interestingly, multiple groups have also studied the role of miRNA expression in CML. BCR-ABL1 activity has been reported to overexpress several miRNAs that activate a variety of oncogenic pathways.[100] On the one hand, the expression of the miR-17-92 cluster, which targets *TGF-β*, *STAT3*, and *PTEN*, was significantly elevated in $CD34^+$ CML-CP progenitor and CML-BC cells compared to normal $CD34^+$ cells.[100,101] Additionally, the BCR-ABL1-dependent overexpression of miR-130 reduced the expression of *CCN3*, which is a growth inhibitor that can

reverse the anti-apoptotic block, allowing CML cells to evade negative growth regulation.[102] Finally, miR-21 is an oncogenic miRNA that targets negative regulators of the PI3K/AKT pathways and miR-21 suppression resulted in the enhancement of IM-induced apoptosis in CML $CD34^+$ cells.[103] On the other hand, tumour suppressive miRNAs (miR-29b, miR-30a, miR-30e, miR-320, miR-424) that target *BCR-ABL1* were reported to be downregulated.[100] Different miRNA expression profiles have also been observed in CML patients at different stages of the disease. A panel of miRNAs (miR-19a, miR-20a, miR-146, miR-150, miR-155, miR-181a, miR-221, miR-222) had a higher level of expression in CML patients that experienced hematological relapse, therapy failure and CML-BP compared to patients at diagnosis. These miRNAs target genes are involved in MAPK and p53 signaling pathways and controlling growth and cell cycle.[104] Additionally, TKI resistance could be predicted by the expression of miRNAs (miR-21, miR-26a, miR-29a, miR-100, miR-191) and the expression of some miRNA can be affected by TKI treatments (let-7d, let-7e, miR-15a, miR-16, miR-145).[105–107] Our lab has also reported the reduced expression of miR-185 in $CD34^+$ stem/progenitor cells compared to normal bone marrow and its expression is significantly decreased in IM-nonresponsive patients compared to IM-responsive patients.[96] Restoration of miR-185 expression using lentivirus sensitized CML LSCs to TKI treatment, significantly inhibited their proliferation, and reduced their engraftment *in vivo*.[96] Studies of miRNA in CML has proved the predictive ability of miRNA for TKI responsiveness and identified new targets for novel therapies to overcome TKI-resistance. However, differences in the cell types profiled, the technologies used, and the heterogeneous treatment outcomes observed in patients pose challenges in identifying reliable biomarkers and predictive models with clinical utility.

1.3 Abelson Helper Integration Site 1 (AHI-1/Ahi-1) Involvement in Diseases

1.3.1 AHI-1 Structure and Regulation of Expression

Abelson helper integration site 1 (*Ahi-1*) was characterized as a common helper provirus integration site in mice that had an increased insertional mutagenesis rate over the expected frequency for random integrations.[108] This insertional mutation was commonly observed in pre-B-cell lymphomas transformed by the oncogene *v-abl* found in Abelson murine leukemia virus (A-MuLV).[108] Full transformation by A-MuLV and its ability to replicate *in vivo* and *in vitro* requires a non-defective helper Moloney MuLV, which harbours the Ahi-1 locus.[108–110] Later, the *Ahi-1* gene was identified within this locus using an exon trapping method.[111] In humans, the *AHI-1* gene is found on chromosome 6 with 33 exons spanning 200 kilobases.[111] Alternate splicing of the *AHI-1* gene occurs at the 3'-region which results in three isoforms.[111] Additionally, a functional promoter was found 1.3 kilobases upstream to the start codon containing two putative TATA boxes, a cis-acting CCAAT box and binding sites for transcription factors like c-fos and Oct-1.[112] AHI-1 protein was found to be a 1096 amino acid protein with three domains: an N-terminal coiled-coil domain, a WD40-repeat domain with seven repeats, and a Src homology 3 (SH3) domain (Figure 1.2A).[111] Coiled-coil domains are comprised of two or more α-helices wrapped around each other, which allows for interactions with another coiled-coil domain, whether on another molecule of the same protein for dimerization or another protein for complex formation.[113] The WD40-repeat domain has a propeller structure, which is a large surface for interactions (including for phosphorylation sites) with other proteins involved in many different cellular processes like cell cycle control, intracellular transport, cytoskeletal organization, and apoptosis.[114] The SH3 domain is one of the most common protein-interacting domains which bind to proline-rich motifs.[115] Our lab has

solved the AHI-1 SH3 domain structure by X-ray crystallography and discovered a unique C-terminal a helix not observed in other SH3 domains, which may act as an additional binding site for increased specificity for residues outside the traditional PXXP motifs.[116] AHI-1 also contains several PXXP motifs, which allows binding to proteins with SH3 domains, and two PEST sequences, which mediate protein degradation.[117] Being well-equipped with many important interaction domains for signal transduction, AHI-1 can mediate multiple protein-protein interactions as a scaffold protein for signaling pathways.

Ahi-1 expression is found in several organs such as the kidney, thymus, and lungs, but was especially highly expressed in the brain and testis.[111] *Ahi-1* is also developmentally regulated during mouse embryo development, with the highest expression just prior to birth.[118] For hematopoiesis in humans and mice, *AHI-1*/*Ahi-1* expression is the highest in the most primitive cells and is reduced as cells become more differentiated, indicating a role in the regulation of stem cell development and it may play a role in human leukemias like CML.[119]

1.3.2 The Role of AHI-1 in CML

The deregulation of AHI-1 expression was first found to be linked to hematopoietic malignancies in a panel of leukemic cells lines with greater *AHI-1* expression compared to normal bone marrow cells.[119] In CML, *AHI-1* expression was increased in all stages of the disease and an *in vivo* model demonstrated a cooperative effect from the overexpression of *AHI-1* and *BCR-ABL1* inducing a more lethal leukemia than either alone.[75,119,120] The highest expression of these genes was also found in the leukemic stem cell-enriched population, which further supports the idea of AHI-1 and BCR-ABL1 cooperative abilities in the transformation of hematopoietic cells and regulating leukemic properties in LSCs.[119] Immunoprecipitation

experiments demonstrated that the Ahi-1 WD40-repeat domain is necessary for the protein-protein interaction between Ahi-1 and BCR-ABL1, while the N-terminus portion of Ahi-1 is required for the interaction between Ahi-1 and JAK2, a BCR-ABL1 substrate that is a protein-tyrosine kinase that is also involved in cell signaling.[75,121] The expression and activities of JAK2 and one of its substrate transcription factor STAT5 were enhanced in cells co-expressing *AHI-1* and *BCR-ABL1*, which contributed to TKI resistance and disease progression.[120] The cooperation between AHI-1 and BCR-ABL1 could be explained by AHI-1's ability to bring BCR-ABL1 and its substrates together to enhance BCR-ABL1's transformative activities (Figure 1.2B).

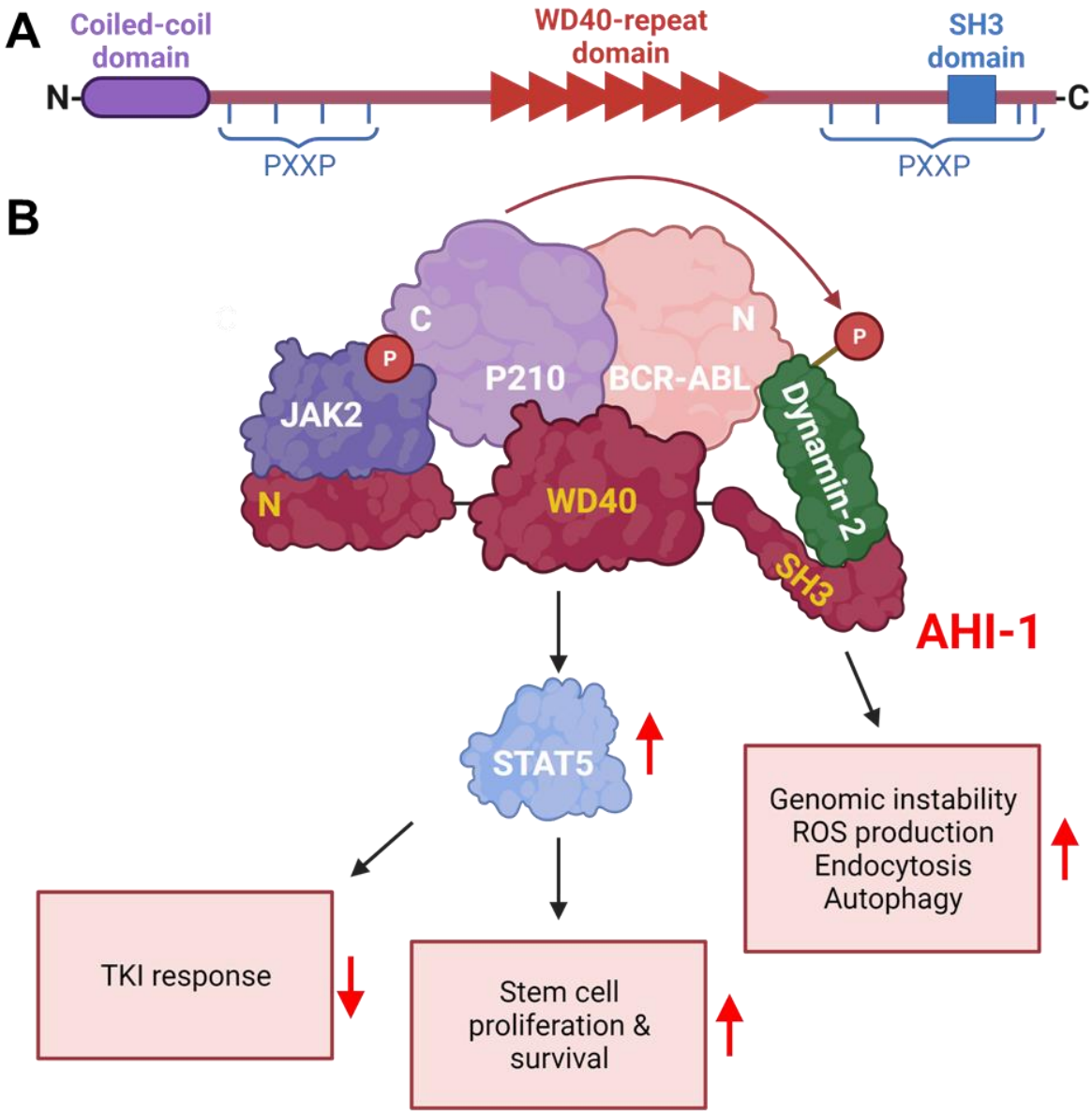

Figure 1.2: AHI-1 as a Scaffold Protein. (A) Schematic of AHI-1 structural motifs including coiled-coil domain (purple), WD40-repeat domain (red), SH3 domain (blue), and proline-rich motifs (PXXP). (B) AHI-1 interacts with multiple proteins to deregulate leukemic properties in CML. AHI-1 interacts with BCR-ABL1 with the WD40-repeat domain and interacts with JAK2 with the N-terminal portion, and dynamin 2 with its SH3 domain. AHI-1 enhances BCR-ABL1 activity by interacting with BCR-ABL1 substrates allowing for increased BCR-ABL1-phosphorylation of substrates resulting in increased activity leading and deregulation of biological processes. Created with BioRender.com

AHI-1 has been demonstrated to contribute to TKI resistance as genetic inhibition by shRNA increased the sensitivity of $CD34^+$ CML stem/progenitor cells to TKI treatment.[120] A combination treatment of TKIs and JAK2 inhibitors were able to reduce the proliferation and colony forming abilities of TKI-resistant CML stem/progenitor cells *in vitro* and *vivo.*[18,75] Co-immunoprecipitation experiments demonstrated the interaction between AHI-1 and PR55α, which is the B subunit of the phosphatase PP2A, and β-catenin.[76] Dual inhibition of PP2A and BCR-ABL1 led to a synergistic effect of targeting CML stem/progenitor cells *in vitro* and LSCs *in vivo.*[76] Mechanistically, this dual inhibition disrupted AHI-1 mediated signaling resulting in the degradation of β-catenin, which is necessary for the maintenance of CML LSCs.[76]

Previous studies have also demonstrated the AHI-1 SH3 domain contributes to TKI resistance and is required for the cytoplasmic anchoring of AHI-1.[122] Furthermore, the AHI-1 SH3 domain was found to interact with the proline rich domain of a mechanoenzyme, dynamin 2 (DNM2), involved in multiple cellular activities such as endocytosis, intracellular trafficking, and the reorganization the cytoskeleton.[122,123] Again, it was demonstrated that AHI-1 bridged the interaction between BCR-ABL1 and DNM2, leading to an increased phosphorylation and activity of DNM2.[122] The AHI-1-BCR-ABL1-DNM2 complex deregulated endocytosis, ROS production, and autophagy to provide enhanced survival of primitive CML cells.[122] Most importantly, dual inhibition of BCR-ABL1 and DNM2 could reverse these deregulated leukemic functions to reduce the proliferative ability and TKI-resistance in CML stem/progenitor cells. These reports demonstrate the oncogenic ability of AHI-1 in regulating CML LSC properties and TKI resistance and support the notion to target key processes involving AHI-1 and its interacting partners to effectively target CML LSCs and TKI resistant cells.

1.3.3 The Role of AHI-1 in Other Diseases

Although AHI-1 has a large role in CML, mutations and deregulation of AHI-1 play a role in many other diseases as well. For example, *AHI-1* transcript levels were found be higher in patient cells with cutaneous T-cell lymphoma (CTCL), which is characterized by the infiltration of malignant T cells on the skin, or the leukemic variant of CTCL, Sezary Syndrome.[124,125] Suppressing *AHI-1* in Hut78 cells, a Sezary Syndrome cell line, resulted in a reduction of transforming phenotypes and impaired tumour growth *in vivo*, suggesting AHI-1's role in CTCL pathogenesis.[124] Additionally, suppression of *AHI-1* led to restoration of the expression of a tumour suppressor, BIN1, in CTCL cells; patient cells with suppressed BIN1 resulted in reduced induction of Fas/Fas ligand-mediated apoptosis allowing for disease persistence.[124,125]

Beyond hematopoietic malignancy, AHI-1 also plays a role in neurological diseases as it is highly expressed in brain tissues. Mutations in *AHI-1* was found to cause Joubert syndrome (JS), a rare autosomal recessive disease characterized by abnormal brain development, and Joubert syndrome related disorders (JSRD), which include renal cystic disease and retinal dystrophy.[118,126,127] The most common *AHI-1* mutations in JSRD are frameshift or nonsense mutations that result in the truncation of AHI-1 missing the WD40-repeat and/or SH3 domains or missense mutations found in these domains.[127–129] JS and JSRD are part of a group of genetic disorder resulting in the dysfunction of the primary cilium called ciliopathies.[130] The non-motile primary cilium is essential as a hub for cell signaling pathways for organ development and maintenance, which AHI-1 plays a crucial role in the structure and function of the primary cilium.[131–134] Additionally, multiple sclerosis, a degenerative disorder of the myelin sheath of neurons, was linked to reduced *AHI-1* mRNA expression resulting in an enhancement of proinflammatory IFNγ^+ T cells development that is implicated in multiple sclerosis.[135] Some

AHI-1 single nucleotide polymorphisms were associated with elevated risk for schizophrenia, autism, and mood disorders.[136–138] Multiple studies demonstrate the consequences of *AHI-1* suppression resulting in a depressive phenotype due to impaired release of neurotransmitters.[139,140] Furthermore, *Ahi-1* deficiency was reported to promote the degradation of glucocorticoid receptors and reduced nuclear translocation in response to stress, which resulted in hyposensitivity to antidepressants in mice.[141] These observations indicate the importance of AHI-1 in proper brain development and function.

There are also strong associations with certain AHI-1 single nucleotide polymorphisms that result in metabolic disorders such as type 2 diabetes.[142,143] AHI-1 expression was also found in skeletal muscle and linked to the regulation of glucose uptake and glucose homeostasis.[143] In the hypothalamus, Ahi-1 mediates feeding behaviour of mice by interacting with serotonin receptor 2C (5-HT_{2C}R), which plays an important role in feeding and appetite control.[144] When fasting, increased Ahi-1 induced the lysosomal degradation of 5-HT_{2C}R, and suppression of hypothalamic Ahi-1 resulted in a decrease of food intake and body weight.[144] These reports demonstrate the importance of proper AHI-1 function and regulation as it is crucial in brain development and function. When AHI-1 function is deregulated, this leads to a wide range of brain and metabolic disorders. Therefore, understanding AHI-1 function in the pathogenesis of these diseases is crucial for the development of potential treatments of these diseases.

1.4 The Eukaryotic Translation Initiation Mechanism

1.4.1 Cap-Dependent Initiation of Translation by eIF4F Complex

Protein synthesis is a critical cellular function that builds a chain of amino acids on ribosomes based on an mRNA template sequence. As most cellular functions are carried out by

proteins, cells are dependent on this process for multiple aspects including survival, proliferation, and stress response. Therefore, it is crucial for cells to have translational control. Protein synthesis is divided into multiple steps: initiation, elongation, termination, and recycling.[145] This process involves the recruitment of an initiator methionyl-tRNA bound ribosome to the start codon of an mRNA transcript; then, the ribosome travels down the transcript and extends the amino acid chain depending on the codons of the transcript.[146] Termination of this process occurs when the ribosome arrives at a stop codon that promotes the release of the nascent protein.[146] Finally, the ribosome is recycled back into subunits to continue another cycle of translation.[146] In this dissertation, the focus will mainly be on the eukaryotic initiation of translation.

The rate-limiting step of translation in eukaryotes is the initiation step as it is highly regulated with multiple controls.[147] Initiation of translation begins with the recruitment of the small 40S ribosomal subunit to the 5' untranslated region (UTR) of an mRNA through the assembly of the 43S preinitiation complex (PIC).[148] The 43S PIC is composed of the 40S ribosomal subunit bound by eukaryotic initiation factors (eIFs) 1, 1A, and 5, the eIF3 complex, and the ternary complex (TC), which is comprised of an initiator methionyl-tRNA and the GTP-bound form of eIF2.[148] The 43S PIC binds to the 5'-cap of the mRNA facilitated by the eIF4F complex.[149] The eIF4F complex is made up of multiple proteins including: the cap-binding protein, eIF4E, the RNA helicase, eIF4A, and the scaffold protein, eIF4G (Figure 1.3).[150] After the 43S is bound near the cap, it scans for an AUG start codon through the sequence complementation of the anticodon of the initiator tRNA forms the 48S PIC.[148] The eIFs that are responsible for scanning are released to allow the 60S ribosome subunit to join and produce an 80S initiation complex that leads into the elongation step.[148]

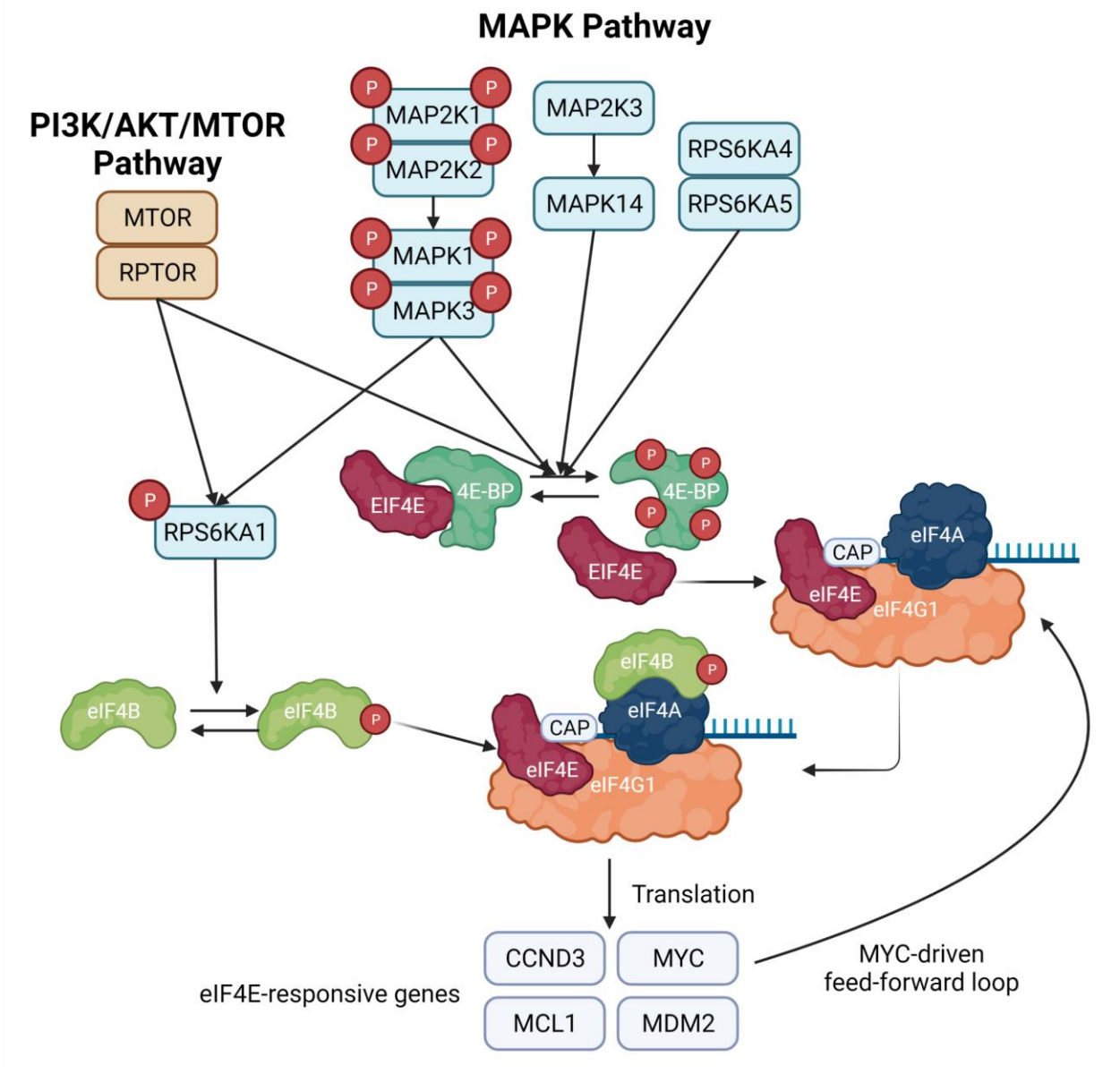

Figure 1.3: The Regulation of eIF4F Complex by Cancer-Related Signaling Pathways. The eukaryotic initiation factor (eIF4F) complex is responsible for the cap-dependent translation of mRNAs. This complex is comprised of the scaffold, eIF4G, the cap-binding protein, eIF4E, and the mRNA helicase, eIF4A. This complex is regulated at multiple points by PI3K/AKT/MTOR and MAPK pathways by phosphorylating the 4E-binding protein (4E-BP) and eIF4B. A subset of mRNAs (*CCND3*, *MYC*, *MCL1*, *MDM2*) are translated at different rates compared to the global translation rate depending on eIF4F activity. The transcription factor c-Myc has also been reported to increase the protein expression of eIF4F complex resulting in a feed-forward loop. Created with BioRender.com

The eIF4F complex serves as the effector for the regulation of translation initiation, containing essential proteins to carry out the recruitment of the 43S PIC. On the one hand, the rate-limiting component for translation is eIF4E as it is the least abundant initiation factor with 0.2 to 0.3 molecules per ribosome.[150] On the other hand, eIF4A is the most abundant initiation factor with 3 to 6 molecules per ribosome and exists in two homologs with 90% similarity: eIF4A1, which is the more abundant form, and eIF4A2 in humans.[151,152] eIF4G also exists in two homologs with 46% similarity, eIF4G1, the more abundant homolog, and eIF4G2.[153] eIF4G contains two separate domains to interact with different regions of the same eIF4A molecule and another defined domain for eIF4E to allow for the interaction with other important factors for the initiation process.[154,155] Additional members of the eIF4F complex include eIF4B and eIF4H, which are RNA-binding proteins that stimulate the helicase activity of eIF4A to unwind stable secondary structures of the transcript.[156] These RNA-binding proteins affect eIF4A activity by increasing the affinity for ATP when helicase activity is inhibited by secondary structure of the 5' end of the transcript.[150,157]

The eIF4F complex contributes to the differences in mRNA translation efficiency. This is due to the rate-limiting levels of eIF4E and eIF4F complex has different affinities for mRNA depending on the degree of secondary structure of the 5'-UTR.[158,159] The first step of the process of recruiting the 43S PIC to the mRNA is the binding of eIF4E to the 5'cap and is stabilized by the RNA-binding sites on eIF4G.[160] Then eIF4A is recruited to unwind any secondary structure proximal to the 5'-cap to allow for the recruitment of the 43S PIC or is recycled to unwind further secondary structures.[150] Differences in the structural barriers of mRNA results in differences in translation efficiency; "weaker" mRNAs often have more secondary structures in their 5'-UTR which require eIF4F complex activity to unwind and efficiently translate the

transcript.[150] Interestingly, most of these "weak" mRNAs that encode for growth and survival factors that are generally suppressed except under the context of cancer, where eIF4F complex activity may be enhanced.[150]

Many efforts have been poured into studying the effects of elevated eIF4F activity on a small subset of mRNA transcripts. eIF4E overexpression models have demonstrated that there was only a small increase in overall protein synthesis rate. However, there was a subset of mRNAs with a substantial, disproportionate increase in translation.[150] Translation of transcripts of housekeeping proteins, like glyceralehyde-3-phosphate dehydrogenase and actin, did not respond to eIF4E expression changes, but transcripts of ornithine decarboxylase, cyclin D1, and c-MYC were identified as eIF4E-responsive mRNAs.[150,161,162] The 5'-UTR structures of "weak" mRNA are longer and highly structured containing more guanine/cytosine content compared to the shorter and easier to unwind "strong" mRNAs of housekeeping proteins.[163] More detailed studies with codon-by-codon resolution using ribosome profiling identified a pyrimidine-rich translation element in 5'-UTR that interacts with eIF4E, which is key to control the translation of a subset of mRNAs encoding proteins with transformative properties for cancer.[164,165] Phosphorylation of eIF4E has a similar effect to overexpression as it stimulates the translation of prosurvival mRNAs, like *MCL1*, and proinvasion mRNAs, like *MMP3*, unproportionally to the global protein synthesis rate.[166,167] Due to the oncogenic potential of increased eIF4F complex activity, it is crucial to understand the regulation of this complex.

1.4.2 Regulation of the eIF4F Complex

Multiple pathways are involved in the regulation of the eIF4F complex that respond to environmental changes, like nutrient availability and stress. The mTOR kinase pathway receives

extracellular signals and information about cellular energy status, nutrient availability, oxygen levels, and hormones and growth factors to induce cellular growth, proliferation, and differentiation.[168–171] There are two forms of mTOR complexes, mTORC1 and mTORC2; mTORC1 is linked to translation control as its substrates, 4E-binding proteins (4E-BPs) and ribosomal S6 kinases, are involved in regulating the eIF4F complex.[172–174] The 4E-BPs are a family of small translation suppressors that bind to cap-binding protein, eIF4E, and have three homologs: 4E-BP1, 4E-BP2, and 4E-BP3.[175] Dephosphorylated 4E-BPs bind to eIF4E, sequestering it to prevent interaction with eIF4G.[175] However, when mTORC1 phosphorylates 4E-BPs, it causes the dissociation with eIF4E, allowing for the eIF4E-eIF4G interaction leading to the assembly of the eIF4F complex (Figure 1.3).[172] On 4E-BP1, mTORC1 phosphorylates T37 and T46, which are primer sites for further phosphorylation of T70 then S65 last and finally allows for dissociation with eIF4E.[172,176] Therefore, phosphorylation by mTORC1 induces eIF4F complex activity for translation, while inhibition of mTORC1 using an inhibitor like rapamycin, will reduce translation rates.

The p70 ribosomal S6 kinase ($p70^{S6K1}$), a member of the ribosome S6 kinases, is also regulated by mTORC1 by phosphorylation. The T389 phosphorylation on $p70^{S6K1}$ is the most important residue for its activation and studies have proven this site to be sensitive to rapamycin treatment, further supporting the fact that mTORC1 is responsible for its phosphorylation.[177,178] Activation of $p70^{S6K1}$ results in the phosphorylation of S422 on eIF4B, which increases its affinity for the 43S PIC and eIF4A to increase translation rates.[179,180] Additionally, $p70^{S6K1}$ can also phosphorylate S67, which is the programmed cell death protein 4 (PDCD4), and its phosphorylation leads to its degradation.[181] PDCD4 is a tumour suppressor which inhibits eIF4A helicase activity to reduce translation rates, in which degrading PDCD4 will enhance translation

rates.[182] Although mTORC1 has a larger role in regulating protein synthesis through the elongation step and ribosome biogenesis, these are a few examples of mTORC1's effect on the eIF4F complex.

Another pathway involved in the regulation of the eIF4F complex is the MAPK pathway, which is involved in transmitting upstream growth factor signals to regulate cell proliferation, differentiation, apoptosis, and survival.[183] MAP kinase-interacting kinase 1 (MNK1 also known as RPS6KA5) and MNK2 (also known as RPS6KA4) may be tightly bound to extracellular signal-regulated kinase 1 (ERK1) and ERK2, which are part of the MAPK pathway.[184] When receiving a mitogen signal, ERKs are activated and phosphorylate MNKs, releasing them and activates their phosphotransferase activities.[184] MNKs then phosphorylate eIF4E on S209, which promotes the translation of mRNAs encode for chemokines and metalloproteases.[185,186] Another kinase that is activated by ERKs is the p90 ribosomal S6 kinase-1 (RSK1 also known as RPS6KA1), which can phosphorylate eIF4B on S422, the same residue phosphorylated by $p70^{S6K1}$ from the mTOR pathway.[180] Since the MAPK and mTOR pathway are often deregulated in cancers and can control eIF4F complex activity, aberrant translation initiation can lead to the overexpression of oncogenes to promote the development of cancers.

1.4.3 eIF4F Complex Involvement in Cancers

Some proto-oncogenes, like c-Myc, have a relatively high degree of sequence complexity in their 5'UTR rendering them "weak" mRNAs that is only translated during very specific times. However, elevated eIF4F complex activity levels unlock the structural barriers to increase the translation of oncogene mRNAs for cancer pathogenesis. Elevated c-Myc expression dramatically increases the protein synthesis rates as it drives the translation of ribosomal RNA

(rRNA) and genes involved in rRNA processing.[150] Interestingly, increased c-Myc expression also increases the expression of eIF4F complex members, eIF4E, eIF4A1, and eIF4G1, resulting in a feed-forward loop in which c-Myc and eIF4F complex enhances the expression of each other.[187,188] With c-Myc being one of the most common oncogenes for cancer pathogenesis, it is not surprising that each member of the eIF4F complex has been demonstrated to play a role in cancer.

Early studies of the cap-binding protein eIF4E demonstrated its overexpression in multiple cancer cell lines and ectopic expression of eIF4E in non-transformed cell lines resulted in cellular transformation and tumourigenesis.[189–192] An eIF4E transgenic mouse model demonstrated its transformative activity that leads to a wide variety of cancers developing in the mice.[193] The elevated expression of eIF4E has been reported in multiple forms of cancers including breast, head and neck, colorectal, bladder, lung, and cervical cancers.[161] Studies on the effects of eIF4E suppression in transformed cells showed impaired the formation and proliferation of tumours.[194,195] Mechanistically, eIF4E activation aids cancers in apoptosis evasion through the cooperation of c-Myc to counter the c-Myc-mediated apoptotic program or increase the expression of anti-apoptotic proteins such as Bcl-XL.[196,197] These studies support the notion elevated eIF4E expression contributes to cancer pathogenesis. Furthermore, the phosphorylation of eIF4E also contributes to its oncogenic capabilities. In AML, overexpression of MNK1 resulted in the increased phosphorylation of S209 on eIF4E, and MNK1 inhibition impaired the proliferation and enhanced differentiation of AML cells.[198] Additionally, MNK inhibitors reduced the S209 phosphorylation of eIF4E, which resulted in reduced cyclin D1 expression and proliferation in breast cancer cells.[199] These studies show that targeting eIF4E expression and phosphorylation has some efficacy to reverse the oncogenic effects of eIF4E.

There are several observations of eIF4A1 overexpression associated with cancer. A panel of 14 melanoma cell lines and primary melanoma and hepatocellular carcinomas samples have been reported to have elevated levels of eIF4A1.[200,201] Additional studies also showed that protein expression of eIF4A1 predicted poorer outcome in estrogen negative breast cancer, while the eIF4A1 inhibitor, PDCD4, was associated with improved outcome.[202] Furthermore, eIF4A1 overexpression in non-small cell lung cancer is associated with metastasis.[203] These studies indicate that increased eIF4A1 may play a role in different cancer types.

The scaffold protein of the eIF4F complex, eIF4G, has also been found to play a role in cancer development. The transformative properties of eIF4G1 were confirmed in NIH-3T3 cells overexpressing eIF4G1 *in vitro,* which resulted in morphological changes, and *in vivo* by tumour formation in nude mice.[204] These findings may be a result of eIF4G1's ability to drive the cap-independent, by internal ribosome entry site (IRES), translation of mRNAs of oncogene instead of cap-dependent translation associated with eIF4E.[201] Many reports have described eIF4G1 overexpression in cancers such as non-small cell lung cancer, prostate cancer, and pancreatic ductal adenocarcinoma.[205–207] eIF4G1 overexpression results in the promotion of the G1/S transition of the cell cycle and increased cell proliferation and tumourigenesis *in vitro* and *in vivo.*[205,206] A pan-cancer study was performed using datasets from The Cancer Genome Atlas (TCGA) and found that most cancers have increased expression of eIF4G1 mRNA expression compared to normal tissues and higher eIF4G1 mRNA level was associated with worse outcome in multiple types of tumours.[208] Another study analyzing large public datasets identified eIF4G1 to be more selectively overexpressed than eIF4E, which in this context displayed a preference for cap-independent translation of cancer-related mRNAs over the translation of the mRNA of housekeeping proteins via cap-dependent initiation.[209] This phenotype is attributed to eIF4G1

hyperphosphorylation resulting in increased binding to eIF4A1 and reduced eIF4E availability.[209] Since eIF4F complex is clearly involved in cancer development, it is critical to explore therapeutic options to reverse the effects of eIF4F complex activity for developing improved treatment strategies for cancer patients.

1.4.4 eIF4F Complex Inhibitors

There has been a large amount of effort in exploring the inhibition of each member of the eIF4F complex in different cancers. Multiple approaches have been utilized to target eIF4E including targeting the cap-binding activity or the expression of eIF4E. A compound called 4Ei-1 was used in preventing the eIF4E to bind to the 5'-cap of mRNAs and reduced cap-dependent translation *in vitro* and *in vivo* in zebrafish embryos.[210] 4Ei-1 is a pronucleotide that is metabolized in the target cells by histidine triad nucleotide binding protein (HINT), which produces 7-benzyl monophosphate guanosine, a cap analogue, to prevent eIF4E binding the 5'cap.[210] Additionally, 4Ei-1 has been demonstrated to sensitize mesothelioma cells, breast and lung cancer cell lines to chemotherapy and reduce their proliferation.[140,211] Mechanistically, 4Ei-1 treatment induces the proteasomal degradation of eIF4E.[211] Other studies have used an eIF4E-specific antisense oligonucleotide (ASO) called LY2275796 to reduce the expression of eIF4E, which demonstrated promising activity in cell lines and xenograft models.[212] Interestingly, LY2275796 treatment did not reduce global protein synthesis, but showed reduced levels of cancer-related and anti-apoptotic protein expression like c-Myc, VEGF, Bcl-2, and survivin.[212] After these preclinical studies, LY2275796 was tested in a phase I clinical trial, which demonstrated reduced eIF4E mRNA and protein expression in patients with stage IV colon, lung, or head and neck cancer with moderate side effects like fatigue, nausea, fever, and vomiting.[213]

Phase II clinical trials are currently being conducted with the combination of LY2275796 and various chemotherapies in NSCLC (NCT01234038) and prostate cancer (NCT01234025).

Drug screens have been performed to identify inhibitors that can target the eIF4A1 helicase activity. Three natural products that selectively targeted eIF4E were identified: hippuristanol, pateamine A (Pat A), silvestrol.[214–216] Hippuristanol binds to the C-terminal end of eIF4A1 and prevents RNA binding by locking eIF4A1 in a closed conformation.[214,217] On the other hand, Pat A and silvestrol work similarly by inducing eIF4A1 dimerization and sequestration onto RNA non-specifically, which results in a depletion of available eIF4A1.[216,218] All three inhibitors demonstrated anti-cancer activity *in vitro* and *in vivo*, but silvestrol had more favourable pharmacologic properties for *in vivo* studies.[150,219–221] A synthetic inhibitor called zotatifin was then developed based on silverstol with improved pharmacokinetics for preclinical and clinical studies.[222] Zotatifin impaired cell proliferation and induced apoptosis in multiple solid tumour cell lines driven by receptor tyrosine kinases and inhibited tumour growth in human lymphoma xenograft models.[223,224] Mechanistically, zotatifin increases the affinity between eIF4A1 and specific polypurine tracts in 5'-UTRs that prevent the scanning of the 43S PIC for initiation of translation leading to decreases in expression of c-Myc and Bcl6.[224,225] Currently, there are ongoing clinical trials for the use of zotatifin in advanced solid tumours (NCT04092673).

Another approach to targeting the eIF4F complex is disrupting the interaction between eIF4G and eIF4E to prevent the assembly of the eIF4F complex. The first identified compound was 4EGI-1 (eIF4E/eIF4G interaction inhibitor) through a high throughput drug screen that involved displacing a fluorescent peptide that bound that eIF4E.[226] This compound is a competitive inhibitor of eIF4G1 binding to eIF4E, which resulted in a reduction of c-Myc and

Bcl-xL protein expression and induced apoptosis in multiple cancer cell lines.[226,227] 4EGI-1 treatment also reduced the tumour growth of human melanoma and breast cancer xenografts showing efficacy *in vivo.*[228] Another high throughput drug screen identified another compound called 4E1RCat, which also binds to eIF4E to disrupt its interaction with eIF4G1 and 4E-BPs, and treatment reversed the doxorubicin chemoresistance in Eμ-Myc lymphoma mice model.[229] Instead of binding to eIF4E, SBI-756 was another compound found to disrupt the eIF4E and eIF4G1 interaction but bound to eIF4G1.[230] SBI-756 dissociated eIF4G1 from eIF4F complex and increased the interaction between eIF4E and 4E-BPs, an indication of reduced eIF4F complex activity.[230] SBI-756 inhibited the growth of *NRAS*, *BRAF*, and *NF1*-mutant driven melanomas and reduced tumour growth *in vivo.*[230] Another study reported a synergistic effect of the anti-apoptotic protein BCL2 inhibitor, venetoclax in combination with SBI-756 in inducing apoptosis *in vitro* and tumour burden *in vivo* in lymphoma cells.[231] Molecularly, SBI-756 treatment disrupted the assembly of eIF4F complex leading to selectively reduced translation of mRNAs encoding ribosomal proteins and translation factors, displaying the specificity of SBI-756.[231] In summary, the eIF4F complex has been demonstrated to play an important role in the translation of mRNAs of cancer-related proteins to which cancers become addicted, and there is also a growing appreciation for eIF4F complex inhibitors to target the overexpression of these specific oncogenes for translation to pre-clinical and clinical studies.

1.5 Thesis Objectives

Drug resistance and disease relapse remain major challenges for curative treatment of CML patients. It is crucial to identify patients who are irresponsive to standard TKI monotherapies, so that they may be considered rapidly for transplant-based or novel combination treatments, to

significantly improve treatment outcomes. However, current clinical scoring systems cannot accurately predict the heterogeneous treatment outcomes observed in patients. It is also essential to identify key targets and develop new treatment strategies to overcome drug resistance by understanding the mechanisms in which CML LSCs and TKI-resistant cells can resist TKI treatments. To achieve these objectives, I focused my work on two specific projects:

1. Development of a predictive model by evaluating miRNA expression changes in $CD34^+$ CML stem/progenitor cells pre- and post-nilotinib therapy and examining the correlation of miRNA expression with patients' $CD34^+$ cell sensitivity to TKIs in a colony formation assay *in vitro*.
2. Identification and characterization of a highly deregulated eIF4F translation initiation complex in drug-resistant BCR-$ABL1^+$ cells by using a phospho-proteomic antibody microarray and various functional assays.

Recent studies have shown that differentially expressed miRNAs can be identified in primitive CML patient cells compared to normal bone marrow, particularly between IM-responders and IM-nonresponders.[96] Additionally, IM sensitivity determined using colony-forming cell (CFC) assays can predict a patient's response.[232] I hypothesize that the correlation of miRNA expression with patients' $CD34^+$ cell sensitivity to TKIs in CFC assays predicts TKI response in CML patients. In Chapter 3 of this dissertation, I describe the use of multiple bioinformatic analysis to develop a model of miRNA expression and *in vitro* TKI sensitivity to predict patient response to NL. I analyzed the expression of differentially expressed miRNAs in $CD34^+$ CML cells pre- and post-NL treatment from 58 patients enrolled in the Canadian sub-analysis of the ENESTxtnd phase IIIb clinical trial and correlated with sensitivity of $CD34^+$ cells to TKI treatments from *in vitro* CFC assays. Cox proportional hazard (CoxPH) analysis was

performed on these miRNAs and applied machine learning algorithms to generate multivariate miRNA panels that can predict NL response at treatment-naïve or post-treatment timepoints.

Understanding resistant mechanisms is important to discovering novel therapeutic strategies for drug resistant CML patients. Previous reports have demonstrated that AHI-1 is highly deregulated in CML LSCs and interacts with BCR-ABL1 to enhance its oncogenic activity.[75,119,120] AHI-1 contains multiple domains involved in signal transduction including the SH3 domain, which mediates TKI resistance.[116,122] I hypothesize that targeting key biological processes regulated by AHI-1 and its interacting partners and their pathways can sensitize drug-resistant cells to TKI treatment. Chapter 4 begins with the presentation of my antibody microarray analysis to identify differences in the proteome and the phosphorylation landscape of BCR-ABL1^{+} cells expressing different Ahi-1 constructs and their response to IM treatment. I observed the greatest number of differential antibody signal intensities in BCR-ABL1^{+} cells co-transduced with wildtype Ahi-1 compared to BCR-ABL1^{+} cells or cells co-expressing Ahi-1 SH3 domain deletion with and without IM treatment. This analysis led me to identify that the regulation of the eIF4F complex is deregulated in BCR-ABL1^{+} cells expressing wildtype Ahi-1, which were relatively more IM-resistant. Furthermore, transcript levels of several eIF4F complex members were found to be elevated in CD34^{+} CML patient cells compared to normal bone marrow. This led me to investigate the protein expression of eIF4F complex members and I discovered that IM-resistant CML cells expressed higher levels of eIF4G1 and eIF4B. Subsequently, I used genetic and pharmaceutical inhibition of eIF4G1 to study the effects of targeting the eIF4F complex and I reported reduced survival and increased sensitivity to IM treatment by inhibition of eIF4G1 in IM-resistant cells. I also demonstrated that eIF4G1

inhibition resulted in significant reduction in eIF4F complex activity, the protein expression of BCR-ABL1, and several eIF4E-sensitive genes.

Chapter 2: Materials and Methods

2.1 Cell Culture

2.1.1 Cell lines

The human CML BC cell lines K562 and IM-resistant K562 cells (K562R, no detectable BCR-ABL1 kinase domain mutations; kindly provided by Dr. A. Turhan, University of Poitiers, France) and BCR-ABL1-transduced murine pro-B cell line, BaF3, (B/A only), BCR-ABL1^{+} BaF3 co-transduced with wild-type mouse Ahi-1 (WT Ahi-1) or SH3 domain-deleted mouse Ahi-1 (Ahi-1 SH3$^{\Delta}$) were cultured in Rosewell Park Memorial Institute (RPMI) 1640 medium containing 2 mM L-glutamine supplemented with 10% fetal bovine serum (FBS) (Life Technologies, Carlsbad, CA), 100 U/mL penicillin (Thermo Fisher Scientific, Waltham, MA), 0.1 mg/mL streptomycin (Thermo Fisher Scientific) and 0.1 mM β-mercaptoethanol (STEMCELL Technologies, Vancouver, BC), henceforth referred to as complete RPMI medium. eIF4G1 knockdown cells were cultured in complete RPMI medium supplemented with 2 µg/mL puromycin. Human HEK-293T cells were cultured in Dulbecco's modified Eagle media (DMEM) (Life Technologies) supplemented with 10% FBS, 100 U/mL penicillin, 0.1 mg/mL streptomycin and L-glutamate (STEMCELL Technologies, Vancouver, BC). All cell lines were maintained in 10 cm Falcon® (Corning Inc., Lowell, MA) or Sarstedt (Nümbrecht, Germany) tissue culture dishes at 37°C and 5% CO_2.

2.1.2 Human Cells and Study Design of Nilotinib Predictive Study

Heparin-anticoagulated peripheral blood (PB) samples were obtained from 62 newly diagnosed CML patients enrolled in the Canadian sub-analysis arm of the ENESTxtnd phase IIIb clinical trial (https://clinicaltrials.gov/ct2/show/NCT01254188, Supplementary Table 1).

Enrichment of $CD34^+$ cells were enriched immunomagnetically using an EasySep CD34 positive Selection Kit (STEMCELL Technologies). However, 4 patients were excluded from the study due to insufficient enrichment of $CD34^+$ cells in the samples (<65%), leaving a total of 58 patient samples for analysis. These patients were newly diagnosed (within 6 months) CML-CP patients who have not been previously treated with IM. PB samples were obtained prior to therapy (BL), 1 month (M1) and 3 months (M3) after 300 mg or 400 mg BID nilotinib (NL) therapy.[233,234] Clinical responses of patients were classified as either NL-responders (R) or NL-nonresponders (NR) at 12 months (46 R, 12 NR) after treatment based on *BCR-ABL1* transcript levels following the European Leukemia Net treatment guidelines.[235]

2.1.3 Small Molecule Inhibitors

IM and NL were obtained from Novartis (Basel, Switzerland) and DA was obtained from Bristol-Myers Squibb (New York, NY). SBI-756 was purchased from Selleck Chemicals (Houston, TX). Cycloheximide solution and MG132 were purchased from Sigma-Aldrich (St. Louis, MO). Stock solutions of 10 mM were prepared with ddH_2O (IM) or dimethyl sulfoxide (NL, DA, SBI-756, MG132) and stored at -20°C.

2.2 Microfluidic Quantification PCR and Bioinformatic Analysis

Microfluidic quantitative PCR (qPCR) was performed as previously described.[96,236] Pooled RT primer mix containing 47 different miRNA stem-loop primers plus RNU48 were prepared and mixed with RNA extracted from $CD34^+$ CML cells. Amplified cDNA from these reactions were combined with Taqman master mix and loaded to sample inlets of a Fluidigm 48.48 Dynamic array device. High-throughput quantitative real-time PCR was then performed

using the BioMark HD system (Fluidigm, San Francisco, CA) to produce image-based fluorescent signals and raw Ct values.

Data quality control and normalization was performed using the *HTqPCR* package.[237] The Ct values were normalized to the endogenous control RNU48 (ΔCt method). Two samples were excluded due to having high RNU48 Ct values and were determined to be outliers as defined as 1.5 times the interquartile range. Univariate Cox Proportional Hazard (CoxPH) analyses were performed on 47 normalized miRNAs at each individual time point applying four different dichotomization cut-offs (median, 1st quartile, 3rd quartile, maximally selected rank statistics calculated cut-off) using the *R survival* packages while treating "non-response" at 12 months as the hazardous event.[238,239] Although maximally selected ranked statistics calculated cut-offs were used as the final cut-offs in the presented models and scores, only variables that were significantly associated with non-response in at least two of the four cut-off categories were considered for multivariate CoxPH analyses and machine learning. All features with significant expression differences between groups determined by Welch t-test were subjected to train two individual types of machine-learning models for "non-response" prediction for treatment-naïve samples, being random forest (RF) and Naïve Bayes (NB), using the *R caret* and *MLeval* packages.[240,241] For samples taken after patients received treatment, only miRNAs with stable association for NL non-response between 1 month and 3 months after treatment were considered for machine learning. Each model was repeatedly 10-fold cross-validated and performance of the two trained model per feature combination was evaluated based on *receiver operating characteristic* (ROC) and precision recall (PR) plots and recorded in the form of area under the curve (AUC) values.

2.3 Antibody Microarray and Bioinformatic Analysis

The Kinex KAM-1325 antibody microarray (Kinexus Bioinformatics Corporation, Vancouver, BC) was performed in accordance with the manufacturer's specification. In brief, cells were lysed and sonicated for 40 seconds in intervals of 10 seconds with 10 seconds intermissions over ice. The resulting homogenates were incubated for 30 minutes with 6 mM NTCB at 37°C for cysteine chemical cleavage and then subjected to ultracentrifugation for 30 minutes at 20°C at 50,000 RPM. The samples were then labeled with 20 µg of NHS-Biotin (APExBIO, Houston, TX) for 1 hour. The resulting labeled protein fragments were then purified using Sephadex G-25 Spin columns (Sigma-Aldrich) and eluted. Samples were then diluted to 400 µL with PBS with 0.05% Tween and 50 mM ethanolamine and then protein concentrations were measured by Bradford protein assay. Lysates were then applied to the antibody microarray and incubated in a humidity chamber for 2 hours. Slides were then washed, and anti-biotin antibody labelled with Alex546/Cy3 was then applied over the slides for 10 minutes in the humidity chamber. The slides were then washed, dried under nitrogen, and scanned at 543 nM using a ScanArray GX Microarray scanner (Perkin-Elmer, Wellesley, MA). Fluorescent signals from the antibody microarray were quantified with ImaGene 9.0 microarray image analysis software (BioDiscovery, El Segundo, CA). Antibody signal intensity was calculated as a function of the net median signal and spot size.

The raw antibody signal intensities were normalized using a semi-global method. Antibodies with the lowest 20% standard deviation across all samples were used as a subset for normalization. The *R* packages *ConcensusClusterPlus* and *pheatmap* was used to generate the heatmap with hierarchical clustering while the UMAP projection was generated using the *R* package *M3C*.[242–244] Differential expression analysis was performed using the *R limma* package

and volcano plots were generated using *EnhancedVolcano*.[245,246] Antibodies with significant differential signal intensities were subjected to pathway enrichment analysis using the g:Profiler toolset.[247] Criteria for enriched pathways include p-value > 0.05, size of pathway contains 10 ≤ number of proteins ≤ 500, and contains at least two proteins with significantly differential antibody signal intensities. Data sources for g:Profiler include GO biological process, KEGG, Reactome, and WikiPathways.

2.4 Molecular Techniques

2.4.1 Protein Extraction and Quantification

Protein was extracted from cells by incubating in lysis buffer on ice for 20 minutes. The lysis buffer contained 900 µL of phosphorylation solubilization buffer (PSB), 100 µL 10% NP-40 Alternative Protein Grade Detergent (Calbiochem, San Diego, CA) solution, 10 µL 10% sodium dodecyl sulfate (SDS) solution, 5 µL phenylmethylsulfonyl fluoride (Sigma-Aldrich), 5 µL protease inhibitor cocktail (Sigma-Aldrich). The lysate was then centrifuged at 13,000 RPM for 20 minutes at 4°C and the clarified lysate was separated into another tube. Protein concentration was quantified using 200 µL of 1:5 diluted Bio-Rad Protein Assay Dye (Bio-Rad, Hercules, CA) with 20 µL of 1:20 diluted protein lysate in triplicate on a 96-well Falcon® plate. The absorbance of each sample was measured using the Sunrise absorbance microplate reader (Tecan, Männedorf, Switzerland).

2.4.2 Immunoblotting

Protein lysates containing 30 µg of protein were mixed with 4x SDS-PAGE loading buffer, followed by heating at 95°C for 10 minutes. Samples were then loaded and separated in

8%-12% SDS-PAGE gels by electrophoresis, then transferred to a low fluorescence PVDF (MilliporeSigma, Burlington, MA). The membrane was blocked with EveryBlot Blocking Buffer (Bio-Rad) for 5 minutes at room temperature. Primary antibody incubation was done overnight at 4°C followed by a wash with Tris-buffered saline with 0.1% Tween 20 (TBST) for 5 x 6 minutes. Secondary antibody incubation was performed at room temperature for 1 hour and followed by a wash with TBST for 5 x 6 minutes. After, the membrane was incubated with Clarity Western Enhanced Chemiluminescence Substrate (Bio-Rad) and was imaged using the ChemiDoc Imaging System (Bio-Rad).

The primary antibodies used for immunoblotting were anti-phospho-mTOR (Ser2448, #2971, Cell Signaling Technology (CST), Danvers, MA), anti-phospho-RSK (Ser227, #3556, CST), anti-phospho-PTK2 (Tyr576/577, #3281, CST), anti-phospho-eIF4G1 (Ser1231, NBP2-04965, Novus Biologicals, Littleton, CO), anti-eIF4G1 (#2858, CST), anti-phospho-eIF4B (Ser422, #3591, CST), anti-eIF4B (#3592, CST), anti-eIF4A (#2013, CST), anti-eIF4E (#610269, Thermo Fisher Scientific), anti-phospho-4EBP (Thr37/46, #2855, CST), anti-4EBP (#9644, CST), anti-cyclin D3 (#2936, CST), anti-ABL (8E9, AB_2220994, BD Biosciences, Franklin Lakes, NJ), anti-MDM2 (sc-13161, Santa Cruz, Dallas, TX), and anti-MCL1 (#16225-1-AP, Proteintech, Rosemont, IL).

2.4.3 Proximity Ligation Assay

Approximately 7.5×10^4 cells were seeded on a 1 cm^2 square drawn using a Super PAP Pen (Electron Microscopy Sciences (EMS), Hatfield, PA) on a poly-L-lysine coated slide (EMS). Cells were then allowed to adhere to slide for 20 minutes in a 37°C incubator. The cells were then fixed with 4% paraformaldehyde (EMS) in PBS for 15 minutes at room temperature. Slides

were washed with PBS 3 times and incubated with 0.1% Triton X-100 (Sigma-Aldrich) in PBS solution for 10 minutes at room temperature for permeabilization. Cells were washed again with PBS 3 times and blocked with Blocking Solution (Sigma-Aldrich) in a 37°C incubator for 1 hour. eIF4G1 (1:125 dilution) and eIF4E (1:250 dilution) primary antibodies were diluted in Antibody Diluent (Sigma-Aldrich) and incubated on the slides overnight at 4°C. The next day, cells were washed twice with Wash Buffer A (Sigma-Aldrich) for 5 minutes with gentle agitation and incubated with PLA probe PLUS and MINUS (Sigma-Aldrich) diluted 1:5 with Antibody Diluent for 1 hour in a 37°C incubator. Cells were washed again with Wash Buffer A twice for 5 minutes and incubated with the Ligase-Ligation solution at 37°C for 30 minutes. Cells were washed again with Wash Buffer A for 5 minutes twice and incubated with the Polymerase-Amplification solution at 37°C for 100 minutes. Cells were then washed with Wash Buffer B for 10 minutes twice with gentle agitation, followed by a 0.01X Wash Buffer B solution for 1 minute. Finally, slides were mounted in Prolong Diamond antifade reagent with DAPI (Thermo Fisher Scientific), and fluorescence signals were detected using a confocal Nikon X1 microscope (Nikon, Minato City, Japan).

After image acquisition, FIJI (FIJI is Just Image J) was used to quantify the PLA foci signal. The background was corrected with “Subtract Background” and a Gaussian Blur was applied to the images. The PLA foci and DAPI channels were split, and threshold were applied using “MaxEntropy” and “Mean”, respectively. “Analyze Particles” was used to quantify the area of the images with threshold and the area ratio between the PLA foci and DAPI signals of each image was calculated.

2.4.4 O-Propargyl-Puromycin Assay

To measure protein synthesis rate, the Click-iT Plus OPP Alexa Fluor 647 Protein Synthesis Assay Kit (Thermo Fisher Scientific) was used. In brief, 2.5×10^5 cells were transferred to a clean FACS tube. Cells were spun down and resuspended with 100 µL of 20 µM Click-iT® OPP solution (Thermo Fisher Scientific) in pre-warmed complete RPMI medium. Cells were incubated in a 37°C incubator for 30 minutes and followed by a wash using 1 mL of PBS. The cells were then fixed using 100 µL of 4% paraformaldehyde solution in PBS (EMS) for 15 minutes at room temperature, followed by a wash using 1 mL of PBS. Cells were then permeabilized using 100 µL of 0.5% Triton X-100 (Sigma-Aldrich) solution in PBS for 15 minutes at room temperature, followed by a wash with 1 mL of PBS. The cells were then incubated with 100 µL of Click-iT® OPP reaction cocktail (Thermo Fisher Scientific) for 30 minutes at room temperature protected from light, followed by a wash using 1 mL of PBS. Cells were then washed with 100 µL of Click-iT® Reaction Rinse Buffer (Thermo Fisher Scientific) and resuspended with 150 µL of 1% FBS in PBS. OPP fluorescent signals were measured using the BD LSRFortessa Cell Analyzer (BD Biosciences) using the red laser and 670/14 filter.

2.4.5 Sucrose Gradient Centrifugation and Polysome Fractionation

Ten minutes prior to harvesting of cells, 100 µg/mL of cycloheximide was added to each condition. Cells were then harvested, washed with PBS supplemented with 100 µg/mL cycloheximide, and the cell pellets were stored at -80°C until lysis. Cells were lysed using a hypotonic lysis buffer containing 20 µM TRIS pH 7.3, 150 mM KCl, 5 µM $MgCl_2$, 0.5X protein inhibitor cocktail, 0.5% NP40, 0.5% deoxycholate, 100 µg/µL cycloheximide and Turbo DNase (Thermo Fisher Scientific). After 5-minute incubation on ice, the lysates were centrifuged at

5000xg for 5 minutes at 4°C to separate the nuclear fraction from the cytosolic fraction. The cytosolic fraction was then collected and loaded onto a sucrose gradient (10%, 34%, 55%) that was prepared the previous day. Then each sucrose gradient was centrifuged at 35,000 RPM for 2 hours at 6°C in a SW60 Ti rotor and a Beckman Coulter Ultracentrifuge (Beckman, Brea, CA). The samples were then fractionated and collected using the BioComp gradient profiler (BioComp Instruments, Fredericton, NB). After, fractions containing peaks that correspond to polysomes with 6 or more ribosomes were pooled together as the heavy polysome fraction and were then used for RNA extraction (Figure 2.1). This definition of heavy polysomes is used in Chapter 4.

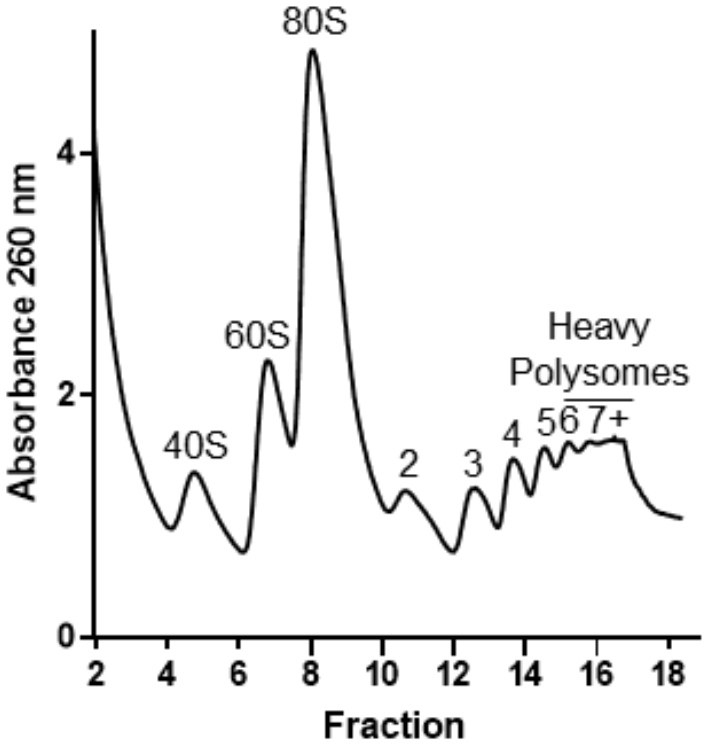

Figure 2.1: Example of Polysome Profile. Trace from a polysome fractionation experiment containing peaks that correspond to ribosome subunits (40S and 60S), monosomes (80S), and polysomes (numbers indicate number of ribosomes). Heavy polysomes are defined as those containing 6 or more ribosomes.

2.4.6 RNA Extraction

Samples were mixed with TRIzol (Thermo Fisher Scientific) for RNA extraction.[248] Glycoblue (Thermo Fisher Scientific) was added as a carrier to visualize the RNA pellet. RNA was dissolved in Nuclease-free water (Thermo Fisher Scientific) and the RNA concentration was measured using the Nanodrop (Thermo Fisher Scientific).

2.4.7 Quantitative Real-time PCR

Approximately 500 ng of RNA were reverse transcribed into cDNA using STEMscript cDNA synthesis kit (STEMCELL Technologies) according to the manufacturer's instructions. The cDNA was then diluted 1:10 using nuclease-free water. Quantitative real-time PCR (qRT-PCR) was performed using 6.25 µL of SYBR Green PCR Master Mix (Thermo Fisher Scientific), 0.25 uL of 20 µM gene specific primer solution, and 6 µL of the diluted cDNA on the 7500 Real Time PCR System (Thermo Fisher Scientific). SYBR was used as the reported dye while ROX was used as the passive reference. The ΔΔCt method was used to calculate relative transcript levels using *β2-microglobulin* (*β2M*) as the housekeeping gene. Primers used in this study for *BCR-ABL1* were 5'-CATTCCGCTGACCATCAATAAG-3' (forward) and 5'-GATGCTACTGGCCGCTGAAG-3' (reverse) and for *β2M* are 5'-TAGCTGTGCTCGCGCTACT-3' (forward) and 5'- TCTCTGCTGGATGACGTGAG-3' (reverse).

2.5 Transfection and Transductions

2.5.1 Lentivirus Production

Lentiviruses were produced in HEK293T cells using polyethylenimine (PEI) as transfection reagent. 18-20 hours prior to transfection, 5.5×10^6 cells were seeded in each of 10-cm Falcon® tissue culture plate in 7 mL DMEM supplemented with 10% FBS and L-glutamine and incubated in a 37°C incubator with 5% CO_2. Seven plates were seeded per construction. Four hours prior to transfection, the medium was removed and replaced with 4.5 mL of medium. For each plate, a 250 µL DNA mixture with 6 µg of shRNA plasmids, packaging vectors (1.5 µg of REV, 3.9 µg of ΔR), 2.1 µg of vesicular stomatitis virus glycoprotein (VSV-G) envelope in Opti-MEM® medium (Thermo Fisher Scientific) was added dropwise into a solution of 40 µL of PEI (1 µg/µL) with 210 µL of Opti-MEM® medium and was incubated at room temperature for 20 minutes. After, this combined 500 µL solution was added dropwise to each plate of HEK293T cells. After 48 hours, the viral supernatant was collected and filtered using a 0.45 µM low-binding filter (Pall Corporation, New York, NY), followed by ultracentrifugation to concentrate the viral particles for 1.5 hours. The virus pellet was resuspended in Iscove's Modified Dulbecco's Medium (STEMCELL Technologies) containing 5% DNase with gentle agitation for 30 minutes at room temperature, which was then aliquoted and stored at -80°C.

2.5.2 Lentiviral shRNA-Mediated Knockdown of eIF4G1

K562 or IM-resistant K562R cells were seeded at 3×10^5 cells in 400 µL of RPMI 1640 medium in a 24-well plate. The cells were then infected with 5 µL of concentrated lentivirus containing MISSION shRNA construct targeting human eIF4G1 (TRCN0000061769, TRCN0000061771) or a non-targeting sequence (SHC002, pLKO.1-puro non-mammalian

shRNA control plasmid, Sigma-Aldrich) in the presence of protamine sulfate for 18 hours. Cells were then washed with PBS and resuspended in complete RPMI medium containing 2 µg/mL puromycin. Cells were exposed to puromycin for 48 hours before setting up assays.

2.6 *In Vitro Assays*

2.6.1 Trypan Blue Viability Assay

Trypan blue exclusion method was used to assess the total cell counts and cell viability. Trypan blue (Thermo Fisher Scientific) remains in unhealthy cells with compromised cell membranes resulting in a dark blue colour to distinguish between healthy cells that have a white appearance. Cells were then counted using a Neubauer hemocytometer. Cells were seeded at a density of 1×10^5 cells/mL with or without inhibitors, and cell counts were performed at 24, 48, and 72 hours.

2.6.2 PI-Annexin V Apoptosis Assay

Apoptosis was detected using an Annexin V-APC apoptosis detection Kit (Thermo Fisher Scientific) and was used according to the manufacturer's instructions. In brief, cells were washed with PBS with 1% FBS and then resuspended with 100 µL of 1x Annexin V binding buffer (Thermo Fisher Scientific). Next, 2.5 µL Annexin V-APC and propidium iodide (PI) (Thermo Fisher Scientific) were added to each sample. After 20 minutes incubation at room temperature protected from light, 500 µL of 1x Annexin V binding buffer were added to each sample as a wash. Cells were then resuspended with 200 µL of 1x Annexin V binding buffer and flow cytometry was performed using the BD LSRFortessa Cell Analyzer. Percent apoptotic cells were

computed using FlowJo 10 software to sum "early" (Annexin V^+/PI^-) and "late" apoptotic cells (Annexin V^+/PI^+) together.

2.6.3 Colony-Forming Cell Assay

Colony-forming cell assays were performed as previously described.[120] Briefly, 3000 primary $CD34^+$ cells were mixed with 1 mL MethoCult H4230 (STEMCELL Technologies) in duplicate with growth factor cocktail in the presence or absence of inhibitors: 10 µM NL, 150 nM DA, 5 µM IM. Colonies were counted 14 days after plating.

2.7 Statistical Analysis

Unless otherwise indicated, results are shown as the mean ± standard deviation obtained from two to four independent experiments. Differences between groups were compared using a two-tailed Student's t-test for unpaired samples with unequal variances or one-way ANOVA, with corrections for multiple comparisons, using GraphPad Prism version 9 (GraphPad Software, San Diego, CA). *P*-values <0.05 were considered statistically significant and were computed applying the Welch Two Sample t-test with a 95 percent confidence interval.

Chapter 3: Identification of Key MicroRNAs as Predictive Biomarkers of Nilotinib Response in Chronic Myeloid Leukemia

3.1 Introduction

CML is a myeloproliferative stem cell disease characterized by the fusion oncoprotein BCR-ABL1.[4,249] TKIs that selectively target BCR-ABL1, such as IM, and second generation TKIs such as DA and NL, have demonstrated remarkable clinical efficacy in the treatment of CML-CP.[33,45,250–254] For example, a 10-year follow up of the ENESTnd clinical trial that evaluated long-term outcomes of NL and IM, demonstrated that NL had increased rates of treatment-free remission (TFR) eligibility and overall survival compared to IM treatment.[234,255] The extension of the ENESTnd clinical trial, ENESTxtnd, further supported the use of NL as a front-line therapy, with 81% of CML-CP patients achieving major molecular response (MMR) by 24 months.[256] These advances in TKI therapy have improved cancer-free survival rates and resulted in faster and deeper levels of molecular response in these patients. However, TKI treatments are not usually curative as some patients develop drug-resistance or are at risk of disease relapse when treatment is discontinued.[38,257–260] Thus, it has been of interest to develop predictive biomarkers to accurately predict whether patients may achieve a deep molecular response with first-line TKI, require a switch to second generation TKIs or can discontinue treatment safely. Patient material from a variety of sources has been profiled using microarrays, RNA-sequencing and, more recently, single cell RNA-sequencing.[89,261–263] Some studies have identified parameters that may indicate poor TKI response in CML patients, such as the detection of additional chromosomal abnormalities in BCR-ABL1^{+} cells at diagnosis or observing a slow rate of change in *BCR-ABL1* transcript levels in the first 3 months of TKI therapy, among

others.[264–266] It was also reported that IM response could be predicted in treatment-naïve CD34$^+$ stem/progenitor cells by an *in vitro* CFC assay.[232] Moreover, analysis of differential gene expression between IM-nonresponders and responders has offered predictive potential: a 17-gene panel quantified via qRT-PCR to classify patients as high-risk or low-risk was able to predict early molecular response failure, based on *BCR-ABL1* transcript levels at 3 months in CML-CP patients treated with IM or NL.[267] However, differences in the cell types profiled, the technologies used, and the inherent complexity associated with the interpretation of molecular data pose challenges in identifying reliable biomarkers with clinical utility.

MicroRNAs (miRNA) are single-stranded non-coding RNAs of about 18-25 nucleotide length that are aberrantly expressed in various malignancies and regulate numerous biological processes including cell differentiation and survival.[268–271] Some miRNA tumor suppressors regulating BCR-ABL1 were reported to be downregulated in CML cells whereas oncogenic miRNAs (oncomiRs) modulated by BCR-ABL1 were found to be overexpressed.[100,272,273] Additionally, BCR-ABL1-dependent and -independent miRNA expression profiles were observed in CML patient cells at different stages of the disease.[104,272] Interestingly, the expression of some of these miRNAs was reported to change in response to TKI-treatment and may therefore be good indicators of TKI-resistance.[101,104–107] Recently, our lab has generated miRNA and strand-specific RNA sequencing profiles on treatment-naïve CD34$^+$ CML cells with known subsequent IM responses and identified several differentially expressed miRNAs, including miR-185 and miR-145, in IM-nonresponders as compared to IM-responders.[96]

The goal of this study was to generate an effective, combinational predictive model consisting of miRNAs and *in vitro* TKI CFC data by analyzing miRNA expression profiles in

CD34$^+$ cells from 58 patients (retrospectively classified as NL-responders or NL-nonresponders) and the sensitivity of these cells to TKIs. Through Cox Proportional Hazard (CoxPH) analysis and machine learning approaches, two predictive miRNA panels were identified and evaluated in treatment-naïve or post-NL treatment in CML patients. Interestingly, incorporation of *in vitro* CFC data into either panel improved the predictive power at each time point. To my knowledge, this is the first study to utilize miRNA expression profiles, CFC data, and clinical response data from matched patient samples to develop a predictive model of response to NL treatment.

3.2 Results

3.2.1 Treatment-naïve CD34$^+$ CML Cells from NL-Responders and NL-Nonresponders Generate Significantly Different CFC Outputs during *in Vitro* Nilotinib Treatment

Previously, it has been demonstrated that CFC assays in IM-supplemented cultures can classify CML patients into IM-responders and IM-nonresponders, based on the colony output from treatment-naïve CD34$^+$ stem/progenitor cells obtained at diagnosis.[232] To determine whether a similar method can be applied to NL, *in vitro* CFC assays were performed with and without TKI treatments on CD34$^+$ cells from 58 newly diagnosed CML patients enrolled in the ENESTxntd trial. NL-responders have a 3-log-fold or greater reduction in *BCR-ABL1* transcripts (< 0.1%) at month 12 of NL therapy, while those that failed to achieve this response were classified as NL-nonresponders (NR, Appendix A). As expected, there was an overall reduction in CFC outputs generated from CD34$^+$ cells upon NL, DA or IM treatment compared to untreated controls. Furthermore, NL-response in patient CFC data correlated with DA-CFC and IM-CFC counts from the same patient sample (DA: Pearson's $R = 0.06831$, $p < 0.0001$; IM: $R =$

0.7243, $p < 0.0001$; Figure 3.1A). However, while most retrospectively classified responders produced overall fewer colonies upon any TKI treatment, a more diverse pattern was observed for nonresponders, clustering into two response fractions in CFC assays. Some of the nonresponder samples showed that they responded poorly and produced high numbers of colonies upon NL or DA or IM treatment, but a few samples produced similar numbers of colonies as $CD34^+$ cells from responders (Figure 3.1B). Nevertheless, a significant difference in CFC output was observed between responder and nonresponder samples for NL ($p = 0.014$) but not for IM or DA (Figure 3.1B). To determine if CFC output was significantly associated with nonresponse, each patient was categorized as CFC *low* or *high* based on maximally selected rank statistics calculated cut-offs (NL = 46.2%, DA = 26.9%, IM = 34.3%). Univariate CoxPH analysis showed that CFC outputs from all three TKIs were significant classifiers in predicting NL clinical response status ($p \leq 0.019$, Table 3.1) and displayed hazard-ratios (HR) <1, associating higher colony output with NL nonresponse.

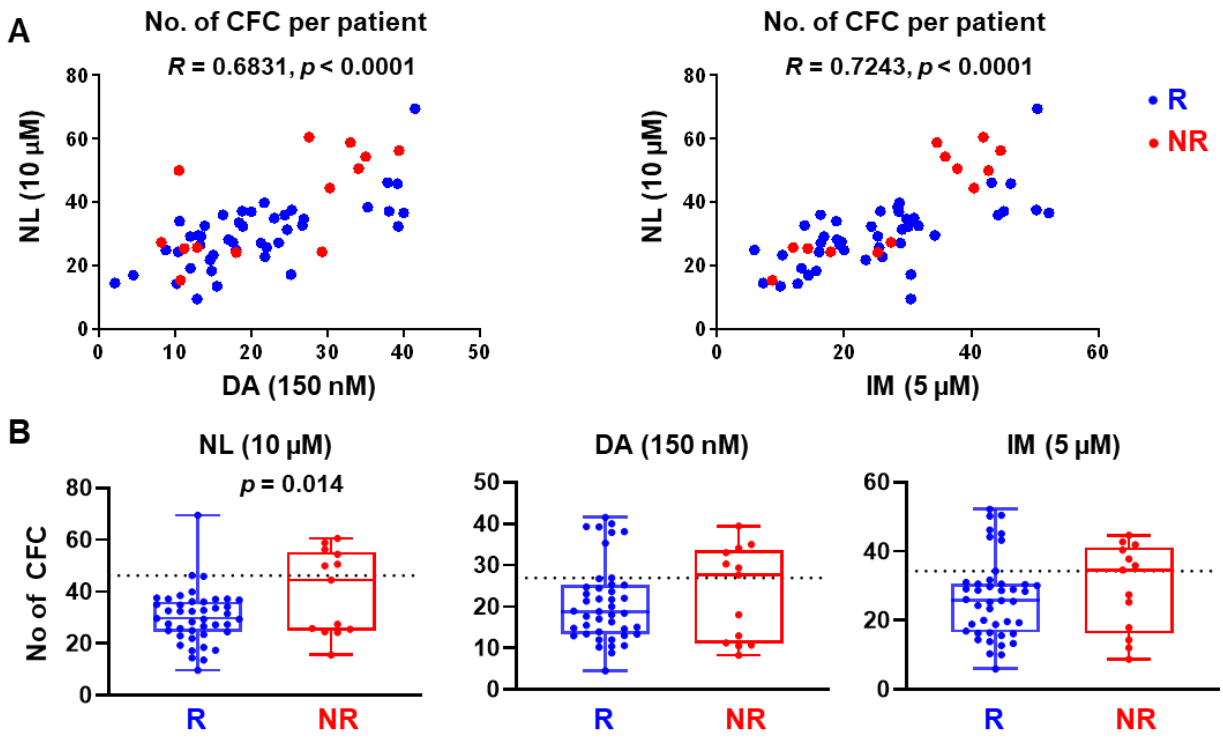

Figure 3.1: Comparison of the Effect of TKIs *in vitro* on CD34$^+$ Cells from NL-Responders and Nonresponders. (A) Correlations of CFC output between NL and IM or DA. (B) Differential CFC output between NL-NR and NL-R patient samples after treatment with NL, DA, and IM. Dashed line represents the calculated cut-offs determined by maximally selected rank statistics for CoxPH analysis. *P*-values for comparing NL-NR and NL-R groups were calculated using a two-tailed unpaired Student *t*-test. Data shown are mean ± standard deviation (SD).

Table 3.1 Cox Proportional Hazard Analysis of CFC Data

TKI	beta	HR	(95% CI for HR)	Wald test	*p*-value	RF ROC	NB ROC
NL (10 µM)	-2.2	0.11	(0.033-0.34)	14	0.00016	0.75	0.75
DA (150 nM)	-1.4	0.26	(0.083-0.8)	5.5	0.019	0.73	0.72
IM (5 µM)	-1.4	0.26	(0.083-0.8)	5.5	0.019	0.58	0.57

3.2.2 Expression of MiR-145 and MiR-708 in Treatment-Naïve CML Cells Predicts Patient Response and Accuracy is Further Improved by Incorporation of *In Vitro* NL-CFC data

Our lab recently published a miRNA-sequencing study highlighting 47 differentially expressed miRNAs identified in $CD34^+$ stem/progenitor cells between normal bone marrow (NBM) and CML patient samples, particularly between IM-responders and IM-nonresponders.[96] In the present study, microfluidic qRT-PCR expression data was collected for this panel of 47 miRNAs in $CD34^+$ cells obtained at diagnosis (BL), 1-month (M1) and 3-month (M3) post-NL treatment from 58 CML patients. The *HTqPCR* R package was used to perform data quality control and test several normalization methods on a large data set generated from 8,256 microfluidic qPCR reactions consisting of TaqMan probes specific for 47 miRNAs and an RNU48 control for each of the 58 patients. Ct values normalized to an endogenous RNU48 control produced a favourable normal distribution and this normalization method was then selected for this study (Figure 3.2). Interestingly, univariate CoxPH analysis identified that expression of 17/47 miRNAs were significantly associated with NL nonresponse (four miRNAs at BL, nine miRNAs at M1, and ten miRNAs at M3; $p < 0.05$, Figure 3.3A and Table 3.2). Some of these miRNAs were significantly associated with nonresponse across all the three time points and overall, 9/47 miRNAs were differentially expressed between NL-responder and NL-nonresponder patients at any time point (BL, M1, M3; $p \leq 0.047$, Figure 3.3B).

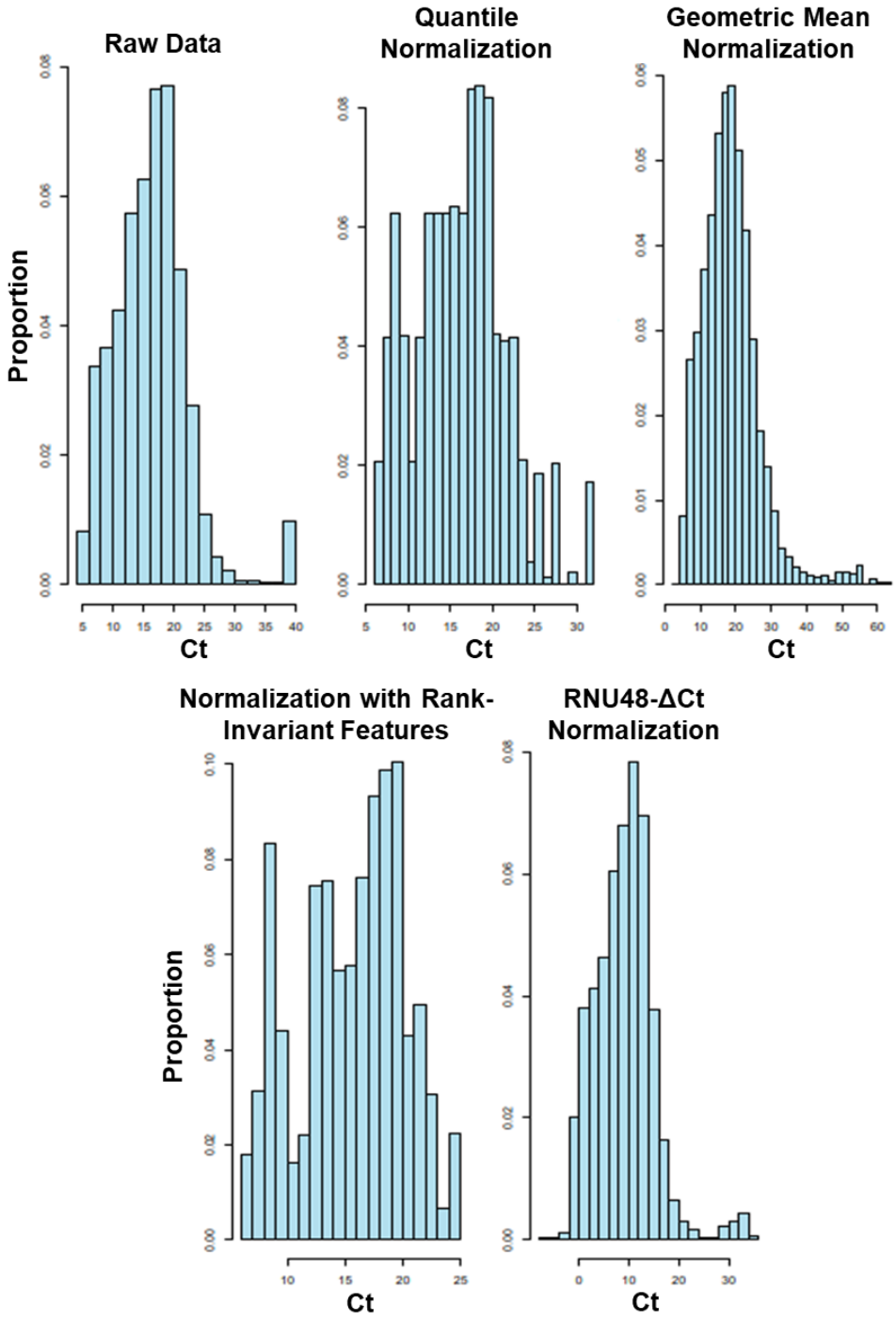

Figure 3.2: Distributions of Ct Values According to Different Normalization Methods from *HTqPCR* package. Frequency plots displaying the distribution of normalized Ct values of all 8,256 microfluidic qPCR reactions after each normalization method was applied with the Ct values plotted along the X-axis and their proportion on the Y-axis. The *HTqPCR* R package was used to calculate and plot the distribution of normalized Ct values.

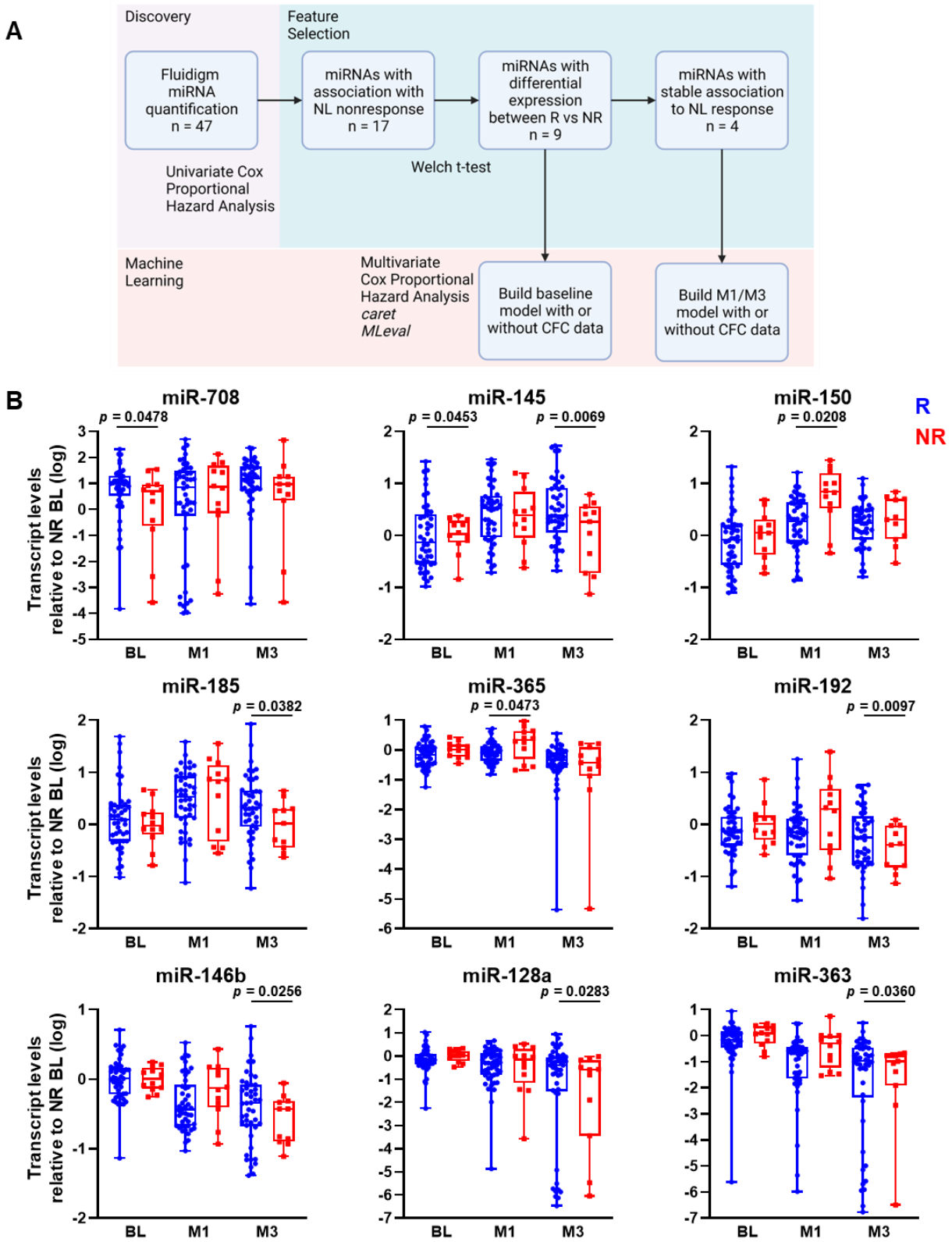
A
Discovery
Feature Selection
Fluidigm miRNA quantification n = 47
miRNAs with association with NL nonresponse n = 17
miRNAs with differential expression between R vs NR n = 9
miRNAs with stable association to NL response n = 4
Univariate Cox Proportional Hazard Analysis
Welch t-test
Machine Learning
Multivariate Cox Proportional Hazard Analysis
caret
MLeval
Build baseline model with or without CFC data
Build M1/M3 model with or without CFC data
B
R
NR
miR-708
p = 0.0478
miR-145
p = 0.0453
p = 0.0069
miR-150
p = 0.0208
miR-185
p = 0.0382
miR-365
p = 0.0473
miR-192
p = 0.0097
miR-146b
p = 0.0256
miR-128a
p = 0.0283
miR-363
p = 0.0360
Transcript levels relative to NR BL (log)
BL
M1
M3

Figure 3.3: Study Design and Univariate Analysis of 47 Differentially Expressed MiRNAs between NL-Responders and Nonresponders. (A) Workflow of statistical and analytical processes. (B) Univariate analysis of differentially expressed miRNAs associated with NL-nonresponse across pre- and post-treatment time points as indicated. Box-plots of transcript levels are displayed relative to NL-NR at the treatment-naïve state (BL) on a log scale. *P*-values were calculated using Welch's t-test.

Table 3.2: Univariate Cox Proportional Hazard Analysis of MiRNAs at Different Time Points

A. miRNAs with significant hazard ratios at baseline

Name	beta	HR	(95% CI for HR)	Wald test	*p*-value
miR-3607-5p	1.5	4.7	(1.4-16)	6.3	0.012
miR-363	1.3	3.8	(1.1-13)	4.7	0.031
miR-708	-1.6	0.2	(0.044-0.92)	4.3	0.038
miR-128a	1.4	3.9	(1.1-14)	4.2	0.041

B. miRNAs with significant hazard ratios after 1 month NL treatment

Name	Beta	HR	(95% CI for HR)	Wald test	*p*-value
miR-150	2.3	10	(3.1-32)	15	0.00011
miR-365	2	7.7	(2.5-24)	12	0.00045
miR-192	1.8	6.3	(2-20)	9.7	0.0018
miR-452	-1.9	0.15	(0.045-0.5)	9.5	0.002
miR-363	1.8	6	(1.9-19)	9.3	0.0023
miR-660	1.7	5.5	(1.8-17)	8.6	0.0033
miR-451	1.6	4.8	(1.5-15)	7.2	0.0071
miR-3607-5p	1.5	4.6	(1.2-17)	5.2	0.023
miR-146b	1.4	3.9	(1.1-14)	4.2	0.041

C. miRNAs with significant hazard ratios after 3 months NL treatment

Name	beta	HR	(95% CI for HR)	Wald test	*p*-value
miR-145	-1.6	0.19	(0.057-0.67)	6.8	0.0092
miR-3676	1.4	4.1	(1.2-13)	5.4	0.02
miR-182	-1.5	0.23	(0.06-0.86)	4.8	0.029
miR-185	-1.3	0.28	(0.085-0.92)	4.4	0.036
miR-192	-1.3	0.28	(0.085-0.92)	4.4	0.036
miR-3607-5p	1.2	3.4	(1-11)	4.2	0.042
miR-660	-1.3	0.28	(0.082-0.95)	4.1	0.042
miR-139-5p	-1.3	0.28	(0.083-0.97)	4	0.045
miR-150	1.3	3.5	(1-12)	4	0.045
miR-324-5p	-1.3	0.26	(0.07-1)	3.9	0.049

To evaluate their predictive capacity, the nine miRNAs that demonstrated significant association with NL nonresponse and were differentially expressed between NL-responders and

NL-nonresponders were combined into multivariate models for each individual time point of sample collection. At the treatment-naïve state (BL), increased miR-145 expression (HR 6.95, $p = 0.013$) and decreased miR-708 expression (HR 0.13, $p = 0.009$) were associated with NL-nonresponse in multivariate CoxPH modeling (Figure 3.4A). Two different classification algorithms were used to evaluate the combinations of miRNAs for robust predictive performance, in which the resulting AUC-ROC values were used to select the combination of miRNAs with the best performance. The random forest (RF) classifier algorithm generates multiple decision trees based on random subsets of the original dataset, which when combined would produce a "forest" of decision trees that averages the performance of each individual tree.[274] The Naïve-Bayes (NB) classifier utilizes Bayesian techniques to form networks based on independent probabilities of each input variable.[275] AUC-ROC values generated by trained RF- and NB-machine learning models also indicated predictive performance of miR-145 and miR-708 (AUC-ROC: $RF = 0.58$, $NB = 0.67$; Figure 3.4C and E).

Next, I tested if the model accuracy could be further improved through incorporation of the TKI-CFC response data (NL, IM, and DA). Indeed, multivariate CoxPH models incorporating CFC output (HR 0.15, $p = 0.003$) but not IM or DA showed superior Concordance in predicting NL nonresponse compared to models based on miRNA expression alone ($C_i = 0.8$ vs $C_i = 0.89$) (Figure 3.4B). Most interestingly, results from the trained RF and NB machine learning models showed that inclusion of NL-CFC increased the AUC-ROC and AUC-PR values by 1.2-fold (RF) and 1.9-fold (NB) (Figure 3.4D and F). Of note, no other clinical factors except for NL-CFC, including WBC count and *BCR-ABL1* transcript levels at BL and 12 months, were identified as important features in machine learning or associated with patient response (Table 3.3). Other factors including age and sex of the patients were not available, which could not be

included in the analysis. Thus, the combination of miR-145 and miR-708 expression was identified as a predictive indicator of NL response at the treatment-naïve state and inclusion of NL-CFC data further enhanced predictive performance.

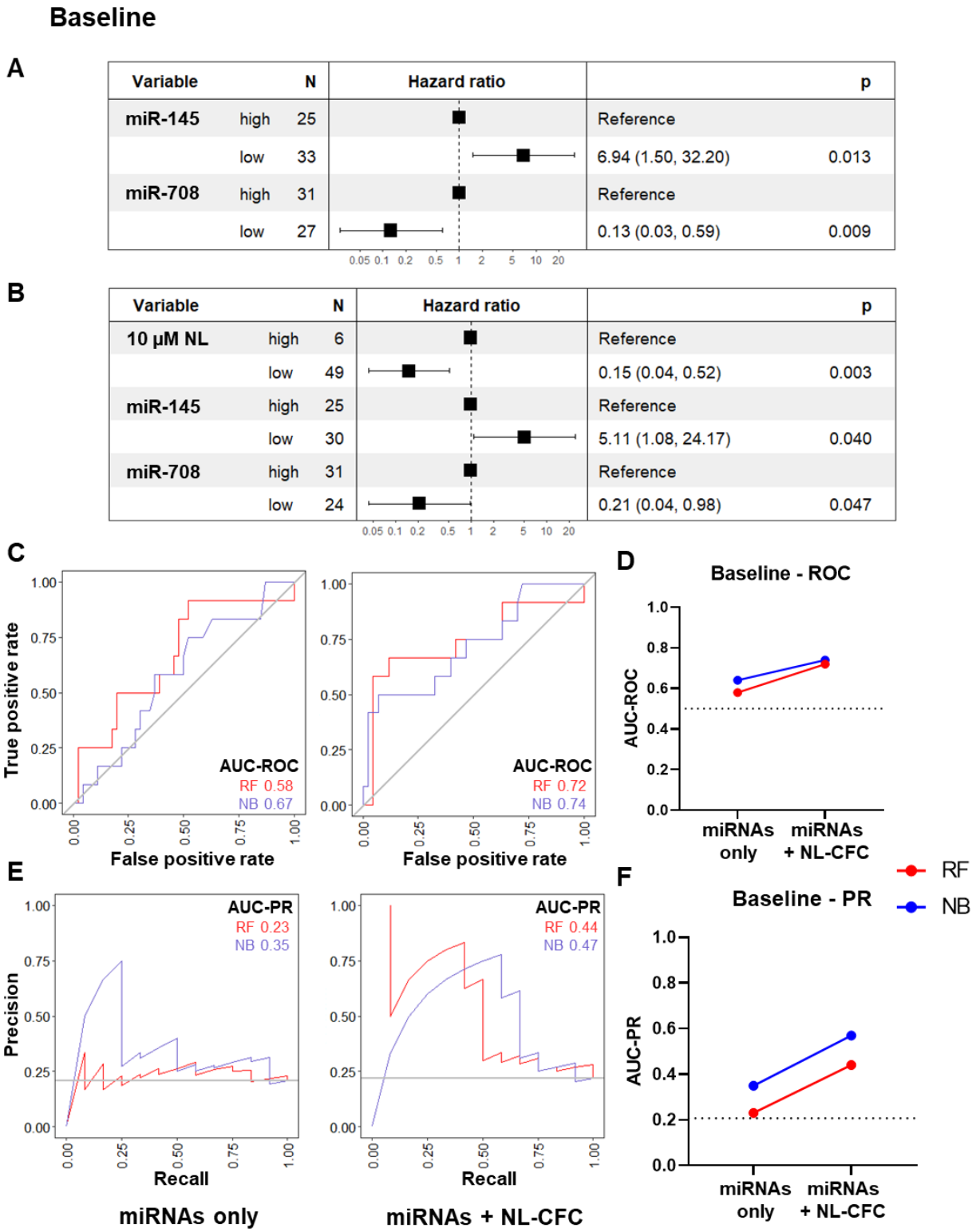

Figure 3.4: Multivariate Analysis of MiRNAs Associated with NL-Nonresponse in Treatment-Naïve Patients (BL). MiR-145 and miR-708 are associated with and can predict

NL-nonresponse as determined by multivariate CoxPH analysis (A) and ROC (C) and PR (E) plots from trained machine learning models. Inclusion of NL-CFC data (B) enhances predictive performance based on AUC-ROC and AUC-PR (C-F). N represents the number of patient samples that were classified as *high* or *low* in miRNA level or CFC output using the calculated cut-offs. The hazard ratios for each variable in the multivariate CoxPH analyses are displayed with 95% confidence and the corresponding *p*-value. ROC and PR plots for each machine learning algorithm, RF and NB, are shown with their corresponding AUC values.

Table 3.3: Univariate Cox Proportional Hazard Analysis of Clinical Parameters

Variable	beta	HR	(95% CI for HR)	Wald test	*p*-value
White blood cell count	-1.4	0.25	(0.055-1.2)	3.1	0.076
% CD34$^+$ cells	-19	4.00E-09	(0-Inf)	0	1
BCR-ABL1 ratio (BL)	-1	0.36	(0.11-1.1)	3.1	0.078
% BCR-ABL1 (12 m)	-24	5.50E-11	(0-Inf)	0	1
Log change 12 m-BL	24	1.80E+10	(0-Inf)	0	1

3.2.3 MiR-150 and MiR-185 Expression Levels in Post-NL CML Samples Predict Treatment Response and Accuracy is Further Improved by Incorporation of *in Vitro* NL-CFC Data

Since the model performed well in treatment-naïve patient cells, I next tested if a similar predictive panel could be generated at the M1 and M3 post-NL treatment. From the nine miRNAs that showed significant association with nonresponse in univariate CoxPH analyses, four miRNAs (miR-145, miR-365, miR-150, miR-185) displayed HR values that remained consistent between M1 and M3 and were therefore selected for further analysis. Overall, combination of miR-150 and miR-185 expression levels into multivariate CoxPH and machine learning models, achieved the best performance (AUC-ROC: *RF* = 0.76, *NB* = 0.73; C_i = 0.8; Figure 3.5A, C and E). Addition of NL-CFC to the M1 model improved Concordance (C_i = 0.88) and overall accuracy (AUC-ROC *RF* = 0.84, *NB* = 0.88, Figure 3.5 B, C and E), overall by up to 1.3-fold (Figure 3.5D and F). Applying the same panel to data collected at M3 validated the predictive potential of miR-150 and miR-185 in multivariate CoxPH analysis (Figure 3.6A) but

underperformed in the machine learning evaluation with lower-than-expected AUC-ROC values (*RF* = 0.52, *NB* = 0.51; Ci = 0.74) (Figure 3.6A, C and E). However, predictive performance was again greatly improved when NL-CFC was included to the M3 model, enhancing Concordance (C_i = 0.84), and increasing AUC-ROC values by 2-fold (*RF* = 0.72, *NB* = 0.68; Figure 3.6C-F). After NL treatment, both at M1 and M3, expression levels of miR-150 and miR-185 were identified as potential classifiers of treatment response and incorporation of NL-CFC data yielded significantly improved predictive accuracy, particularly after 1 month of treatment.

Month 1

A

Variable		N	Hazard ratio	p
miR-150	high	52	Reference	
	low	6	16.26 (4.28, 61.81)	<0.001
miR-185	high	6	Reference	
	low	52	0.13 (0.03, 0.60)	0.009

0.05 0.1 0.2 0.5 1 2 5 10 20 50

B

Variable		N	Hazard ratio	p
10 µM NL	high	6	Reference	
	low	49	0.21 (0.06, 0.76)	0.017
miR-150	high	49	Reference	
	low	6	9.12 (2.15, 38.75)	0.003
miR-185	high	6	Reference	
	low	49	0.17 (0.04, 0.76)	0.021

0.05 0.1 0.2 0.5 1 2 5 10 20

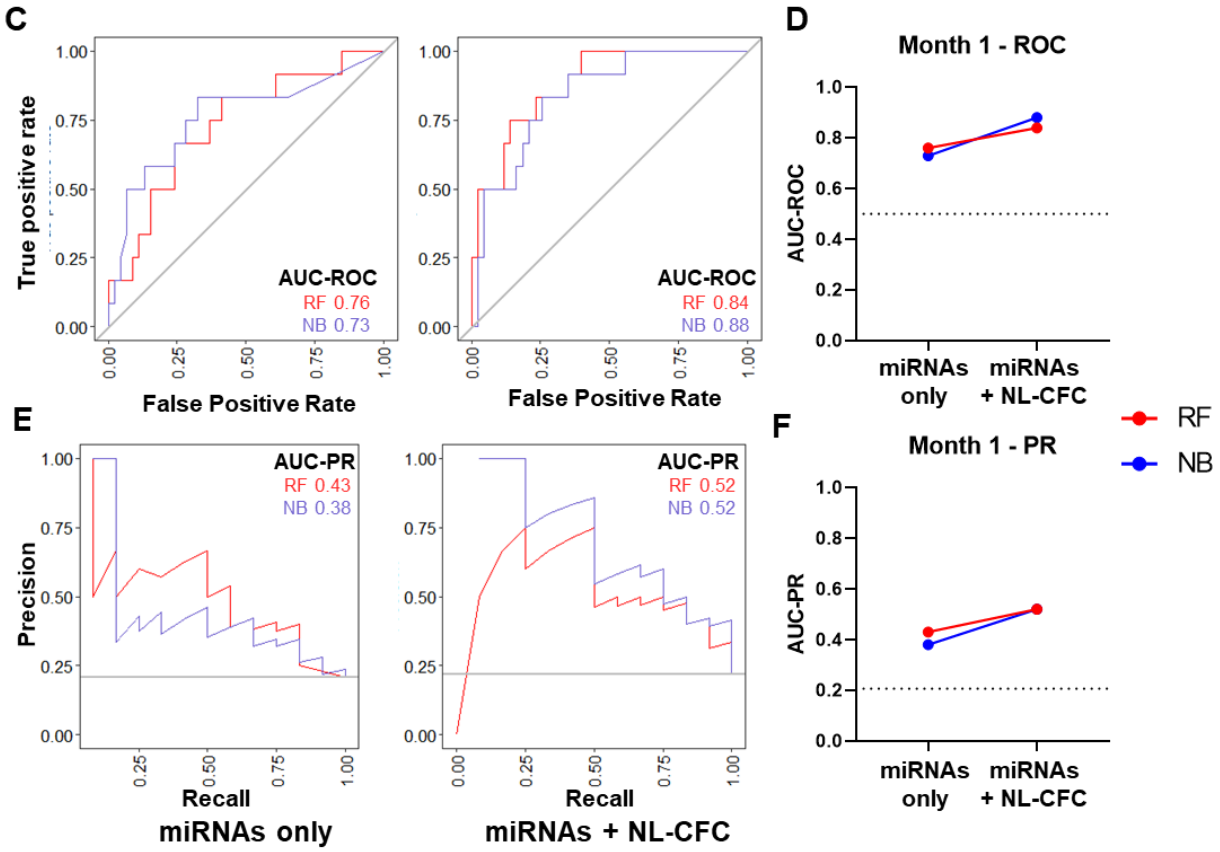

Figure 3.5: Multivariate Analysis of MiRNAs Associated with NL-Nonresponse in 1-Month Post-Treatment Patients (M1). MiR-150 and miR-185 are associated with and can predict NL-nonresponse, as determined by multivariate CoxPH analysis (A) and ROC (C) and PR (E) plots from trained machine learning models (C). Inclusion of NL-CFC data (B) enhances predictive performance based on improved AUC-ROC and AUC-PR (C-F). N represents the number of patient samples that were classified as *high* or *low* in miRNA level or CFC output using the calculated cut-offs. The hazard ratios for each variable in the multivariate CoxPH analyses are displayed with 95% confidence and the corresponding *p*-value. ROC and PR plots for each machine learning algorithm, RF and NB, are shown with their corresponding AUC values.

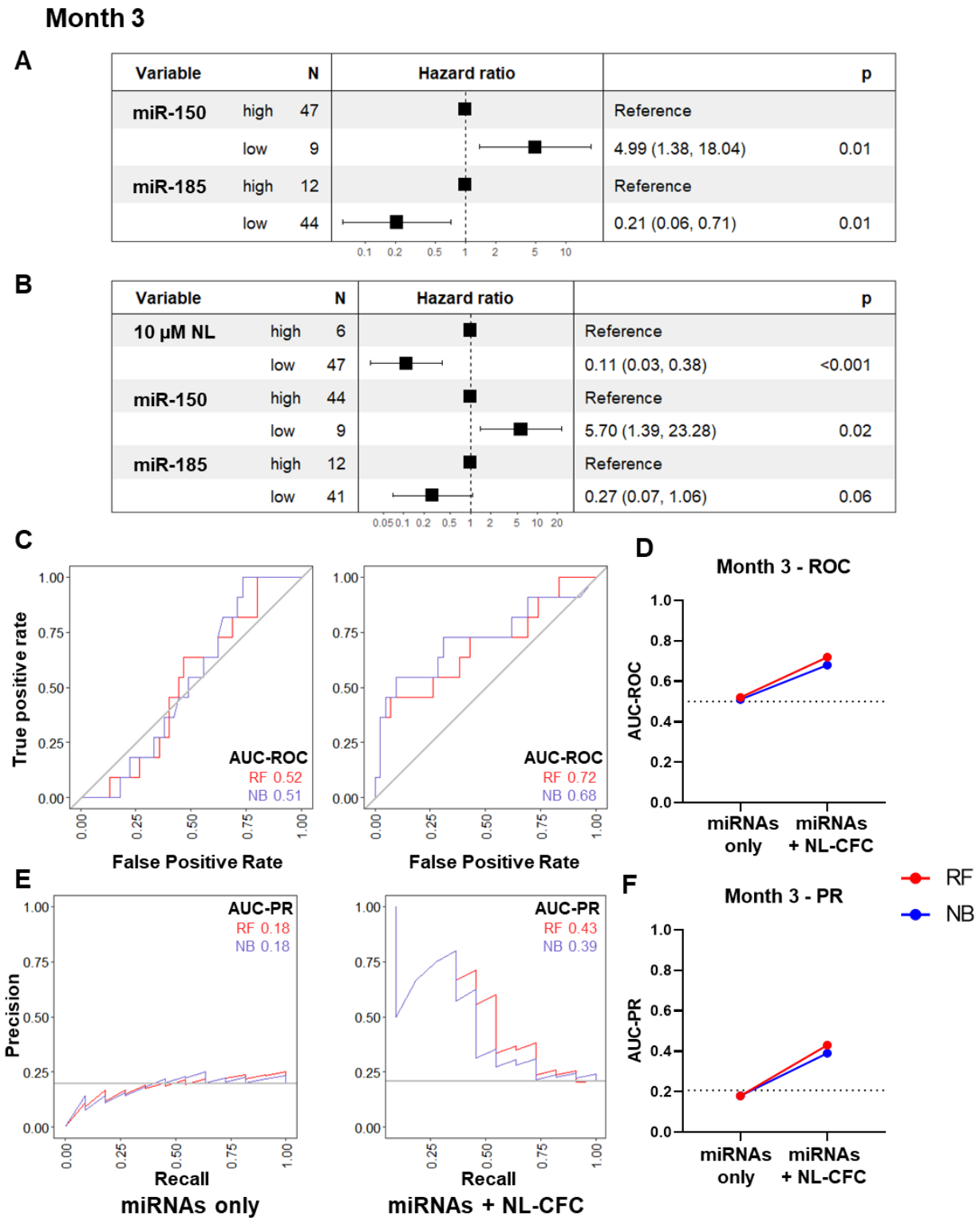

Figure 3.6: Multivariate Analysis of MiRNAs Associated with NL-Nonresponse in 3-Month Post-Treatment Patients (M3). MiR-150 and miR-185 are associated with and can predict NL-

nonresponse, as determined by multivariate CoxPH analysis (A) and ROC and PR plots from trained machine learning models (C). Inclusion of NL-CFC data (B) enhances predictive performance based on improved AUC-ROC and AUC-PR (C-F). N represents the number of patient samples that were classified as *high* or *low* in miRNA level or CFC output using the calculated cut-offs. The hazard ratios for each variable in the multivariate CoxPH analyses are displayed with 95% confidence and the corresponding *p*-value. ROC and PR plots for each machine learning algorithm, RF and NB, are shown with their corresponding AUC values.

3.3 Discussion

TKI therapies induce high rates of initial hematological and molecular responses in CML-CP patients, but TKI resistance and disease progression continue to pose a challenge for some patients. Current clinical scoring systems cannot accurately predict the heterogeneous treatment outcomes that are observed. From the analyses of CML patient samples at the treatment-naïve and post-NL treatment states from 58 patients, there are two proposed panels of NL-nonresponse predictors: The first panel consists of NL-CFC, miR-145 and miR-708, which predicts NL-nonresponse at diagnosis. The second panel of NL-CFC, miR-150 and miR-185 predicts NL-nonresponse at M1 and M3 post-NL treatment. Although miRNA signatures have alluded to TKI response prediction in CML, this study shows merit for combining matched miRNA expression profiles with *in vitro* CFC output to predict NL-specific response.

Previously, it has been demonstrated that IM response could be predicted in treatment naïve $CD34^+$ cells by an *in vitro* CFC assay in a small cohort study.[232] Here, CFC output data from patient $CD34^+$ cells obtained at diagnosis can also predict NL response in a larger cohort. Since singular predictive variables alone may not be sufficient to predict response due to cellular variations and molecular complexity among patients, we generated a multivariate predictive panel based on a combination of expression of specific miRNAs and patient's NL-CFC response. This combination improved the predictive value of using miRNA levels alone, as demonstrated

by improved Concordance, AUC-ROC, and AUC-PR at all time points. It has been well-documented that CML stem cells and their progenitor cells are the least TKI responsive and are responsible for disease recurrence when TKIs are discontinued.[42,63,64,249,276,277] Notably, *BCR-ABL1* transcript and protein levels are significantly elevated in $CD34^+$ cells and even more so in the $CD34^+CD38^-$ stem cell-enriched population compared to the bulk $CD34^-$ population.[63,278] Therefore, it has been of interest to determine whether distinguishing features of $CD34^+$ leukemic stem/progenitor cells from CML patients might vary amongst patients in correlation with the subsequent clinical response to TKI therapy. In this study, primitive $CD34^+$ CML cells from individual CP patients show that they indeed display cellular and molecular differences. In particular, clinically defined responders and nonresponders differ significantly from each other with respect to the growth response of their pre-treatment CFC to NL, and their miRNA expression changes. The two newly identified predictive panels, based on stably down- and up-regulated miRNAs whose expression levels differ significantly and associate with treatment response pre- and post-NL therapy, might therefore form the basis of prospective tests for predicting early treatment response and ultimately for optimizing CML patient management.

In this study, miR-145 and miR-708 are highlighted as potential predictive biomarkers in treatment naïve patients. MiR-145 expression changes were significantly different between IM-responders and IM-nonresponders in $CD34^+$ CML cells obtained at diagnosis, adding to previous reporting that miR-145 is differentially expressed between CML peripheral blood patient samples and normal hematopoietic progenitor cells and between CML-AP versus CML-CP cells.[96,106] NL treatment also seems to be able to increase expression of miR-145 in $BCR\text{-}ABL1^+$ cell lines.[107] Although overall miR-145 expression in $CD34^+$ cells differed significantly between NL-responders and NL-nonresponders in this study, the variation in miR-145 expression level

among responders is relatively high with some responder patient cells expressing levels similar to NL-nonresponders; a trend that was also observed in other miRNAs in this study. These observations indicate heterogeneous and differential expression of miRNAs in individual CML patients even before NL treatment. Thus, it is critical to use advanced multivariable statistical and bioinformatics tools to precisely identify useful miRNA predictors among other clinical, biological, and molecular parameters. Mechanistically, the role of miR-145 in CML has yet to be fully explored. However, miR-145 was found to be downregulated and has been suggested to sensitize resistant cancer cells to treatment by modulating drug efflux and apoptotic pathways in solid tumors.[279,280] A conflicting report shows that miR-145 is overexpressed in later stage breast cancer and supports cancer cell survival by promoting epithelial to mesenchymal transition and hypermethylating apoptotic genes.[281] However, miRNA expression is highly context-dependent and downstream effects can differ greatly between tumour types. While expression of miR-708 was found to be significantly reduced in $CD34^+$ CML cells compared to normal $CD34^+$ bone marrow cells, there is a lack of understanding of miR-708 in CML and other myeloid leukemias.[96] MiR-708 has been studied most extensively in lymphoblastic leukemias like acute lymphoblastic leukemia (ALL) where it is speculated to have both oncogenic and tumor suppressive functions depending on the subtype of ALL.[282] Clinically, ALL patients with low miR-708 levels were reported to have an increased risk of relapse.[282] Based on the analysis from this study, reduced miR-708 expression in NL-nonresponder cells may also be indicative of more aggressive and drug-resistant properties. Although the role of miR-145 and -708 in TKI sensitivity in CML patients have not been elucidated, reports of their participation in drug resistance of other cancers encourages further studies regarding their roles in TKI sensitivity. Furthermore, these miRNAs were identified prior to NL treatment and were used to predict NL

sensitivity. The changes in miRNA expression in response to NL treatment may differ compared to other TKI treatments as each TKIs have different specificities and off-target effects. The expression of these miRNAs could be useful for clinicians to select the most suitable TKI for their patients at the start of their treatments to reduce the risk of nonresponse.

In $CD34^+$ CML cells obtained 1-month and 3-month post-NL treatment, NL-nonresponder patients had increased levels of miR-150 and decreased levels of miR-185 compared to NL-responders. Combining both miRNAs into multivariate models predicted NL-nonresponse at both time points. Interestingly, both miR-150 and miR-185 have been demonstrated to have tumour suppressive properties in CML.[96,283–285] MiR-150 was suggested to be negatively regulated by BCR-ABL1 via MYC which in turn increases MYB expression and contributes to CML pathogenesis.[283] CML patients who were able to achieve early treatment response (ETR) after IM treatment were observed to have higher miR-150 levels.[284,285] MiR-185 can be repressed by BCR-ABL1 in IM-nonresponder patients, which contributes to leukemic stem cell survival and TKI-resistance through increased PAK6 and OXPHOS mechanisms.[96] Furthermore, restoration of miR-185 could sensitize IM-resistant cells to TKIs.[96] In summary, these studies support the identification of that both miR-150 and miR-185 as key players in CML pathogenesis and rationalize their association with TKI-resistance.

The differences in significant miRNA classifiers among the two predictive panels, generated at the treatment naïve and post-NL treatment state, are likely attributed to dynamic changes in miRNA expression in response to NL treatment. The observation of increased miR-150 expression in NL-nonresponder patients appears to conflict with other studies that reported miR-150 to be downregulated in CML and that its increased expression following IM treatment

is an early positive predictor for IM response.[284] This discrepancy may be due to the use of enriched $CD34^+$ stem/progenitor cells in this study as opposed to unpurified peripheral blood and bone marrow cells or because miRNA expression may be modulated differently between NL and IM treatments.[263] Furthermore, it is not uncommon for miRNAs to possess conflicting roles, *e.g.*, serving as oncogenic and tumour suppressive properties in the same cancer type, mainly owed to their ability to regulate expression of multiple target genes, which in turn also include both oncogenes and tumour suppressors.[286] Therefore, independent validation of these proposed predictive panels using greater numbers of patient samples and further exploration of the mechanistic roles of these select miRNAs in CML is warranted to facilitate their utility as prognostic tools in the clinic. Unique to this study, miRNA expression data were combined with patient-matched *in vitro* CFC outputs. In both BL and M1/M3 models, the inclusion of NL-CFC data in the multivariate panels improved predictive performance compared to miRNAs alone. It is widely agreed that treatment response may be affected by multiple factors not just related to biological mechanisms, such as pharmacokinetic variations between CML patients. Thus, prognostic algorithms that rely on genetic signatures alone may not be sufficient to model these extrinsic factors, highlighting the need for multifaceted molecular panels to improve predictive accuracy. The ability to develop rapid and robust tests to predict individual patients' response to TKI therapy could ultimately have a profound impact on CML patient management, providing a foundation for more effective treatment decisions.

Chapter 4: Identification and Characterization of a Highly Deregulated eIF4F Translation Initiation Complex in Drug-Resistant BCR-ABL1^{+} Cells by a Phospho-Proteomic Antibody Microarray

4.1 Introduction

CML is a multi-lineage myeloproliferative disease arising from the overactivation of growth and survival signaling pathways driven by BCR-ABL1 kinase activity.[5,10] Introduction of TKIs, like IM, to block BCR-ABL1 activity has greatly improved the outcomes of CML patients at the chronic phase, which is characterized by the expansion of the granulocyte population.[37] Due to the nature of targeted monotherapies, like TKIs, primary and acquired resistance remains an issue for CML patients as they are not curative and some patients experience early relapses and disease progression.[68] Furthermore, there is a population of quiescent LSCs that are not effectively eliminated by TKIs.[63] Therefore, improved treatments, such as combination therapy are necessary to reduce the prevalence of resistant LSCs and drug-resistant cells. Although targeting BCR-ABL1 activity is key to treating CML, finding other therapeutic targets could help to develop more effective treatment strategies to overcome TKI resistance in CML patients.

AH1-1 is a potential target of interest as it contains multiple important signaling domains and interacts with BCR-ABL1.[75] *AHI-1* was found to be highly expressed in CML patient cells, especially in the LSC-enriched population.[119] Further studies demonstrated AHI-1 directly interacts with BCR-ABL1 with its WD40-repeat domain and a synergistic effect on leukemogenesis was observed with cells co-expressing both AHI-1 and BCR-ABL1 than either alone in a xenograft mice model.[75,120] At the N-terminus, human AHI-1 also contains a coiled-coil domain that allows for interactions with other coiled-coil domains and in mouse, the N-

terminal is crucial for interaction with a BCR-ABL1 substrate involved in cell signaling, JAK2.[75,111,121] At the C-terminus, AHI-1/Ahi-1 contains another important signaling domain, the Src homology 3 (SH3) domain, that can interact with proline-rich motifs (PXXP).[111] The Ahi-1 SH3 domain mediates TKI resistance and interacts with another BCR-ABL1 substrate, dynamin 2, to deregulate multiple biological processes including endocytosis, ROS generation, and autophagy.[116,122] AHI-1 has also been reported to interact with the B subunit of the phosphatase PP2A and β-catenin; dual inhibition of BCR-ABL1 and PP2A disrupted AHI-1 mediated signaling leading to β-catenin, which is required for LSC maintenance.[76] These studies demonstrate the important role of AHI-1 as a scaffold protein to bring together BCR-ABL1 and its substrates to deregulate leukemic properties in CML. Therefore, it is interesting to study the biological processes downstream of AHI-1 and its interacting partners to find potential mechanisms of TKI resistance.

In this study, a high content antibody microarray was used to investigate the differences in the proteome and the phosphorylation landscape of BCR-ABL1$^+$ cells expressing different constructs of mouse Ahi-1 in the presence or absence of IM. I performed bioinformatic analyses and uncovered the eIF4F complex to be highly deregulated in BCR-ABL1$^+$ cells co-expressing wildtype Ahi-1. In an RNA-sequencing dataset, the transcript level of several eIF4F complex members were elevated in CD34$^+$ CML patient cells compared to normal bone marrow, which prompted for further investigation of differences in eIF4F complex member expression in BCR-ABL1$^+$ cell line models. Interestingly, I demonstrated that several key members of eIF4F complex and downstream genes were highly expressed in IM-resistant cells, particularly eIF4G1. Indeed, suppression of eIF4G1 by genetic inhibition using lentiviral-mediated shRNA and pharmacological inhibition of eIF4G1 by SBI-756 resulted in reduced survival, an increased

sensitivity to IM in resistant cells, and reduced eIF4F complex activity. Most notable, the protein expression of BCR-ABL1 was significantly suppressed by the inhibition of eIF4G1. These findings have demonstrated a proof of concept for the novel targeting BCR-ABL1 through the eukaryotic translation initiation machinery.

4.2 Results

4.2.1 An eIF4F Translation Initiation Complex is Identified in BCR-ABL1^{+} Cells Co-Expressing Wildtype Ahi-1 Cells by Antibody Microarray Analysis

Previously, BaF3 cells transduced to co-express BCR-ABL1 (B/A only) and various mouse Ahi-1 constructs including wildtype Ahi-1 (WT Ahi-1) or SH3 domain-deleted Ahi-1 (Ahi-1 SH3$^{\Delta}$) have demonstrated differential sensitivity to TKI treatments.[116,122] The Kinex antibody microarray platform was used to investigate the differences in the proteome expression and phosphorylation landscape between these cells that contribute to TKI sensitivity. The KAM-1325 antibody microarray consisted of antibodies targeting proteins involved with cell signaling including 875 antibodies for specific phosphorylation sites and 451 pan-specific antibodies.[287] To identify differences in IM response, cells were also treated with 5 µM of IM for 3 hours which resulted in a differential reduction in BCR-ABL1 tyrosine phosphorylation levels. Therefore, this dose selected as the optimized IM treatment for the antibody microarray analysis (Figure 4.1A). Each of the 6 samples were applied onto two fields of the antibody microarray, with each field containing duplicate antibody spots; this yielded a total of 4 technical replicates for each sample.

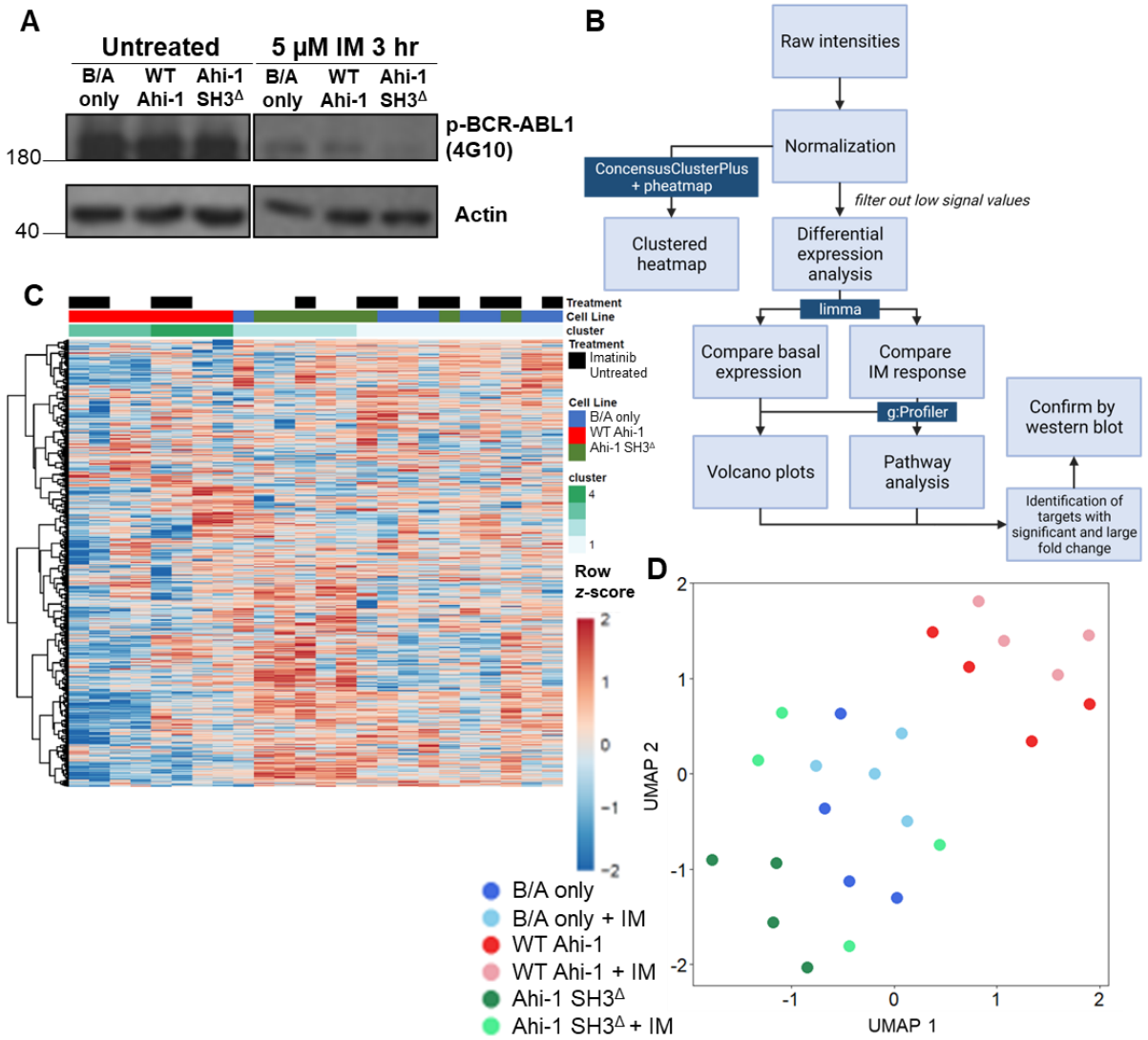

Figure 4.1: Antibody Microarray Analysis Study Design and Overview of Antibody Signal Intensities. (A) Cells expressing BCR-ABL1 only (B/A only), BCR-ABL1 with wildtype Ahi-1 (WT Ahi-1), or BCR-ABL1 with SH3 domain-deleted Ahi-1 (Ahi-1 SH3$^{\Delta}$) were treated with or without imatinib (IM) for 3 hours and were then used for the antibody microarray. Western blot analysis was performed on these cells for detection of phosphorylation of BCR-ABL1 using a 4G10 antibody, which demonstrated a reduction in phospho-tyrosine signals of BCR-ABL1 after IM treatment. (B) Workflow of statistical and analytical processes. (C) Heat map of antibody signal intensities with hierarchical clustering of the sample replicates used for the antibody microarray. (D) UMAP projection of the antibody signal intensities for each sample replicate. The row z-scores were used to display changes in antibody signal intensities changes across all replicates.

The pipeline for the bioinformatic analysis of the antibody microarray data is outlined in Figure 4.1B. First, the raw intensities of each antibody spot were normalized using a semi-global normalization method to eliminate any technical variations during the experiment. This approach used a subset of antibodies with the lowest standard deviation across all samples to normalize for any differences but still preserved the reduction in total signal intensities after IM treatment. As many of the antibodies are for specific phosphorylation sites, it is expected that IM treatment would reduce the global phosphorylation levels. After normalization, hierarchical clustering using Consensus Cluster Plus and UMAP projection was performed for a macroscopic look at the antibody microarray data. This revealed that WT Ahi-1 cells were the most different compared to the other cells as these replicate samples were clustered together in both analysis (Figure 4.1C, D). Next, differential expression analysis was performed by filtering out antibodies with low signal intensities and using *limma*. Aligning with the previous observation, WT Ahi-1 cells had the greatest number of significantly differential antibody signals (29 decreased, 3 increased, Table 4.1 & Figure 4.2A-C) when compared to B/A only cells, while Ahi-1 SH3$^{\Delta}$ cells resulted in fewer significantly differential antibody signals (2 decreased, 12 increased, Table 4.1). Furthermore, there were more significantly differential antibody signals (42 decreased, 7 increased, Table 4.1 & Figure 4.3A-C) in the comparison between WT Ahi-1 and Ahi-1 SH3$^{\Delta}$ cells. In response to IM treatment, WT Ahi-1 cells had the greatest number of significantly differential antibody signals (56 decreased, 7 increased, Table 4.1 & Figure 4.4A-C) compared to B/A only cells (5 decreased, Figure 4.1) and Ahi-1 SH3$^{\Delta}$ cells (9 decreased, 2 increased, Table 4.1).

Table 4.1: Summary of Significant Changes in Antibody Signal Intensities

Comparison	Decreased Signals	Increased Signals
WT Ahi-1 vs B/A only	**29**	**3**
WT Ahi-1 vs Ahi-1 SH3$^{\Delta}$	**42**	**7**
Ahi-1 SH3$^{\Delta}$ vs B/A only	2	12
B/A only + IM vs B/A only	5	0
WT Ahi-1 + IM vs WT Ahi-1	**56**	**7**
Ahi-1 SH3$^{\Delta}$ + IM vs Ahi-1 SH3$^{\Delta}$	9	2

As the comparisons with WT Ahi-1 yielded the greatest number of differential antibody signals, these targets were subjected to a pathway enrichment analysis using g:Profiler to find pathways that could be altered in these comparisons. In the comparison of WT Ahi-1 and B/A only cells, there were 77 pathways enriched from the decreased targets and 3 pathways from the increased targets (Figure 4.2D, E). Interestingly, a pathway involving the eukaryotic translation initiation machinery, "translation inhibitors in chronically activated PDGFRA cells", was enriched in the decreased targets from this comparison. Additionally, there were also multiple enriched pathways involving the MAPK and the PI3K/AKT/mTOR pathways, which play a role in the regulation of translation initiation.[150] Furthermore, there were multiple pathways again involving the MAPK and PI3K/AKT/mTOR pathways that were also enriched between WT Ahi-1 and Ahi-1 SH3$^{\Delta}$ cells with 85 enriched pathways for decreased targets and 23 for increased targets (Figure 4.3D, E). Finally, the presence of these enriched pathways of the MAPK and PI3K/AKT/mTOR pathways, were found in the WT Ahi-1 cells with IM treatment with 111 enriched pathways from decreased targets and 27 from the increased targets (Figure 4.4D, E). Most interestingly, the "translation inhibitors in chronically activated PDGFRA cells" pathway was enriched for with the lowest *p*-value ($p = 4.1 \times 10^{-6}$) from targets with increased antibody signal intensities. The full list of enriched pathways for each comparison can be found in

Appendix B. These findings highlight the deregulation of the translation initiation machinery (eIF4F complex) through the MAPK and PI3K/AKT/mTOR pathways in WT Ahi-1 cells, which may explain the increased resistance to TKI treatment in these cells.

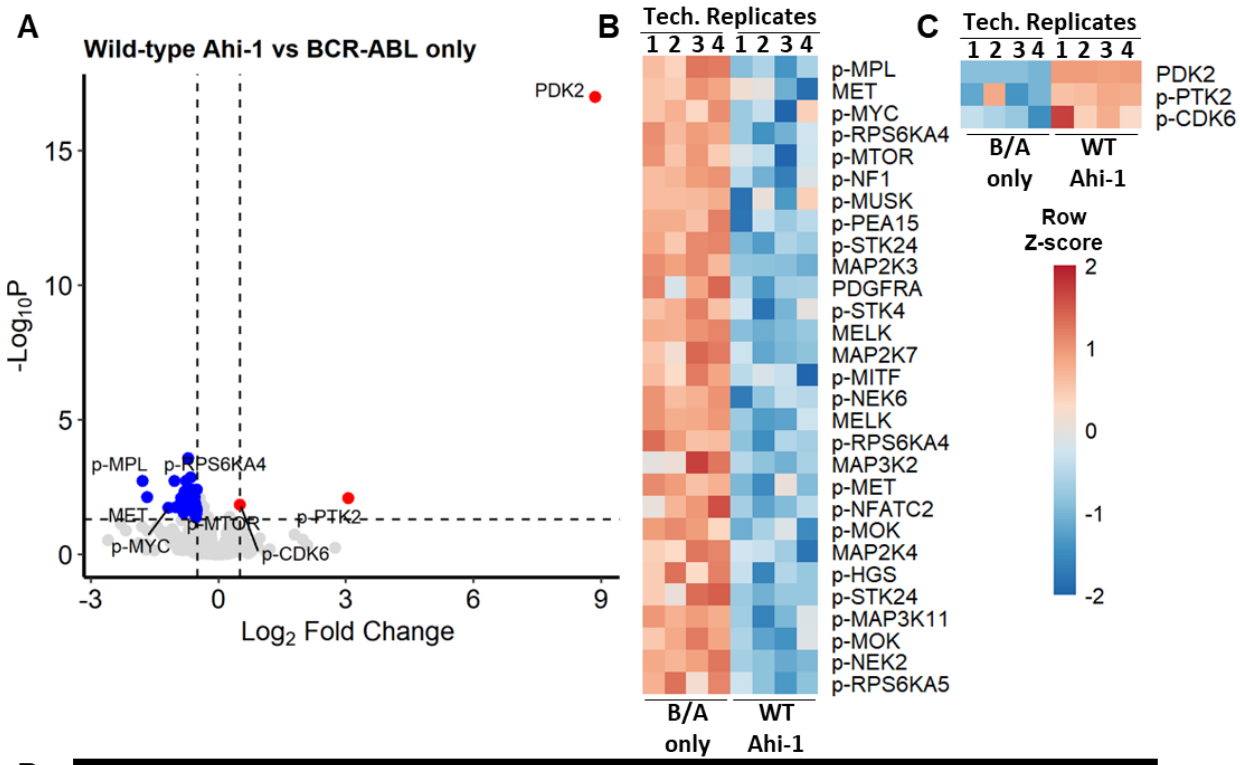

D

Selected Enriched Pathways for Decreases (Total: 77)			
Pathway Name	***p*-value**	**Pathway Size**	**Targets**
Regulation of Translation Initiation Complex (eIF4F Complex)			
Translation inhibitors in chronically activated PDGFRA cells	7.5E-08	45	6
MAPK Signaling (Total: 12)			
MAPK signaling pathway	6.9E-13	286	12
MAPK signaling pathway	4.7E-09	241	10
MAPK cascade	1.1E-04	33	4
Host-pathogen interaction of human coronaviruses - MAPK signaling	1.6E-04	36	4
MAP kinase activation	0.0018	63	4
MAPK family signaling cascades	0.0061	308	6
p38 MAPK signaling pathway	0.0081	34	3
Stress-activated MAPK cascade	0.011	239	5
RANKL/RANK signaling pathway	0.032	54	3
VEGFA-VEGFR2 signaling pathway	0.037	415	6
RAF/MAP kinase cascade	0.039	264	5
MAPK1/MAPK3 signaling	0.042	269	5
PI3K-AKT-mTOR Signaling (Total: 2)			
RANKL/RANK signaling pathway	0.032	54	3
VEGFA-VEGFR2 signaling pathway	0.037	415	6

E

Enriched Pathways for Increases (Total: 3)			
Pathway Name	***p*-value**	**Pathway Size**	**Targets**
Small cell lung cancer	0.0061	95	2
Small cell lung cancer	0.020	90	2
Regulation of cell-matrix adhesion	0.048	119	2

Figure 4.2: Changes in Antibody Signal Intensities in WT Ahi-1 Cells Compared to B/A Only Cells. (A) Volcano plot displaying significant changes ($p < 0.05$, $-0.5 < \log_2(\text{fold change}) < 0.5$) in antibody signal intensities. Heat maps of targets with decreased (B) or increased (C) signal intensity in WT Ahi-1 cells. Selected enriched pathway from decreased (D) or increased I targets in WT Ahi-1 cells with the total number of enriched pathways displayed at the top. For each enriched pathway, the *p*-value, number of proteins (Pathway size), and number of targets with significant differential antibody signal intensities (Targets) are displayed. The row z-scores were used to display changes in antibody signal intensities changes across the replicates.

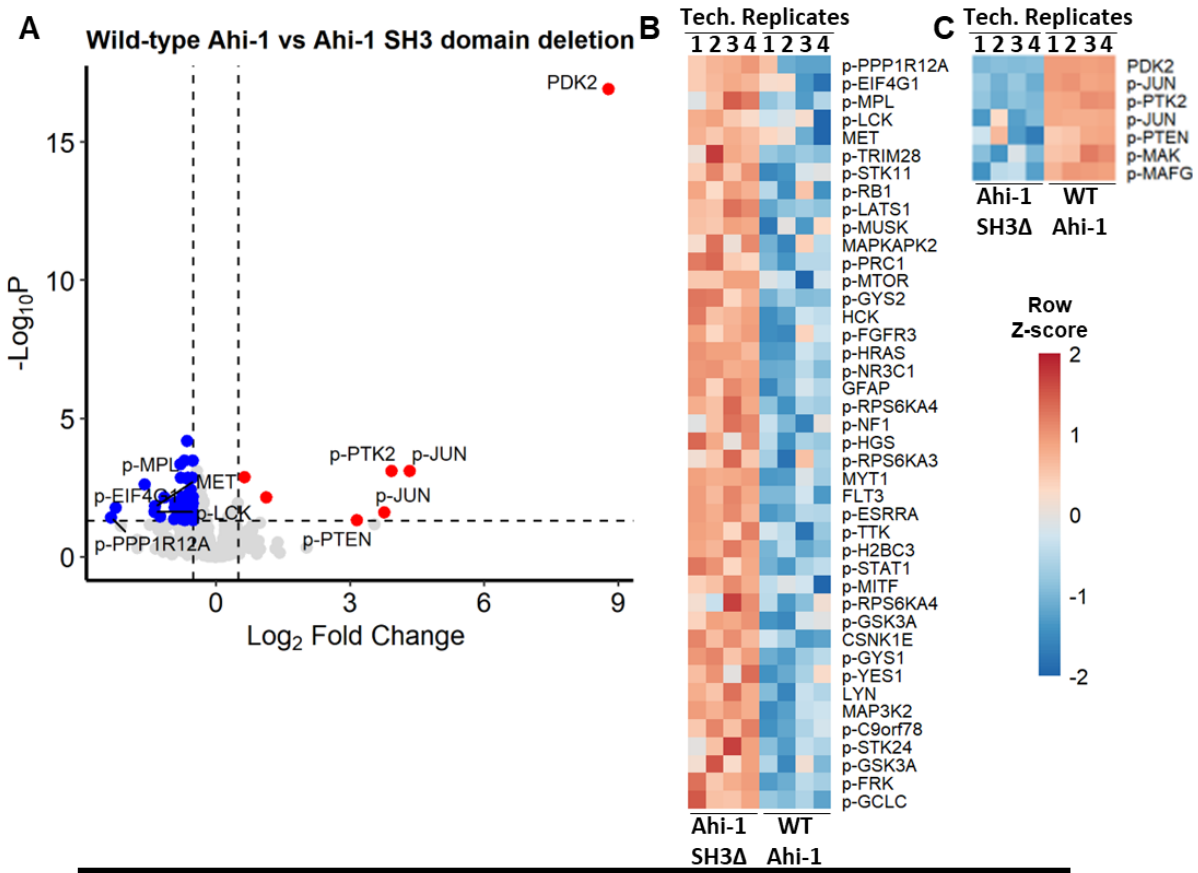

D

Selected Enriched Pathways for Decreases (Total: 85)			
Pathway Name	***p*-value**	**Pathway Size**	**Targets**
MAPK Signaling (Total: 6)			
Signaling by KIT in disease	5.9E-07	17	5
Thymic stromal lymphopoietin (TSLP) signaling pathway	4.8E-06	47	6
Signaling by SCF-KIT	5.2E-05	39	5
MAPK signaling pathway	9.2E-05	286	9
Regulation of MAP kinase activity	0.042	182	5
PI3K-AKT-mTOR Signaling (Total: 8)			
Signaling by KIT in disease	5.9E-07	17	5
Thymic stromal lymphopoietin (TSLP) signaling pathway	4.8E-06	47	6
PI3K-Akt signaling pathway	0.0035	342	8
AMP-activated protein kinase (AMPK) signaling	0.022	66	4
Focal adhesion: PI3K-Akt-mTOR-signaling pathway	0.027	295	7

E

Selected Enriched Pathways for Increases (Total: 23)			
Pathway Name	***p*-value**	**Pathway Size**	**Targets**
MAPK Signaling (Total: 2)			
EGF/EGFR signaling pathway	0.0074	159	3
RANKL/RANK signaling pathway	0.040	54	2
PI3K-AKT-mTOR Signaling (Total: 3)			
Focal adhesion	0.0033	192	3
EGF/EGFR signaling pathway	0.0074	159	3
RANKL/RANK signaling pathway	0.040	54	2

Figure 4.3: Changes in Antibody Signal Intensities in WT Ahi-1 Cells Compared to Ahi-1 SH3$^{\Delta}$ Cells. (A) Volcano plot displaying significant changes ($p < 0.05$, $-0.5 < \log_2$(fold change) < 0.5) in antibody signal intensities. Heat maps of targets with decreased (B) or increased (C) signal intensity in WT Ahi-1 cells. Selected enriched pathway from decreased (D) or increased I targets in WT Ahi-1 cells with the total number of enriched pathways displayed at the top. For each enriched pathway, the *p*-value, number of proteins (Pathway size), and number of targets with significant differential antibody signal intensities (Targets) are displayed. The row z-scores were used to display changes in antibody signal intensities changes across the replicates.

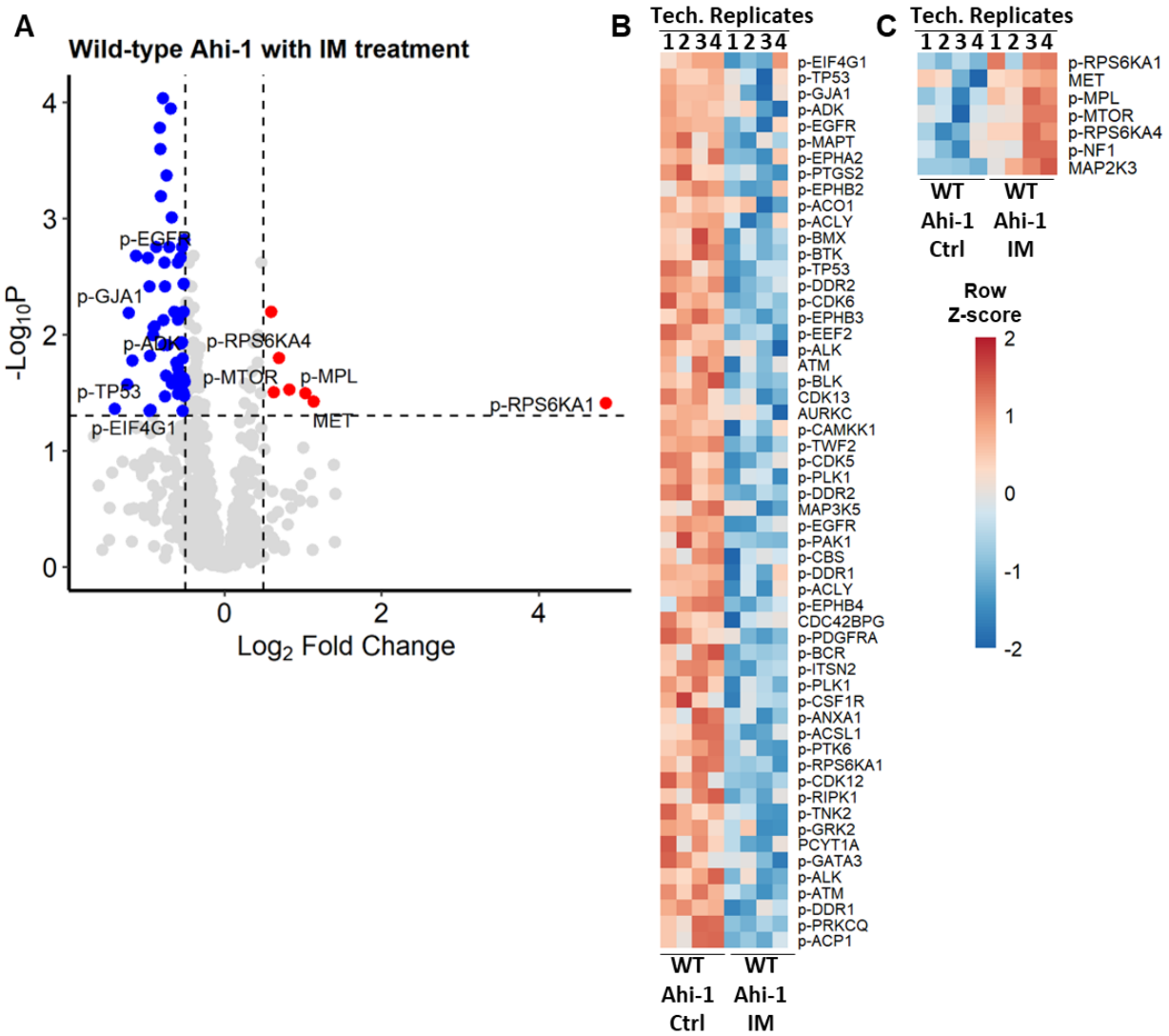

D Selected Enriched Pathways for Decreases (Total: 111)

Pathway Name	*p*-value	Pathway Size	Targets
MAPK Signaling (Total: 4)			
MAPK signaling pathway	3.2E-04	286	9
VEGFA-VEGFR2 signaling pathway	0.010	415	10
Positive regulation of MAPK cascade	0.019	479	8
EGF/EGFR signaling pathway	0.031	159	6
PI3K-AKT-mTOR Signaling (Total: 2)			
VEGFA-VEGFR2 signaling pathway	0.010	415	10
EGF/EGFR signaling pathway	0.031	159	6

E Selected Enriched Pathways for Increases (Total: 27)

Pathway Name	*p*-value	Pathway Size	Targets
Regulation of Translation Initiation Complex (eIF4F Complex)			
Translation inhibitors in chronically activated PDGFRA cells	4.1E-06	45	4
MAPK Signaling (Total: 2)			
MAPK signaling pathway	7.4E-05	286	5
Host-pathogen interaction of human coronaviruses - MAPK signaling	0.047	36	2

Figure 4.4: Changes in Antibody Signal Intensities in WT Ahi-1 Cells after IM treatment. (A) Volcano plot displaying significant changes ($p < 0.05$, $-0.5 < \log_2(\text{fold change}) < 0.5$) in antibody signal intensities. Heat maps of targets with decreased (B) or increased (C) signal intensity in WT Ahi-1 cells after IM treatment. Selected enriched pathway from decreased (D) or increased I targets in WT Ahi-1 cells after IM treatment with the total number of enriched pathways displayed at the top. For each enriched pathway, the *p*-value, number of proteins (Pathway size), and number of targets with significant differential antibody signal intensities (Targets) are displayed. The row z-scores were used to display changes in antibody signal intensities changes across the replicates.

Some of the targets with significant differential antibody signals in these enriched pathways were probed to validate the findings from the antibody microarray. The phosphorylation of mTOR at S2448, the protein-serine/threonine kinase in the mTORC complexes, was reduced in WT Ahi-1 cells compared to B/A only (0.9-fold) and Ahi-1 $SH3^{\Delta}$ cells (0.7-fold, Figure 4.5A). Furthermore, the Y576 and Y577 phosphorylation of PTK2, a non-receptor protein-tyrosine kinase which promotes the activation of the PI3K/AKT pathway, was increased in WT Ahi-1 cells compared to B/A only (2.2-fold) and Ahi-1 $SH3^{\Delta}$ cells (1.3-fold, Figure 4.5B). However, the S221 phosphorylation of RPS6KA1, a kinase downstream of the MAPK pathway that is involved in eIF4F complex regulation, and S1231 phosphorylation of eIF4G1, the scaffold protein of the eIF4F complex, did not match the significant antibody signal intensity changes observed from the antibody microarray (Figure 4.5C, D). Interestingly, the phosphorylation of eIF4G1 was instead increased in WT Ahi-1 cells compared to B/A only (1.9-fold) and Ahi-1 $SH3^{\Delta}$ cells (3-fold), which prompted for further investigation of the expression of eIF4F complex members, particularly, the protein level of eIF4G1 (Figure 4.5D).

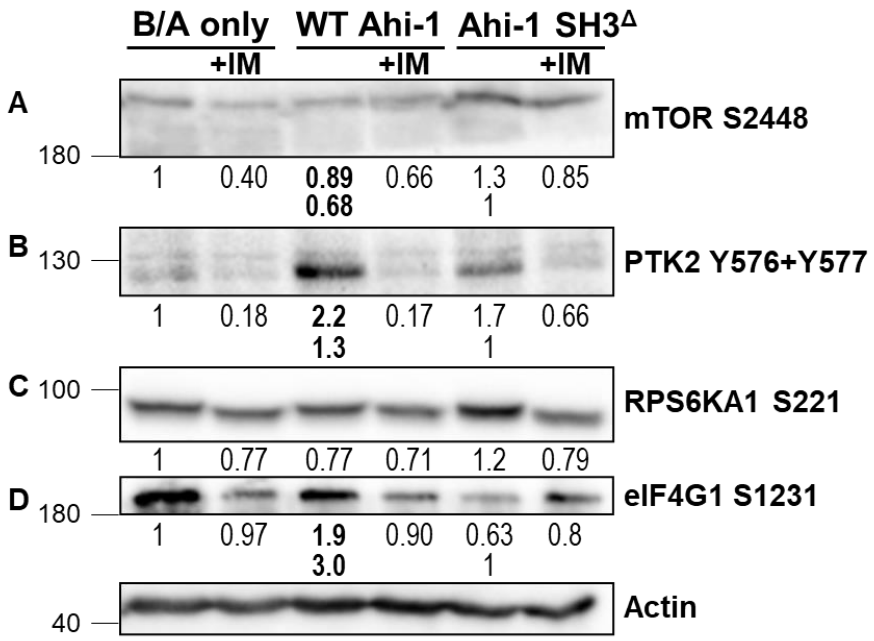

Figure 4.5: Validation of Targets with Significant Changes from Antibody Microarray. Immunoblots of several targets identified from antibody microarray analysis. Lysates of BCR-ABL1 only cells (B/A only), BCR-ABL1^{+} cells expressing wildtype Ahi-1 (WT Ahi-1) or SH3 domain deleted Ahi-1 (Ahi-1 SH3$^{\Delta}$) with or without 3-hour 5 µM IM treatment were used for an immunoblot to validate significant changes observed from antibody microarray analysis. The numbers displayed below each band represents the average relative expression to B/A only cells from three experiments. Additional numbers represent the average relative expression normalized to the condition indicated as 1. Bolded values are those referenced in the text. The blots shown are representative of those from two other independent experiments.

4.2.2 Transcript Levels and Protein Phosphorylation/Expression of Several eIF4F Complex Members are Increased in CD34^{+} CML Patient Cells and IM-Resistant Cells

Due to the observations of changes in the regulation of the translation initiation machinery from the pathway enrichment analysis of the antibody microarray and eIF4G1 phosphorylation changes in WT Ahi-1 cells, I first investigated whether the differential expression of eIF4F complex members could be observed in primitive CML patient cells compared to normal bone marrow, based on our RNA-sequencing dataset of CD34^{+} cells

obtained from 6 CML-CP patients at diagnosis and NBM of 3 healthy donors.[96] Interestingly, this analysis revealed elevated transcript levels of several eIF4F complex members in CML patients including *EIF4G1* (p = 0.0013), *EIF4A1* (p = 0.0019), and *EIF4BP1* (p = 0.0001, Figure 4.6), indicating that eIF4F complex expression is indeed demonstrated in CML stem/progenitor cells, which encouraged me to further study the molecular relevance of the eIF4F complex in regulation of TKI response/resistance in cell line models.

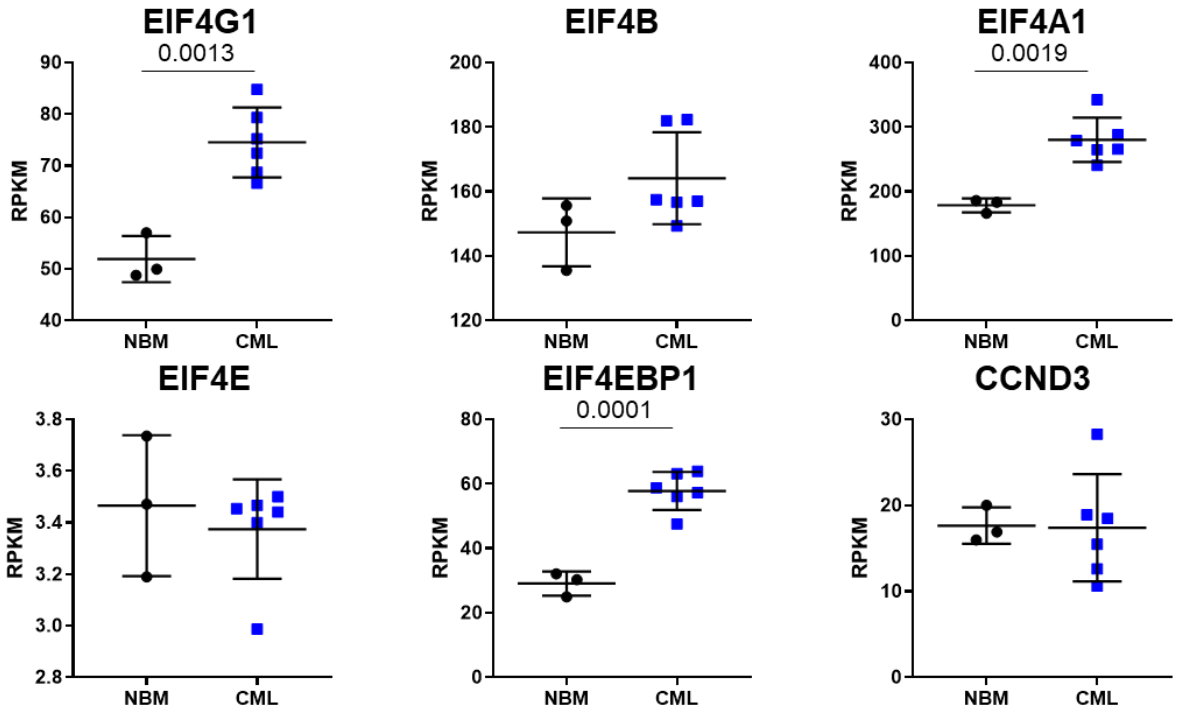

Figure 4.6: Differential Expression of eIF4F Complex Members in CD34$^+$ CML Patient Cells. RPKM values in CD34$^+$ cells from 3 normal bone marrow (NBM) samples and 6 CML patient samples from an RNA sequencing dataset with displayed p-values from two-tailed Student's t-test. Data shown are mean ± standard deviation.

To investigate differences in the protein expression of eIF4F complex members, two cell line models were used: the BaF3 model used in the antibody microarray and an IM-resistant CML cell line model (K562/K562R). Interestingly, WT Ahi-1 cells had a >2-fold increase (p = 0.044) in eIF4G1 S1231 phosphorylation and >2.7-fold increase in eIF4G1 protein expression,

while the IM-resistant K562R cells had 1.9-fold increase in S1231 phosphorylation with a 2.1-fold increase in eIF4G1 protein expression than parental K562 cells (Figure 4.7A, B). Additionally, both IM-resistant cells showed a 4.6-fold increase (p = 0.05, Figure 4.7C) in S422 phosphorylation, which induces eIF4F complex activity, with a >1.3-fold increase in eIF4B protein expression compared to the IM-sensitive cells (Figure 4.7D). Activation of eIF4B results in an increase in eIF4A helicase activity, but differences in eIF4A protein expression was not observed between IM-resistant and IM-sensitive cells (Figure 4.7E). Unexpectedly, a 0.6-fold reduction in the cap-binding protein, eIF4E, protein expression was observed in IM-resistant cells compared to IM-sensitive cells (Figure 4.7F). Furthermore, the hyperphosphorylation of eIF4E binding protein (4E-BP), which frees eIF4E to bind to 5'caps of mRNA transcripts, was increased in both WT Ahi-1 and IM-resistant cells, demonstrated by the increased intensity of the upper band (Figure 4.7G, H). The observation of increased expression and/or activation of these members of eIF4F complex indicates an overall increase in eIF4F complex activity in the IM-resistant cells. To test this, I also probed for the expression of cyclin D3, a gene reported to be sensitive to eIF4F complex activity and demonstrated an increase in cyclin D3 protein expression (4.3-fold, p = 0.019) in K562R cells compared to K562 cells supporting this statement (Figure 4.7I). These findings indicate that eIF4F complex members are highly activated in CML stem/progenitor cells or IM-resistant cells that may contribute to enhanced survival and reduced apoptosis of these cells.

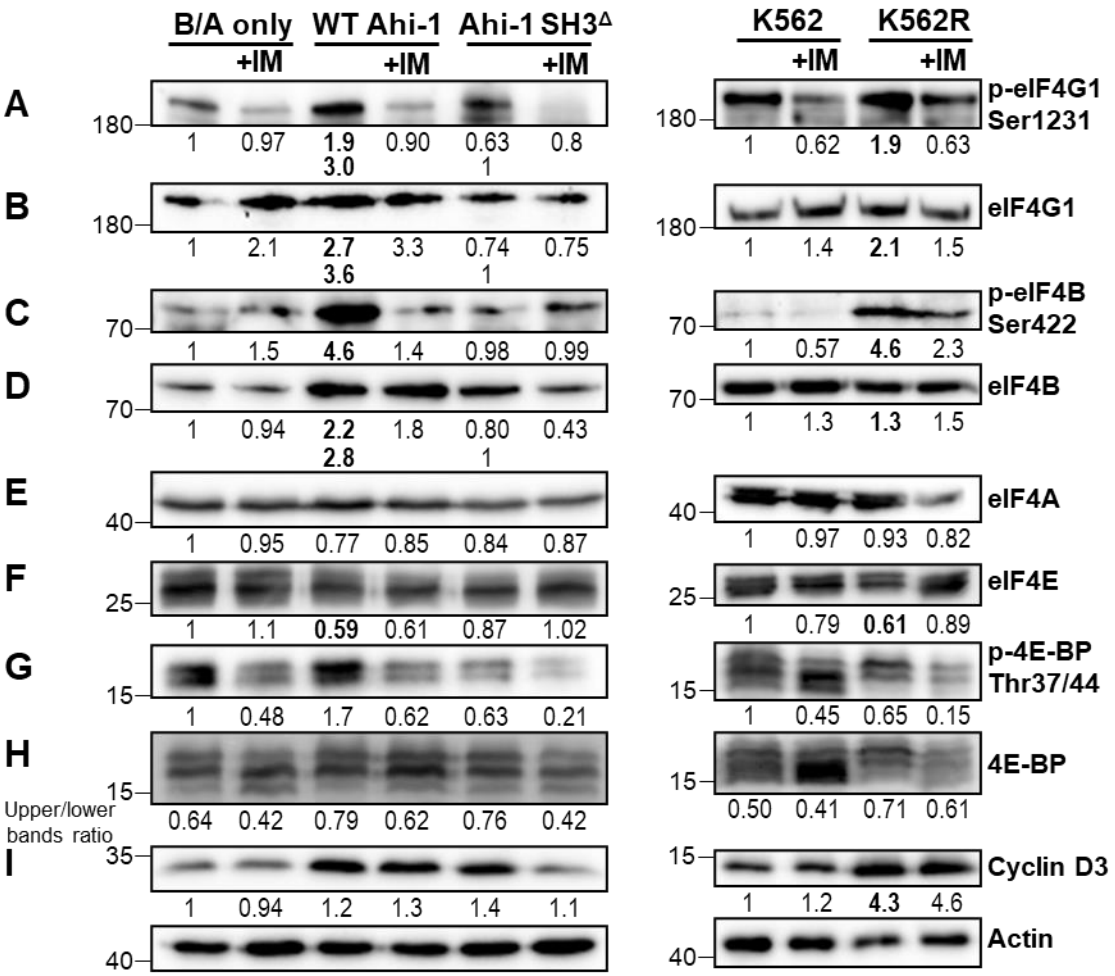

Figure 4.7: Protein and Phosphorylation Levels of Several eIF4F Complex Members are Elevated in IM-Resistant Cells. Immunoblots of eIF4F complex members in Ba/F3 cell line model and K562 and IM-resistant K562R cells with or without 5 µM IM treatment for 3 hours. Displayed values under each band represent the average relative expression to B/A only or K562 cells, except for 4E-BP (H) which is the average ratio of intensities of the hyperphosphorylated upper band to the phosphorylated/non-phosphorylated lower bands from three experiments. Additional numbers represent the average relative expression normalized to the condition indicated as 1. Bolded values are those referenced in the text. The blots shown are representative of those from two other independent experiments.

4.2.3 Lentiviral-Mediated Suppression of eIF4G1 by shRNA Impairs Cell Proliferation, Apoptosis, TKI Response, and eIF4F Complex Activity in IM-Resistant Cells

Due to the observations of increased eIF4G1 phosphorylation and protein expression in K562R cells, the effects of eIF4G1 knockdown on IM sensitivity and eIF4F complex activity were investigated using a short hairpin RNA (shRNA) approach. The transduction of K562 and K562R cells using two shRNAs that targeted the coding region of eIF4G1 resulted in the reduction of eIF4G1 levels (87%, 61%, for shRNA A, B in K562, 94%, 77% for shRNA A, B in K562R, $p < 0.042$, Figure 4.8A, B). Knockdown of eIF4G1 from both shRNAs significantly impaired survival of K562 and K562R cells ($p < 0.019$) at 48 and 72 hours (Figure 4.8C, D). Furthermore, K562R cells with eIF4G1 knockdown displayed increased sensitivity to IM treatment ($p < 0.0021$, Figure 4.8F) but not in K562 cells (Figure 4.8E). Apoptosis was also induced in K562 cells with eIF4G1 knockdown ($p < 0.038$) but not statistical significantly increased in K562R cells (Figure 4.8G, H). Observing these interesting biological effects of the eIF4G1 knockdown, I then investigated the changes in eIF4F complex activity.

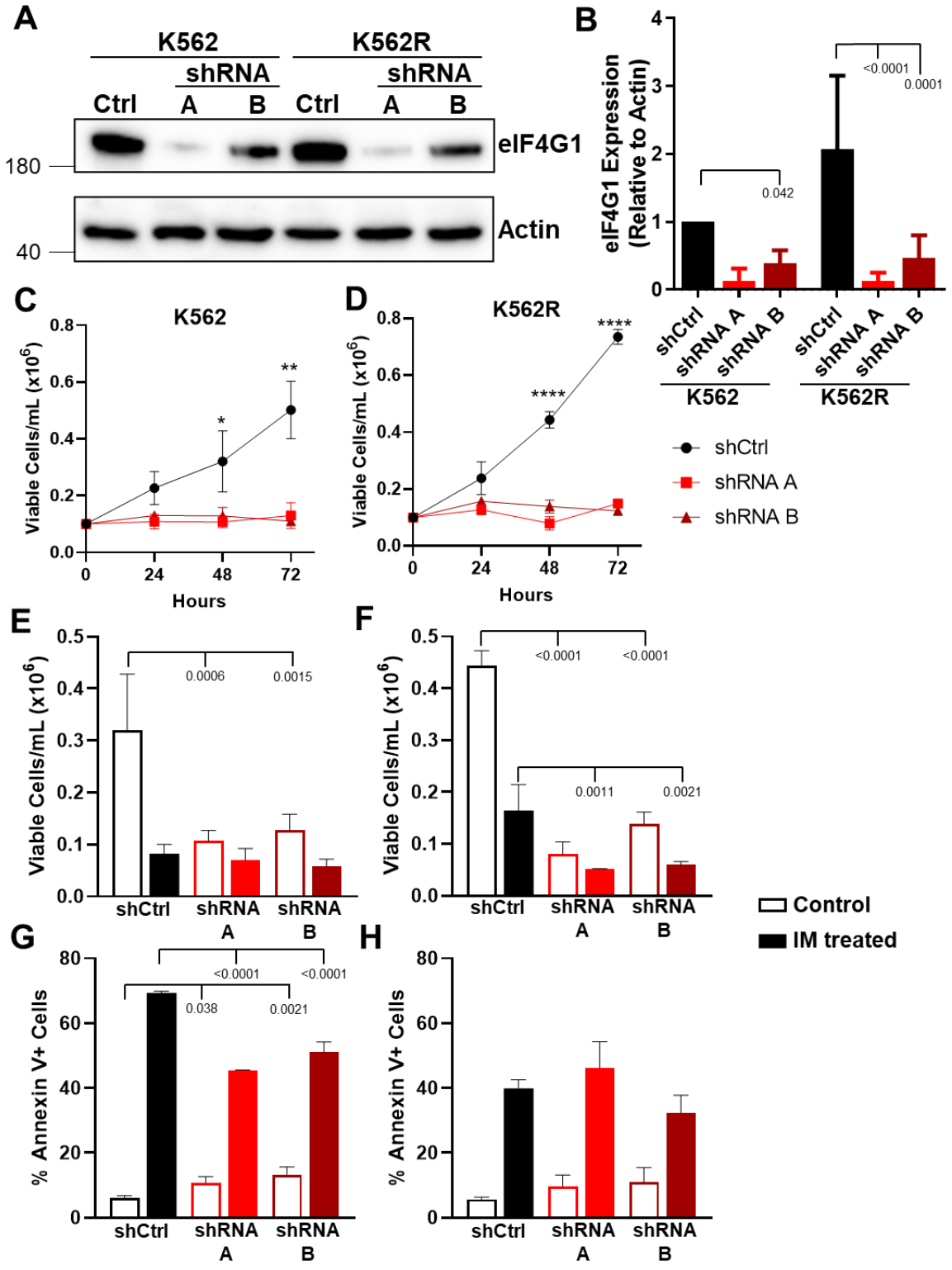
A
K562
K562R
shRNA
Ctrl
A
B
Ctrl
A
B
eIF4G1
Actin
180
40
B
eIF4G1 Expression (Relative to Actin)
<0.0001
0.0001
0.042
shCtrl
shRNA A
shRNA B
K562
K562R
C
K562
Viable Cells/mL (x10^6)
Hours
D
K562R
shCtrl
shRNA A
shRNA B
E
0.0006
0.0015
F
<0.0001
<0.0001
0.0011
0.0021
Control
IM treated
G
% Annexin V+ Cells
<0.0001
<0.0001
0.038
0.0021
H

Figure 4.8: The Effect of eIF4G1 Knockdown on Cell Proliferation, IM Sensitivity, and Apoptosis. (A) Immunoblot of eIF4G1 expression in K562/K562R cells transduced with lentivirus containing a scrambled control (Ctrl), or shRNAs targeting eIF4G1. (B) Densitometry of relative eIF4G1 protein expression to K562/K562R cells expressing the scrambled control (shCtrl) from five independent experiments of (A). Growth curves of K562 (C) or K562R (D) cells expressing shCtrl or shRNAs targeting eIF4G1. Cell counts of K562 (E) or K562R (F) cells expressing shCtrl or shRNAs targeting eIF4G1 with or without IM (K562 = 0.5 µM or K562R = 5 µM) after 48 hours. Apoptosis assays were performed in K562 (G) or K562R (H) cells using the same treatments. Data shown are mean ± standard deviation. *P*-values shown are calculated from Šídák's multiple comparisons tests after a one-way ANOVA was performed from three independent experiments. (*$p < 0.05$, ** $p < 0.01$, *** $p < 0.001$, ****$p < 0.0001$)

To assay the activity of the eIF4F complex, the proximity ligation assay was used to measure the level of eIF4F complex assembly through the interaction between eIF4G1 and eIF4E, which is an important step in forming the eIF4F complex. K562R cells transduced with the scrambled control displayed a reduction in PLA foci formation compared to K562 cells transduced with the scrambled control ($p = 0.0021$, Figure 4.9A, B). Furthermore, K562 and K562R cells with both shRNAs targeting eIF4G1 showed reduced levels of PLA foci formation compared to control indicating a reduction in eIF4F complex formation ($p < 0.013$, Figure 4.9A, B). After demonstrating a reduction in the assembly of the eIF4F complex, I examined the protein expression of several eIF4E-sensitive genes. In the knockdown cells, I observed a reduction in the protein expression of cyclin D3 ($p < 0.01$), MDM2, and MCL1 ($p < 0.026$, Figure 4.9C). Most interestingly, cells transduced with the eIF4G1 shRNA construct A, with >90% suppression of eIF4G1 targeting, greatly reduced the protein expression of BCR-ABL1 (70% reduction, Figure 4.9C). These findings demonstrate that eIF4G1 plays an integral role in the translation of several key genes, particularly *BCR-ABL1*, and pharmaceutical inhibition of eIF4G1 may have a synergistic effect with TKI in CML cells.

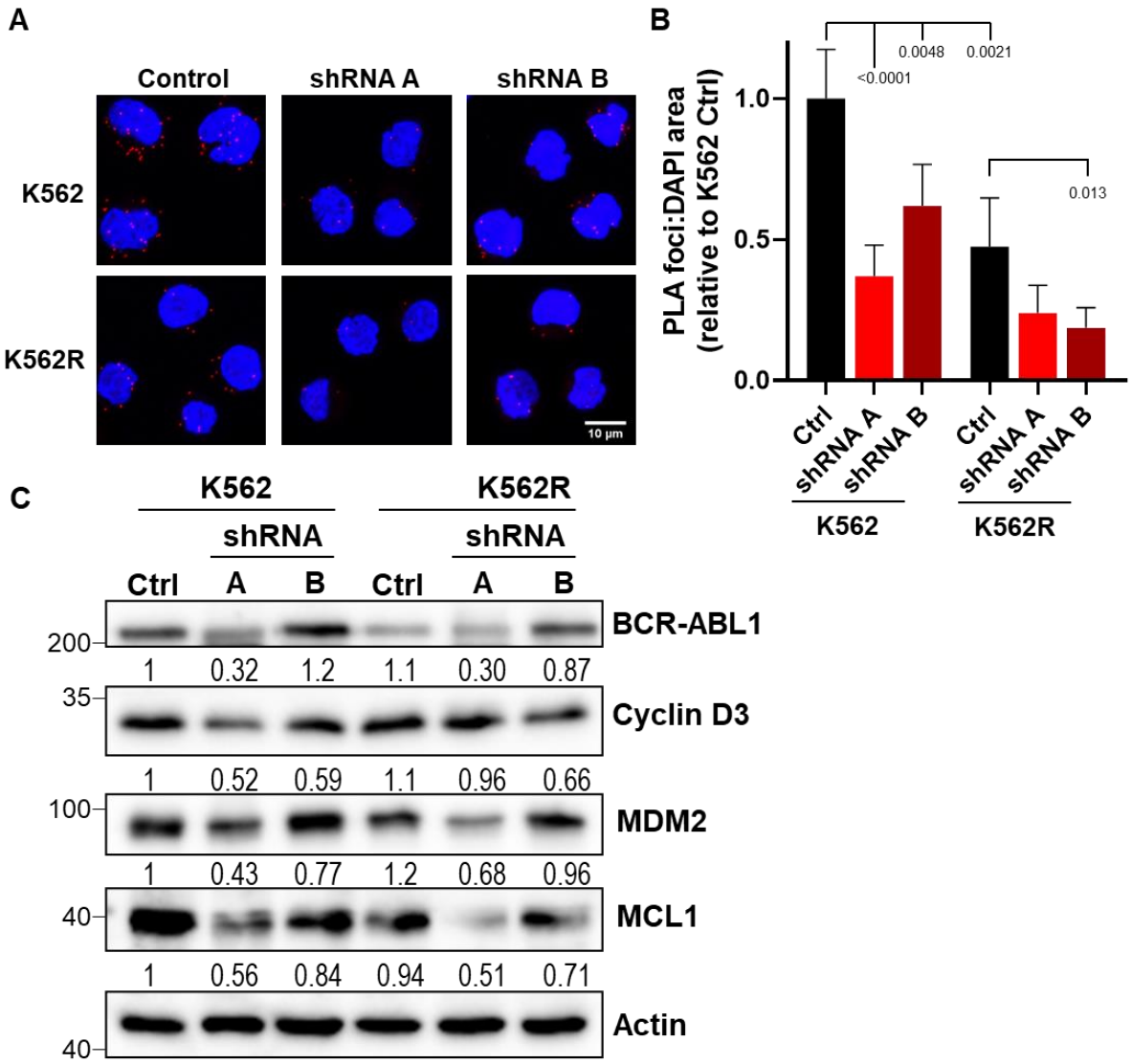

Figure 4.9: The Effect of eIF4G1 Knockdown on eIF4F Complex Assembly and the Expression of eIF4E-Sensitive Genes. (A) Confocal images of K562/K562R cells expressing control or eIF4G1 targeting shRNAs with PLA foci (red) and DAPI (blue) staining. (B) Quantification of the ratio between PLA foci and DAPI area relative to K562 with the scrambled control of three independent experiments from three separate field of views containing at least 30 cells each. Data shown are mean ± standard deviation. *P*-values shown are calculated from Šídák's multiple comparisons tests after a one-way ANOVA was performed. (C) Immunoblots of BCR-ABL1 and several eIF4E-sensitive genes. Displayed values under each band represents the average relative expression to K562 cells with the control shRNA from three experiments. The blots shown are representative of those from two other independent experiments.

4.2.4 The eIF4G1 Inhibitor SBI-756 Reduces Cell Survival and Enhanced IM-Sensitivity of CML Cells

To investigate the effects of pharmaceutical inhibition of eIF4G1 in CML cells, a selective, small molecule inhibitor, SBI-756, was used to target eIF4G1 to mimic the effects of eIF4G1 knockdown. SBI-756 specifically binds to eIF4G1 to prevent the binding of eIF4E, which prevents disrupts the assembly of the eIF4F complex.[230] First, the half maximal inhibitory concentration (IC_{50}) was determined in BCR-ABL1^{+} BaF3 cell lines expressing the different Ahi-1. Although the differences in the IC_{50} were small between the cell lines, the Ahi-1 SH3$^{\Delta}$ cells was the most sensitive to the compound (IC_{50} = 233 nM, 95% confidence interval (CI) = 160 – 318 nM), then WT Ahi-1 cells (IC_{50} = 315 nM, 95% CI = 260 – 374 nM), and the most resistant was the B/A only cells (IC_{50} = 480 nM, 95% CI = 356 – 608 nM, Figure 4.10A). After determining the IC_{50}, 300 nM of SBI-756 was used to treat these cells in combination with 500 nM of IM. A statistically significant decrease in proliferation after 48 hours of SBI-756 treatment was observed in WT Ahi-1 cells (p = 0.001) and Ahi-1 SH3$^{\Delta}$ cells (p = 0.032) but not for B/A only cells (Figure 4.10B). Although an additive effect was observed with the combination treatment in all three cell lines, it was not statistically significant. Furthermore, there was small but statistically insignificant increase in apoptotic cells after 48 hours of SBI-756 treatment in all three cell lines (Figure 4.10C). However, the combination of SBI-756 with IM significantly increased apoptotic cells in B/A only cells compared to either treatment alone and also in Ahi-1 SH3$^{\Delta}$ cells compared to SBI-756 single treatment (Figure 4.10C).

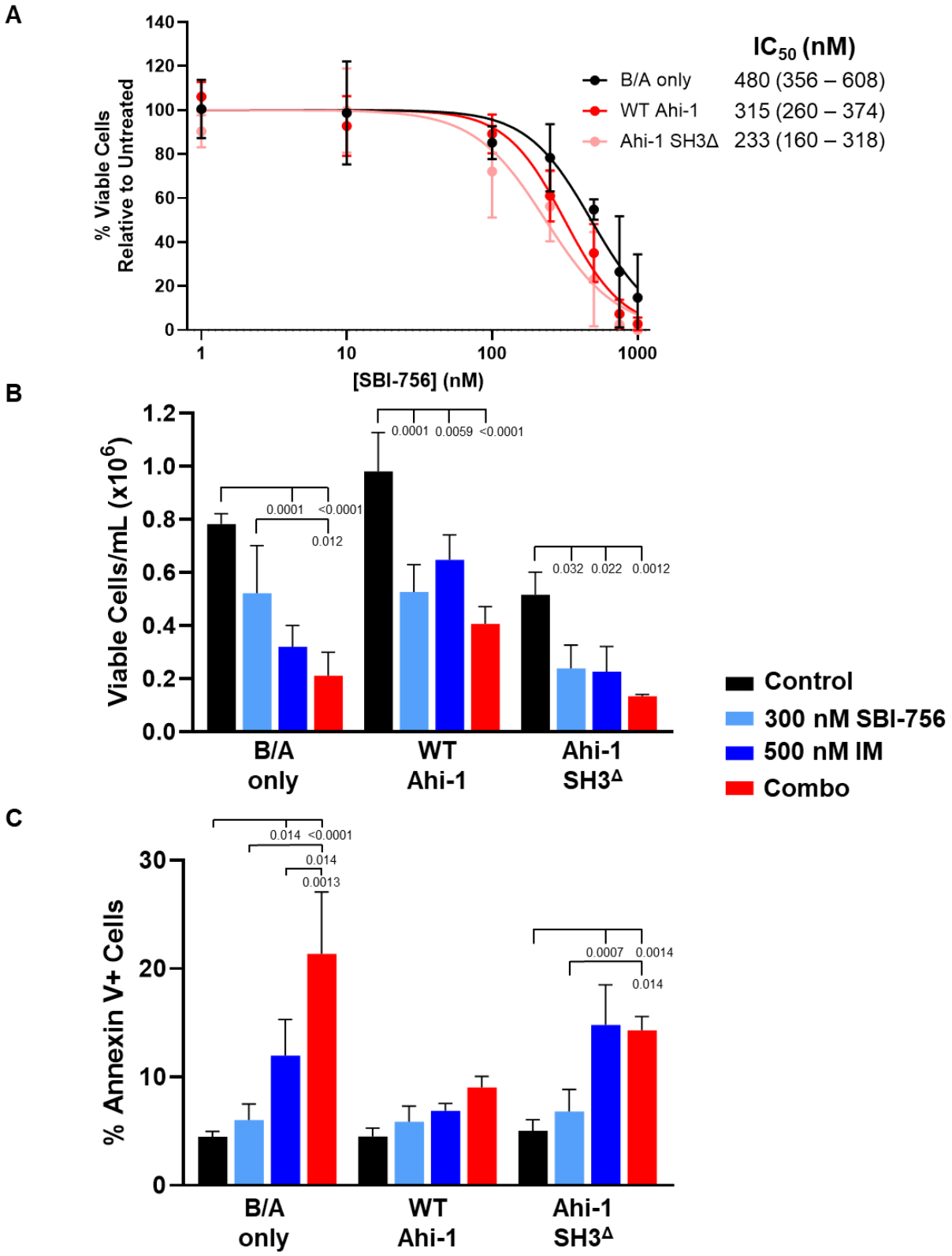
A
% Viable Cells Relative to Untreated
[SBI-756] (nM)
IC50 (nM)
B/A only 480 (356 – 608)
WT Ahi-1 315 (260 – 374)
Ahi-1 SH3Δ 233 (160 – 318)
B
Viable Cells/mL (x10^6)
0.0001 <0.0001
0.012
0.0001 0.0059 <0.0001
0.032 0.022 0.0012
B/A only
WT Ahi-1
Ahi-1 SH3Δ
Control
300 nM SBI-756
500 nM IM
Combo
C
% Annexin V+ Cells
0.014 <0.0001
0.014
0.0013
0.0007 0.0014
0.014
B/A only
WT Ahi-1
Ahi-1 SH3Δ

Figure 4.10: The Effect of SBI-756 Treatment in the Ba/F3 Cell Line Model on Cell Proliferation, IM Sensitivity, and Apoptosis. (A) IC_{50} curves from SBI-756 treatment after 48 hours. IC_{50} values are displayed with the 95% confidence interval in parentheses. Cell counts (B) or apoptosis (C) of B/A only, WT Ahi-1, and Ahi-1 $SH3^{\Delta}$ cells with 300 nM SBI-756, 500 nM IM, or combination treatment after 48 hours. Data shown are mean ± standard deviation. *P*-values shown are calculated from Šídák's multiple comparisons tests after a one-way ANOVA was performed from three independent experiments.

Next, I observed that IM-resistant K562R cells were more sensitive to SBI-756 treatment (IC50 = 667 nM, 95% CI = 505 – 868 nM) than parental K562 cells (IC50 = 892 nM, 95% CI = 770 – 1020 nM, Figure 4.11A). Although the difference in IC_{50} values were minimal, 48-hour SBI-756 treatment was able to reduce the growth of K562R cells with 500 nM (p = 0.0055) and 750 nM (p = 0.0001) but was not statistically significant in K562 cells (Figure 4.11B, C). Additionally, SBI-756 treatment sensitized K562R cells to IM treatment (p = 0.018) and was also reflected with an increase in apoptotic cells (p = 0.0185) but was not observed in K562 cells (Figure 4.11B-E). These findings demonstrate that K562R cells are more sensitive to SBI-756 treatment and can sensitize these resistant cells to IM treatment.

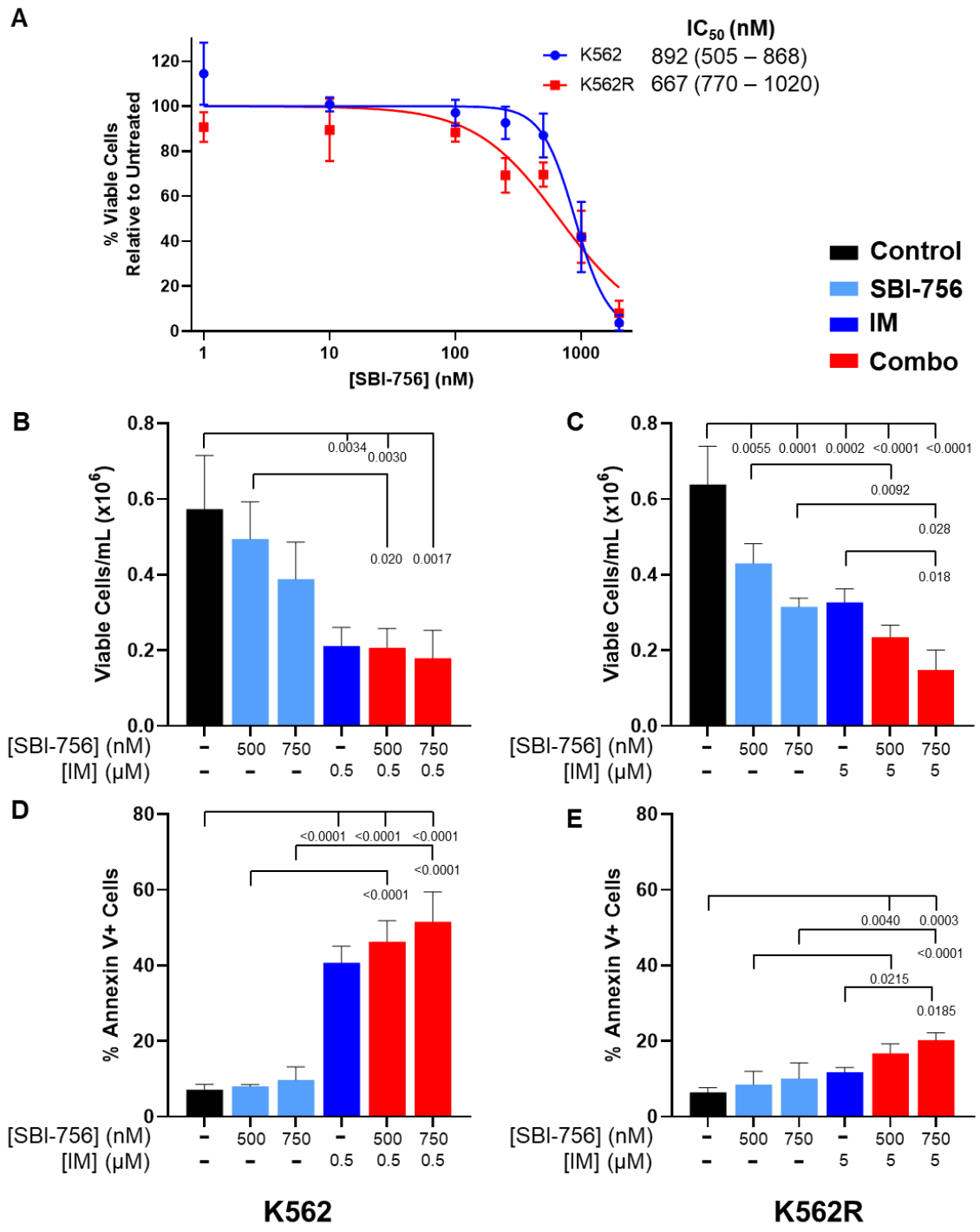

Figure 4.11: The Effect of SBI-756 Treatment in K562/K562R Cells on Cell Proliferation, IM Sensitivity, and Apoptosis. (A) IC_{50} curves from SBI-756 treatment after 48 hours. IC_{50} values are displayed with the 95% confidence interval in parentheses. Cell counts were performed in K562 (B) and K562R (C) cells with the indicated concentrations of SBI-756 and/or IM. Apoptosis assays in K562 (D) or K562R (E) cells were also performed using the same

treatments. Data shown are mean ± standard deviation. *P*-values shown are calculated from Šídák's multiple comparisons tests after a one-way ANOVA was performed from three independent experiments.

4.2.5 The eIF4G1 Inhibitor SBI-756 Reduces eIF4F Complex Activity and the Protein Translation Process in IM-Resistant Cells

To study the molecular mechanisms of the observed biological effects of SBI-756, a PLA assay was used again to determine if SBI-756 can disrupt the interaction between eIF4G1 and eIF4E in the K562 cell line model. A reduced level of PLA foci formation was observed using 5 µM SBI-756 in K562 treatment ($p < 0.0001$) and K562R ($p = 0.014$) cells (Figure 4.12A, B). Interestingly, 5 µM IM treatment also reduced PLA foci in K562R cells ($p = 0.0037$) and in combination with SBI-756 treatment further reduced PLA foci formation ($p < 0.023$), but this was not observed using a combination of 5 µM SBI-756 and 0.5 µM IM in K562 cells (Figure 4.12A, B).

To further assay the activity of eIF4F complex involved in the translation process, an o-propargyl-puromycin (OPP) assay was used to measure the global protein synthesis rate. SBI-756 treatment reduced the OPP MFI in both K562 and K562R cells ($p < 0.0001$), which confirmed a reduction of the translation process by SBI-756 treatment. Furthermore, IM treatment significantly reduced the protein synthesis rate in K562 cells ($p = 0.0017$), but not in K562R cells, and the combination of SBI-756 and IM further reduced the protein synthesis rate in both cell lines (Figure 4.12C, D).

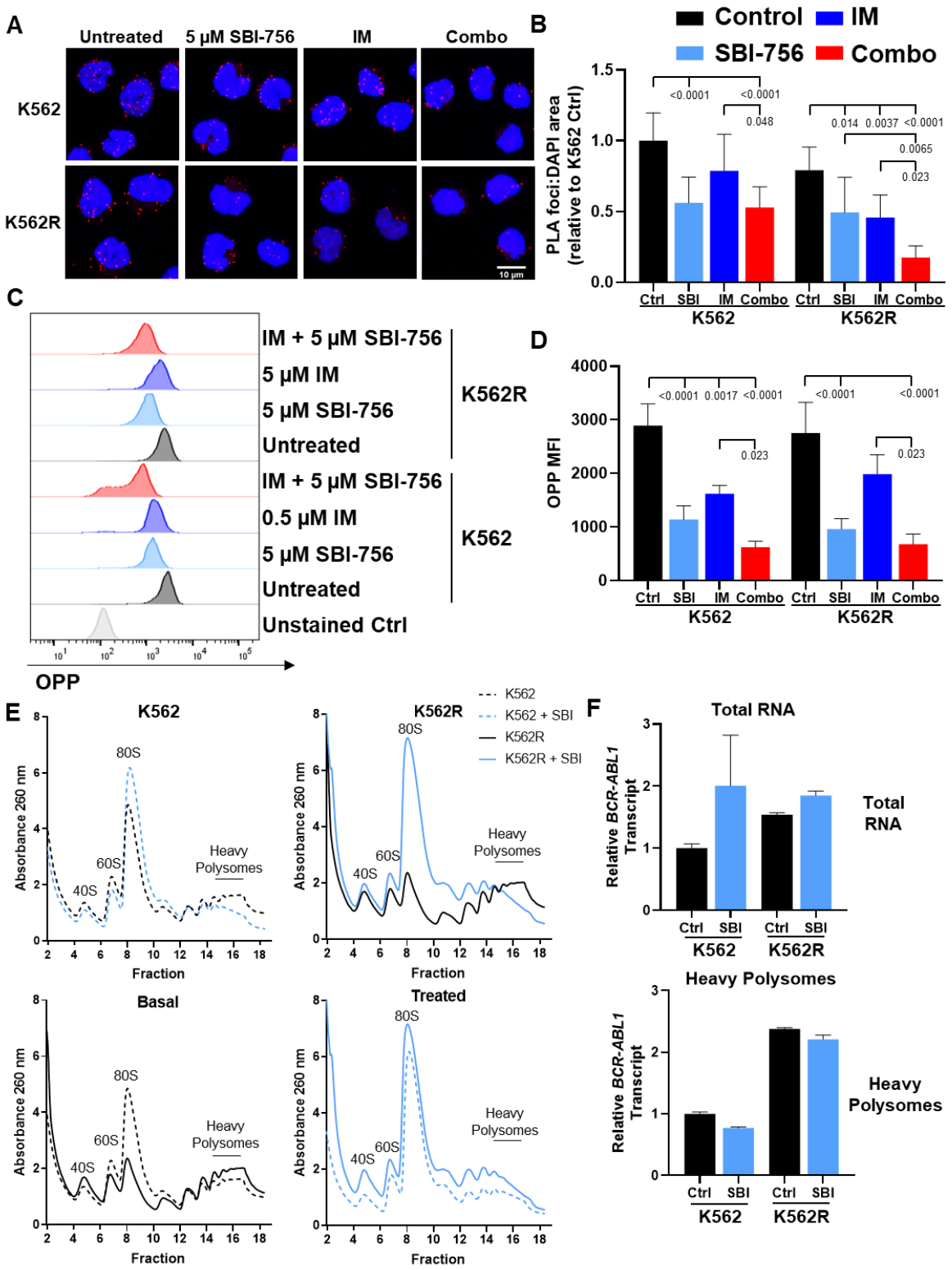
A
Untreated
5 μM SBI-756
IM
Combo
K562
K562R
10 μm
B
Control
IM
SBI-756
Combo
PLA foci:DAPI area (relative to K562 Ctrl)
<0.0001
<0.0001
0.048
0.014
0.0037
<0.0001
0.0065
0.023
Ctrl
SBI
IM
Combo
K562
K562R
C
IM + 5 μM SBI-756
5 μM IM
5 μM SBI-756
Untreated
K562R
IM + 5 μM SBI-756
0.5 μM IM
5 μM SBI-756
Untreated
Unstained Ctrl
K562
OPP
D
OPP MFI
<0.0001
0.0017
<0.0001
0.023
<0.0001
<0.0001
0.023
Ctrl
SBI
IM
Combo
K562
K562R
E
K562
K562R
K562
K562 + SBI
K562R
K562R + SBI
Absorbance 260 nm
Fraction
40S
60S
80S
Heavy Polysomes
Basal
Treated
F
Total RNA
Relative BCR-ABL1 Transcript
Ctrl
SBI
K562
K562R
Heavy Polysomes

Figure 4.12: The Effect of SBI-756 Treatment on eIF4F Complex Assembly, Protein Synthesis Rates, and Translation. (A) Confocal images of K562/K562R cells with 1-hour 5 µM SBI-756 treatment and/or 18-hour 5 µM IM treatment with PLA foci (red) and DAPI (blue) staining. (B) Quantification of the ratio between PLA foci and DAPI area relative to K562 control of three independent experiments from three separate field of views containing at least 30 cells each. (C) Histogram of OPP signals from K562/K562R cells with the same treatments. (D) Plot of the mean fluorescent intensity of OPP signals from three independent experiments. Data shown are mean ± standard deviation. *P*-values shown are calculated from Šídák's multiple comparisons tests after a one-way ANOVA was performed. (E) Polysome profiles of K562 (dashed line)/K562R (filled line) in the absence (black) or presence of SBI-756 (blue). (F) Relative *BCR-ABL1* transcript levels in K562/K56R cells with or without SBI-756 treatment in total RNA (top) or fractions containing heavy polysomes (bottom). Data shown are mean of duplicate values ± standard deviation from a single experiment.

Next, to analyze the level of translation initiation that can be affected by SBI-756 treatment in IM-resistant cells, especially if it directly inhibits the translation of *BCR-ABL1* transcripts in these cells, polysome profiling analysis was then performed. K562R cells had a higher absorbance in the fractions containing heavy polysomes and smaller 80S peak than K562 cells which is indicative of higher global translational levels (Figure 4.12E, bottom left). Following SBI-756 treatment, the absorbances of fractions containing heavy polysomes were reduced with an increase in 80S peak in both cell lines, but this effect was more dramatic in K562R cells. This increase in the 80S peak represents an accumulation of 80S monosomes due to blocked translation initiation and preventing the formation of polysomes, which supports SBI-756 as a translation initiation inhibitor. These findings may explain the increased sensitivity for SBI-756 treatment in the K562R cells. Following the polysome fractionation, qPCR was performed to analyze *BCR-ABL1* transcript levels from total RNA or in fractions containing heavy polysomes (as defined in Section 2.4.5 and Figure 2.1) and observe the changes after SBI-756 treatment. In total RNA samples, *BCR-ABL1* transcript levels were higher in K562R cells than K562 cells and SBI-756 treated cells appeared to have higher levels of *BCR-ABL1* transcript levels (Figure 4.12F, top). Interestingly, *BCR-ABL1* transcript levels were further increased in

K562R cells in heavy polysomes compared to total RNA, indicating *BCR-ABL1* transcripts are more actively translated in K562R cells (Figure 4.12F, bottom). Furthermore, SBI-756 treatment slightly reduced the *BCR-ABL1* transcript levels in the fractions containing heavy polysomes in both cells, indicating a decrease in translation of *BCR-ABL1* transcript after SBI-756 treatment. However, additional experiments to optimize these experimental conditions and inclusion of IM to this assay are still needed.

Finally, to further analyze the effects of SBI-756 treatment on the protein expression of BCR-ABL1 and several eIF4E-sensitive genes in K562/K562R cells, western blot analysis was performed. Interestingly, BCR-ABL1 expression was reduced upon SBI-756 treatment in both K562 and K562R cells (approximately 0.3-fold, Figure 4.13A). Of the eIF4E-sensitive genes, cyclin D3 expression was obviously reduced after SBI-756 treatment in K562 (0.5-fold) and K562R cells (0.4-fold) and a combination of SBI-756 and IM reduced expression of MDM2 and MCL1, but not SBI-756 or IM alone (Figure 4.13A). To dissect the mechanisms of BCR-ABL1 and cyclin D3 protein expression reduction after SBI-756 treatment in a specific process of translation, cycloheximide (CHX) and MG132 treatments were performed in K562R cells in the presence or absence of SBI-756 over the span of two hours. BCR-ABL1 levels were relatively steady during CHX treatment but were greatly reduced in the presence of SBI-756 (Figure 4.13B). However, cyclin D3 levels were reduced in the presence of CHX alone as well as in combination with SBI-756 treatment. These results indicate that reduction in BCR-ABL1 is due to inhibition of the eIF4F complex, which is the initiation step of translation, whereas CHX inhibits the elongation step of translation, which occurs after. Next, K562R cells were treated with MG132, a proteasome inhibitor, with or without SBI-756 treatment over a span of two hours to determine if protein expression reduction is a result of degradation by the proteasome.

BCR-ABL1 protein levels were reduced with MG132 treatment, but there was an accelerated reduction in combination of SBI-756 treatment (Figure 4.13C). Cyclin D3 levels were steady throughout these treatments. These results indicate that BCR-ABL1 protein level reduction is independent of the proteasomal degradation, but it is indeed interesting to observe BCR-ABL1 protein expression reduction upon eIF4G1 inhibition by SBI-756. These findings support potential treatment strategy by targeting BCR-ABL1 through the inhibition of eIF4F complex in drug-resistant CML cells.

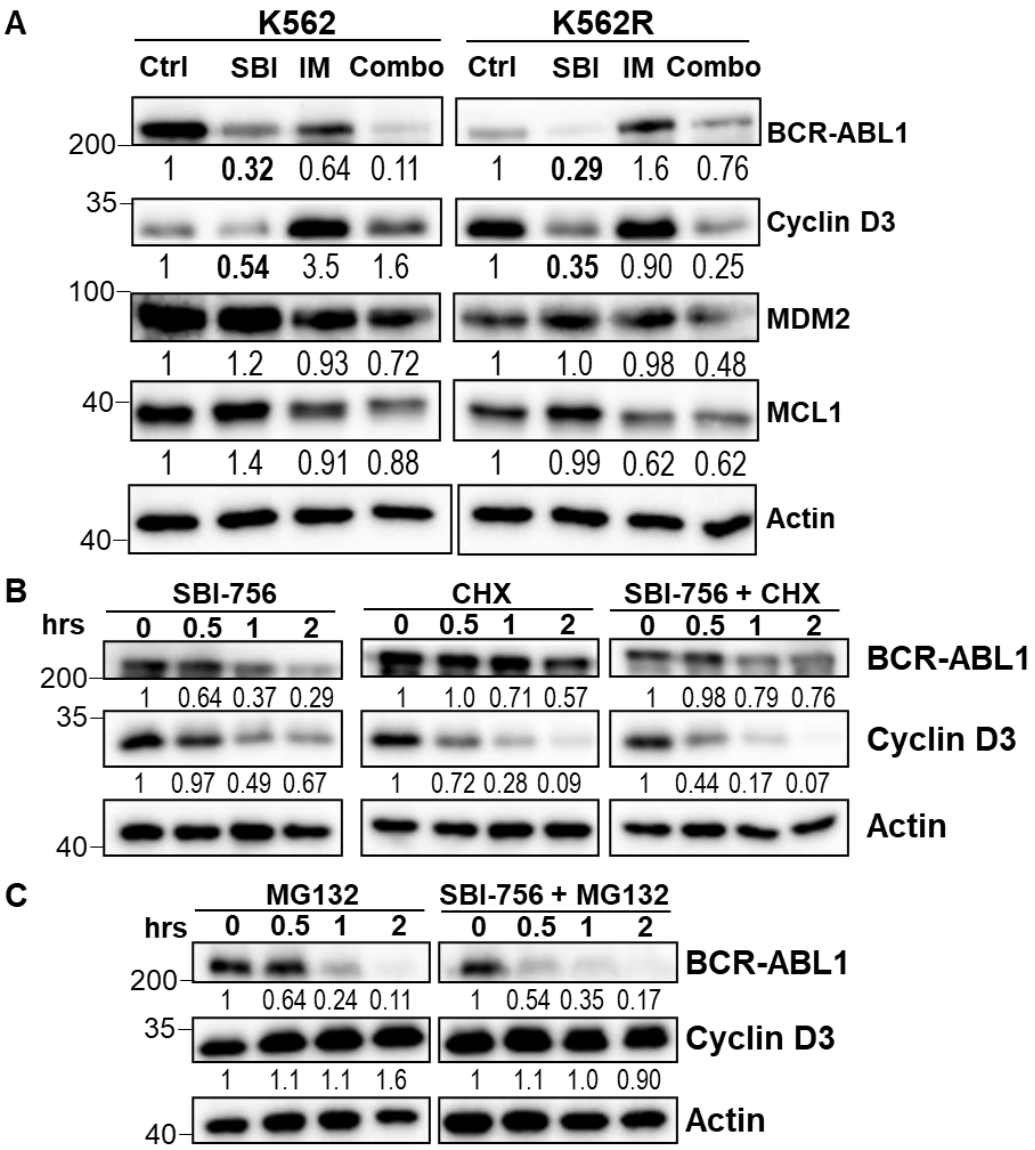

Figure 4.13: The Effect of SBI-756 Treatment on BCR-ABL1 and Several eIF4E-Sensitive Genes. (A) Immunoblots of BCR-ABL1 and several eIF4E-sensitive genes in K562/K562R cells treated with 1 hour of 5 µM SBI-756 and/or 18 hours of 0.5/5 µM IM. Numbers below each band represent the average relative expression to control from two experiments. Bolded values are referenced in the text. The blots shown are representative of those from one other experiment. (B) Immunoblots of K562R cells treated with 5 µM SBI-756, 100 µg/mL cycloheximide (CHX), or a combination over 2 hours. (C) Immunoblots of K562R cells treated with 10 µM MG132 with or without 5 µM SBI-756 over 2 hours. Numbers below each band represent the average relative expression to the start of the experiment (0 hours) from two experiments. The blots shown are representative of those from one other experiment.

4.3 Discussion

In this study, decreased expression and/or phosphorylation of proteins involved in the regulation of the translation initiation machinery, the eIF4F complex, was identified in BCR-ABL1$^+$ cells co-expressing wildtype Ahi-1 using an antibody microarray analysis. This finding was further supported by the enrichment of the MAPK and PI3K/AKT pathways from targets with decreased antibody signals, since these pathways are integral parts of eIF4F complex-mediated network.[150,180] Although the antibody microarray revealed that the WT Ahi-1 cells yielded the greatest number of differential antibody signals when compared to the other cell lines and after IM treatment, the activity of eIF4F complex and its relevant pathways were found to be mostly decreased in these cells compared to control BCR-ABL1$^+$ cells. It is possible that this unexpected result is partially mediated by BCR-ABL1 kinase-independent mechanisms in WT Ahi-1 cells as they still responded to IM-treatment by showing reduced phosphorylation of BCR-ABL1 (Figure 4.1A). Thus, their IM-resistant phenotypes observed may be caused by impaired activity of the eIF4F complex and its network. In addition, an overexpression model system was used in this study and both BCR-ABL1 and Ahi-1 were highly expressed in these cells as compared to their endogenous levels in human CML cells, and the construct of mouse Ahi-1 used in this model system is different from human AHI-1 as the mouse Ahi-1 lacks an N-terminal coiled-coil domain.[75,111] Considering all of these possibilities, I evaluated expression changes of eIF4F complex members in CD34$^+$ CML patient cells and found that several members of the eIF4F complex were highly expressed in these cells, in comparison with normal bone marrow cells, and this is also confirmed in a human CML cell line model. Thus, functional changes of the eIF4F complex were further explored in CML cells.

I also attempted to validate my potential targets from the antibody microarray analysis with immunoblotting. However, there were only a few changes that I was able to confirm. Firstly, the sensitivity between the antibody microarray and immunoblotting is different, where the antibody microarray can detect target antigens with one to two magnitude greater sensitivity compared to immunoblotting. The difference in detection methods, fluorescence for the antibody microarray and enhanced chemiluminescence for immunoblotting, could also attribute to different sensitivities and protein expression being too low to appear on an immunoblot. Furthermore, the proteins in the lysate used for the antibody microarray has been chemically cleaved by NTCB at the amino terminal of cysteine residues prior to the application on the slides, but this process was not performed during immunoblotting. Chemical cleavage can reduce the number of false positives resulting from interactions between proteins, since they are cleaved into peptides. Additionally, it can reveal the intended epitopes buried within the protein for antibodies on the microarray. However, this process can also reveal epitopes on other proteins resulting in off-target antibody binding and new interactions between peptides could also result in false positives on the antibody microarray. While the antibody microarray could potentially have fewer cross-reactivities, immunoblots resolve the proteins based on size, which leads to further confirmation of the correct target determined by the molecular weight. All the potential immunoreactivity with an antibody, both target and off-target proteins, are all combined into one spot with the antibody microarrays. It is difficult to predict *a priori* the potential cross-reactivity of antibodies in different tissues and cell lineages. In addition, some antibodies used were obtained from different sources between the antibody microarray and immunoblotting, which may lead to different specificities and sensitivities to validate the results. Nevertheless, I was

able to find differences in the protein expression and phosphorylation of several eIF4F complex members in IM-resistant CML cells by immunoblotting.

Most notably, I was able to detect the overexpression of eIF4G1 protein and its phosphorylation at S1231 in IM-resistant cells compared to their IM-sensitive counterparts. The increase in phosphorylation of eIF4G1 (S1231), was found to mediate translation.[288,289] It was also reported that overexpression of BCR-ABL1 increased the eIF4F complex activity by phosphorylating 4E-binding protein (4E-BP), leading to an increase in cyclin D3 expression.[290] I confirmed these findings in my study by demonstrating a reduction in the hyperphosphorylation of 4E-BP (Figure 4.7G, H). I observed an increase in cyclin D3 protein expression in IM-resistant CML cells, which indicated a higher level of eIF4F complex activity in these cells. However, the IM treatment at the dosage that I used did not reduce cyclin D3 levels and may require a longer time treatment to observe this effect or other mechanisms may also be involved in regulation of cyclin D3 expression. In addition, the increase in eIF4B S422 phosphorylation and protein expression was also observed in the IM-resistant CML cells compared to IM-sensitive cells. eIF4B is a cofactor to induce eIF4A activity by increasing its affinity for ATP and RNA to allow for the unwinding of secondary structures of the transcript.[150,156,157] The S422 phosphorylation on eIF4B through both the MAPK and PI3K/AKT/mTOR pathways can also induce translation and demonstrate another route of regulation of the eIF4F complex by these pathways.[180] It is of interest to follow up on the effect of increased eIF4B phosphorylation and protein expression on TKI sensitivity using additional biological and molecular assays.

Although the results of western blot analysis of eIF4F complex members and cyclin D3 could hint towards an increased eIF4F complex activity, I performed multiple assays to dissect some molecular details. The proximity ligation assay (PLA) displayed a great reduction in the

eIF4F complex assembly in K562R cells compared to parental K562 cells in eIF4G1 knockdown cells (Figure 4.9B). Although this result is interesting, the assembly of the eIF4F complex does not entirely dictate the translation process as there are also multiple points of regulation in the initiation, elongation, and termination of translation. Furthermore, the global protein synthesis rate assayed by o-propargyl-puromycin was not different between K562R and K562 cells, which did not reflect the observation of increased eIF4F complex activity in K562R cells (Figure 4.12D). However, the most telling difference between K562 and K562R cells is from the polysome profiling experiment, which displayed two completely different profiles and indicated a difference in translation initiation. K562R cells had a higher absorbance in the fractions containing heavy polysomes and a much lower 80S peak compared to K562 cells, indicating an increased level of translation initiation in IM-resistant cell than IM-sensitive cells (Figure 4.12E, bottom left). These differences strongly support the observations from the immunoblots in which the eIF4F complex activity is increased in the IM-resistant K562R cells and supported the notion that targeting the eIF4F complex by reducing abnormal activity of translation initiation may help to overcome drug resistance in CML cells.

To test this hypothesis, a selective eIF4G1-targeting small molecule, SBI-756, was used to investigate its ability to inhibit the cell growth and the eIF4F complex activity in IM-resistant cells. Notably, SBI-756 has been used in other cancer models, including melanoma, diffuse large B-cell lymphoma and BCR-ABL1^{+} B-acute lymphoblastic leukemia, to sensitize drug-resistant cells to chemotherapies, which supported its potential for pre-clinical studies.[230,231,291] In my study, SBI-756 treatment significantly inhibited cell viability and increased apoptosis in IM-resistant cells and this effect was enhanced by a combination of SBI-756 and IM. Additional studies will be needed to determine if this is an additive or synergistic effect and the ability of

SBI-756, alone or in combination with TKI, can effectively eradicate CML LSCs and their progenitor cells from TKI-nonresponders. Mechanistically, the PLA assay demonstrated a reduction in the assembly of the eIF4F complex, while polysome profiling revealed a reduction in heavy polysomes and an accumulation in 80S ribosomes, which indicated a global reduction in translation initiation after SBI-756 treatment (Figure 4.12E). Furthermore, o-propargyl-puromycin assay showed that SBI-756 treatment reduced the global protein synthesis rate (Figure 4.12D). Strikingly, BCR-ABL1 protein expression was significantly inhibited by SBI-756 treatment in IM-resistant cells to a lesser extent in IM-sensitive cells (Figure 4.13A). This was further supported by observing the slight reduction in *BCR-ABL1* transcript levels in fractions containing heavy polysomes after SBI-756 treatment in both cell lines (Figure 4.12F). More experiments are necessary to optimize and confirm the observed changes in *BCR-ABL1* transcript specific translation. These findings demonstrate the efficacy of SBI-756 in inhibiting the growth of IM-resistant cells and its inhibition to reduce the activity of eIF4F complex involved in translation initiation, particularly targeting BCR-ABL1 protein expression in CML cells.

To determine that the effects observed with SBI-756 treatment were due uniquely targeting eIF4G1, I further demonstrated that knockdown of eIF4G1 in IM-resistant cells significantly reduced the cell growth and made them more susceptible to IM treatment, including reduction in the functional activity of eIF4F complex. In particular, knockdown of eIF4G1 demonstrated significant reduction in BCR-ABL1 expression as observed by SBI-756 treatment. This consistent finding strongly supports a novel therapeutic approach to targeting BCR-ABL1 by SBI-756. Since BCR-ABL1 is a driver of CML pathogenesis, TKIs are used to inhibit the BCR-ABL1 phosphotransferase activity, but there are still problems with resistance due to

mutations within the BCR-ABL1 kinase domain, particularly the T315I mutation that is resistant to most TKIs.

There have been multiple approaches attempted to reduce the protein expression of BCR-ABL1. Proteolysis targeting chimera (PROTAC) is the chemical modification of TKIs to include a moiety to recruit an E3 ligase that would ubiquitinate BCR-ABL1 to tag for degradation by the proteasome.[292] However, point mutations in BCR-ABL1 could still prevent the binding of TKIs, which would render it ineffective. To overcome this, some studies have demonstrated the use of small interfering RNA targeting the fusion point of *BCR-ABL1* transcript to reduce its protein expression in primary CML patient cells.[293,294] Another study used the antimalarial drug artesunate to target the ubiquitin-specific protease 7, which stabilizes BCR-ABL1 by removing ubiquitin, and results in the degradation of BCR-ABL1.[295] In my study, SBI-756 treatment can still reduce BCR-ABL1 protein expression in the presence of the protease inhibitor MG132 (Figure 4.13C). It is feasible that the BCR-ABL1 protein still underwent partial proteolysis by proteases despite inhibition of the 20S proteasome complex by MG132. One potential alternative degradation pathways was homoharringtonine (HHT)-induced lysosomal degradation of BCR-ABL1 through autophagy.[296] HHT, which also targets translation like SBI-756, was found to synergize with sequential IM treatment by first reducing BCR-ABL1 levels to increase the antileukemic property of IM.[297] The 5'UTR of *BCR-ABL1* transcript is long and highly structured, similar to other "weak" mRNAs like *c-myc*, which is dependent on eIF4F complex activity for translation.[193,298]

In summary, I present a proof-of-concept for targeting BCR-ABL1 protein expression through the inhibition of eIF4F complex by SBI-756. Increase in eIF4F complex activity leads to an increase in expression of cyclin D3 and reduced TKI response. However, when eIF4G1 is

suppressed, there is a reduction in eIF4F complex activity leading to a reduced expression of BCR-ABL1 and cyclin D3 expression, which in turn reduces survival and increase TKI response in these cells (Figure 4.14). As these experiments were only performed in a cell line model, these findings must be confirmed in primary CML patient and normal healthy donor samples to establish the efficacy and safety of this targeting strategy. These studies provide evidence in targeting the eIF4F complex as alternative strategies in addition to TKIs to overcome drug-resistance in CML patients.

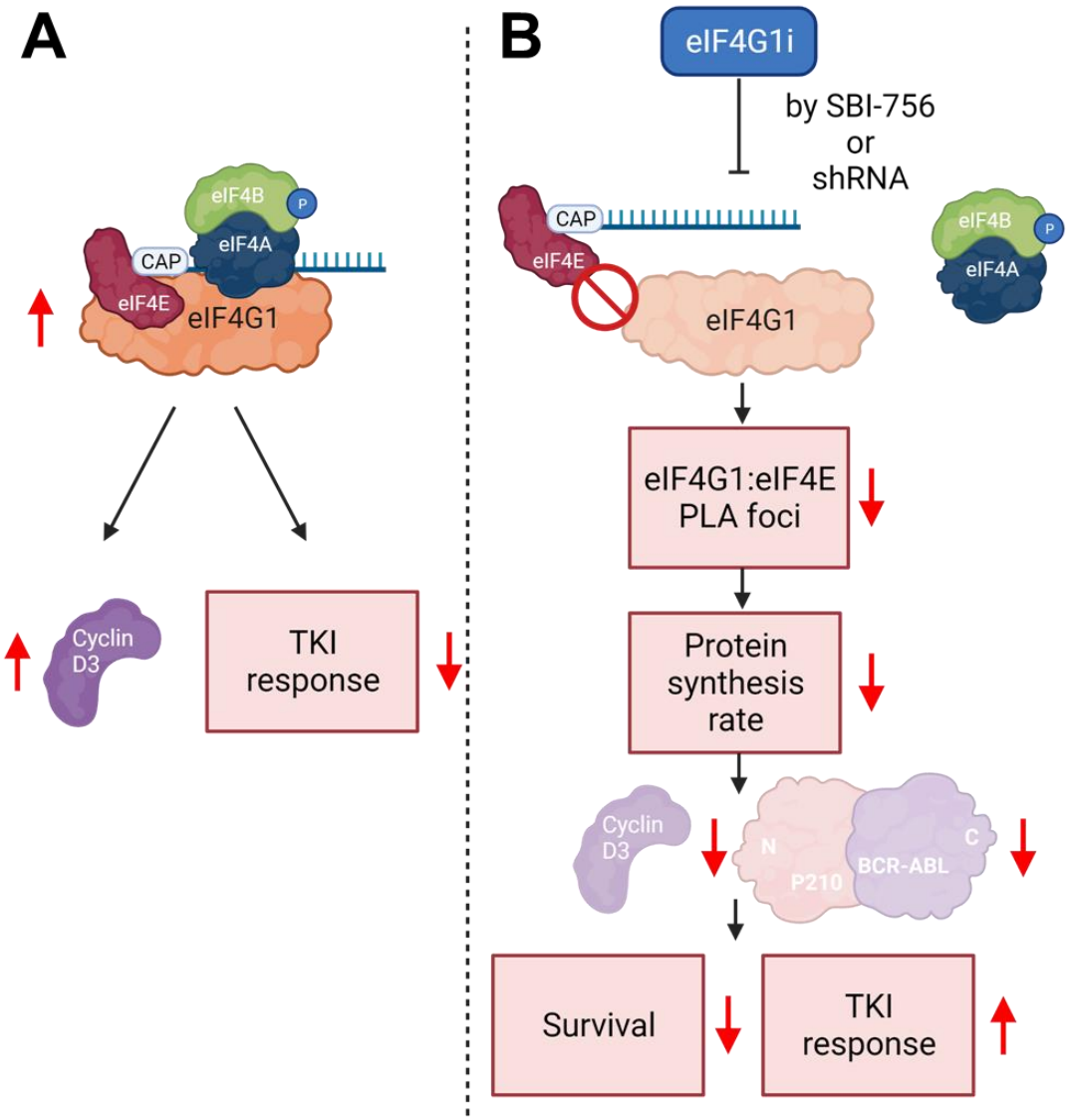

Figure 4.14: Working Model of eIF4G1 Inhibition in CML Cells. (A) eIF4G1 is overexpressed in IM-resistant CML cells resulting in an increase in eIF4F complex activity leading to an increase in cyclin D3 expression. (B) When eIF4G1 is targeted by shRNA or SBI-756 treatment, eIF4F complex assembly is reduced, leading to a reduction in translation and protein synthesis rate. This then results in a reduction in BCR-ABL1 and cyclin D3 protein expression with reduced survival and increased TKI response in drug-resistant CML cells. Created with BioRender.com

Chapter 5: General Summary and Discussion

5.1 Summary

The introduction of TKIs has revolutionized the treatment of CML-CP patients. Unfortunately, primary and acquired resistance to TKIs remains an issue for a proportion of CML patients. Therefore, it is necessary to develop robust tests to predict patients' response to TKI treatment and identify novel targets to overcome TKI resistance in CML patients. Here, I believe I have made new and insightful contributions to the field by identifying panels of miRNAs with *in vitro* TKI sensitivity data that can predict NL response in CML patients. Importantly, I also uncovered that the eIF4F complex plays a critical role in TKI resistance and the regulation of BCR-ABL1 protein expression. These studies are important in finding novel strategies to overcome TKI resistance in CML.

My work in Chapter 3 demonstrates the use of *in vitro* TKI CFC output combined with the expression of miRNAs to predict NL response. By using multiple bioinformatic analyses, I have identified that the expression of miR-145 and miR-708 can predict NL response in $CD34^+$ treatment-naïve CML patient cells, while the expression of miR-150 and miR-185 can predict NL response in post-treatment patient cells. Additionally, inclusion of NL-CFC data improved the predictive performances of both miRNA panels for NL response. Therefore, these findings offer a predictive model with two specific panels for prediction of NL response in pre- and post-treatment CML patients, which could be used as potential prognostic biomarkers for clinical uses to predict resistance.

In Chapter 4, I focused on studying the biological processes that are affected by different constructs of Ahi-1 using a high content antibody microarray. I identified the deregulation of the eIF4F complex in IM-resistant CML cells, which showed increased expression and

phosphorylation of two members, eIF4G1 and eIF4B. Moreover, I demonstrated that the inhibition of eIF4F complex activity by eIF4G1 suppression by shRNA and SBI-756 treatment led to an impaired survival and increased sensitivity to IM in resistant cells, using multiple biological and molecular assays. Most interestingly, I observed a significant reduction of BCR-ABL1 protein expression by targeting eIF4G1 and I have suggested a novel approach of targeting BCR-ABL1 through the inhibition of the eIF4F complex, which could be developed as a novel combination therapy with TKIs.

5.2 Limitations of the Work and Future Directions

Due to the prevalence of drug-resistant cells from CML patients in response to TKI monotherapies, there is still a need for better strategies to treat patients with resistant CML stem cells and BCR-ABL1 mutant cells. It is critical to identify useful biomarkers to predict TKI response as clinicians can change the drug regiment for CML patients as necessary. In the first part of my studies, I demonstrated the predictive capabilities of integrating matched *in vitro* TKI sensitivity data with the expression of miRNA to predict NL response in CML patients. Although this study already included a relatively large cohort of 58 patients with more than 8,000 microfluidic qRT-PCR reactions of TaqMan probes specific for 47 miRNAs and an RNU48 control for each patient sample that were extensively analyzed, only 12 NL nonresponder patients were available, which could reduce the statistical power of the analysis used. However, through the limitations of the number of NL nonresponder samples, the association of NL nonresponse to the expression of several miRNAs was still found to be statistically significant. Even though several miRNAs were identified and associated with NL nonresponse, additional studies to evaluate a different patient cohort or include more patient

samples will further confirm these findings and ensure the robustness of this predictive model. Furthermore, the preselection of miRNAs used in this study limited the assessment of the predictive potential of other miRNAs.

In the predictive panels, the expression of miR-145, -708, -150, and -185 were identified to have association to NL nonresponse. Currently, the role of miR-145 and -708 has yet to be fully investigated in CML. However, miR-145 has been hypothesized to play a role in drug sensitivity in solid tumours by affecting drug efflux.[280] MiR-708 has been found to play both oncogenic and tumour suppressive roles depending on the subtype of acute lymphoblastic leukemia.[282] In CML, miR-150 has been suggested to play a tumour suppressive role, which is negatively regulated by BCR-ABL1 via MYC, which results in increased MYB expression and contributes to CML pathogenesis.[283] Furthermore, miR-185 is also found to be repressed by BCR-ABL1 in IM-nonresponder patients, which increases PAK6 levels and OXPHOS mechanisms contributing to leukemic stem cell survival and TKI-resistance.[96] Although overall expression of these miRNAs in $CD34^+$ cells differed significantly between NL-responders and NL-nonresponders, I also observed that the variations in these miRNA expression levels among responders are relatively high with some responder patient cells expressing levels similar to NL-nonresponders. These observations indicate heterogeneous and differential expression of miRNAs in individual CML patients even before NL treatment. Thus, it would be important to further explore the role of these miRNAs on how they contribute to NL response/resistance. Further molecular studies of these miRNAs could potentially reveal common targets that could explain their significance to predicting NL response. Moreover, it would also be interesting to find if these miRNAs would also have predictive power for detection of responses to other TKIs including IM or DA. These studies also demonstrated the importance of the inclusion of NL-

CFC data, which improved the predictive performance of the miRNA panels. The predictive performance may be further improved with the inclusion of other clinical prognostic parameters that also predict survival of CML patients including Sokal and EUTOS scores.[299,300] Integration of multiple variables from different sources could potentially produce a panel that could have predictive abilities encompassing a larger proportion of CML patients; thus, more studies are necessary to develop these panels for clinical use.

In the second project of my studies, I identified the deregulation of the eIF4F complex in IM-resistance CML cells using the Kinex antibody microarray platform. Deregulated eIF4F complex activity has been observed in multiple different cancers and play a role in development of cancers through the elevated translation of transcripts of specific oncogenes.[150,161,200,201,205–207] With several bioinformatics analyses, I identified significant changes to the MAPK and PI3K/AKT/mTOR pathways, which are directly involved in the regulation of eIF4F complex, using pathway enrichment from targets of antibodies with significant differences in comparisons with WT Ahi-1 cells. Although there were 1,326 antibodies in total, these were preselected and focused mainly on phosphorylation sites and proteins involved with cellular signaling pathways. Therefore, the antibody microarray analysis and the following bioinformatic analyses were limited to predefined subset of targets, which may not show all the processes that were different in the WT Ahi-1 cells and introduce bias for the enrichment of cellular signaling pathways. Moreover, the number of significant targets from the bioinformatic study were limited due to the variations in the data, which could be improved using more replicates. Perhaps the inclusion of other proteomic techniques, such as mass spectrometry, could reveal more processes that are deregulated in WT Ahi-1 cells compared to BCR-ABL1^{+} cells expressing the other constructs of Ahi-1. Applying phosphopeptide enrichment by titanium oxide prior to mass spectrometry, the

phosphorylation landscape could also be further explored and extend the findings from the antibody microarray analysis. Inclusion of multiple proteomic techniques can improve the confidence of the significant differences identified by the bioinformatic analysis.

The antibody microarray platform could also be used to identify specific phosphorylation and protein expression that could potentially predict TKI response in CML patient cells. The advantage of this technology compared to mass spectrometry is that less material is required for detection of differences in phosphorylation sites with higher sensitivities. The phospho-proteomic antibody microarray could identify differential phosphorylation and expression of proteins between TKI-responsive and nonresponsive CML patient cells, which a TKI-nonresponsive signature could be developed based on this dataset. This phospho-proteomic signature would need to be evaluated if it could be used to predict TKI response in CML patient cells. Furthermore, antibodies with the best predictive ability could be used to develop for a flow cytometry-based panel for clinical use.

Interestingly, the overexpression and deregulated phosphorylation of the eIF4F complex was observed in two cell line models involved in IM resistance. I primarily explored the eIF4F complex members, but the other pathways involved in the regulation of the eIF4F complex would still be important to explore, because these pathways, such as the MAPK and PI3K/AKT/mTOR pathways, are also highly activated by BCR-ABL1 in CML cells.[301,302] There are still multiple points of eIF4F complex regulation that I have not explored and could also contribute to the observed increased eIF4F complex activity.

To identify proteins that have increased expression due to increased eIF4F complex activity, mass spectrometry can be utilized in IM-resistant cells with SBI-756 treatment or in eIF4G1 knockdown cells. Due to the observation of a subset of “weak” mRNAs that are

dependent of eIF4F complex activity, there may be proteins identified that could contribute to the IM resistance of these cells. Another approach could be performing RNA sequencing of the transcripts found in the different fractions after polysome fractionation in the presence or absence of SBI-756 treatment. Identifying transcripts that change in abundance in the heavy polysome fractions after SBI-756 treatment could potentially reveal eIF4E-sensitive genes in a CML context to support the hypothesis of selective translation. Furthermore, the proteomic and RNA sequencing datasets could be intersected to find common genes and proteins that are changed after SBI-756 treatment. Identification of these changes will be very interesting and potentially find specific targets that could explain the mechanism of IM-resistance due to an increase in eIF4F complex activity.

Strikingly, I observed a significant reduction in BCR-ABL1 protein levels after eIF4G1 knockdown or SBI-756 treatment. I also demonstrated that this reduction process is independent of the elongation step of translation by CHX treatment and the proteasome by MG132. However, there are still some explanations for BCR-ABL1 protein level reduction by SBI-756 treatment. For example, BCR-ABL1 could be reduced by lysosomal degradation induced by homoharringtonine treatment, which would be an independent process of the proteasome.[296] Moreover, the quantification of *BCR-ABL1* transcript from the polysome fractionation experiment followed by qPCR must be further studied as SBI-756 demonstrated a global inhibition on translation and protein synthesis. Thus, changes of *BCR-ABL1* transcript levels in the polysome fraction can be further validated by treating IM-resistant cells with SBI-756 or IM, alone or in combination. Therefore, more studies are necessary for a better understanding of the mechanism of the reduction of BCR-ABL1 protein levels that could lead to more optimized targeting of BCR-ABL1 protein expression.

Finally, the majority of my experiments were performed in cell lines, particularly K562/K562R cells. These biological and molecular observations must be validated in primary CML patient cells, especially in CML stem and progenitor cells from TKI-nonresponders, to confirm the efficacy of the combination treatment of SBI-756 and TKIs both *in vitro* and *in vivo*. In particular, the inhibition of the eIF4F complex by SBI-756 treatment must be confirmed in primary patient cells, including the reduction in PLA foci formation between eIF4G1 and eIF4E to demonstrate the disruption of the eIF4F complex and the reduction global protein synthesis rates by SBI-756 treatment. Most importantly, it is crucial to demonstrate reduction of BCR-ABL1 protein expression by SBI-756 treatment in primitive CML patient cells, which may differ in the regulation of the translation initiation process and may not be observed in quiescent leukemic stem cells. In addition, potential toxicity or off-target activity of SBI-756 against normal cells should be assessed and $CD34^+$ bone marrow cells from healthy individuals will be included to determine optimized inhibition doses that eradicate CML cells, but not healthy cells. These experiments are necessary to demonstrate this proof-of-concept study by targeting the eIF4F complex as a new therapeutic approach, which may lead to a more effective treatment strategy in CML.

Bibliography

1. Jabbour, E. & Kantarjian, H. Chronic myeloid leukemia: 2020 update on diagnosis, therapy and monitoring. *Am J Hematol* **95**, 691–709 (2020).
2. Apperley, J. F. Chronic myeloid leukaemia. *The Lancet* **385**, 1447–1459 (2015).
3. Nowell, P. C. & Hungerford, D. A. A minute chromosome in human chronic granulocytic leukemia. *Science* **142**, 1497 (1960).
4. Rowley, J. D. A new consistent chromosomal abnormality in chronic myelogenous leukaemia identified by quinacrine fluorescence and Giemsa staining. *Nature* **243**, 290–293 (1973).
5. Goldman, J. M. & Melo, J. V. Chronic myeloid leukemia — Advances in biology and new approaches to treatment. *N. Engl. J. Med.* **349**, 1451–1464 (2003).
6. Eaves, C. J. & Eaves, A. C. 4 Stem cell kinetics. *Baillières Clin. Haematol.* **10**, 233–257 (1997).
7. Perrotti, D., Jamieson, C., Goldman, J. & Skorski, T. Chronic myeloid leukemia: mechanisms of blastic transformation. *J. Clin. Invest.* **120**, 2254–2264 (2010).
8. Arber, D. A. *et al.* The 2016 revision to the World Health Organization classification of myeloid neoplasms and acute leukemia. *Blood* **127**, 2391–2405 (2016).
9. Baccarani, M. *et al.* European LeukemiaNet recommendations for the management of chronic myeloid leukemia: 2013. *Blood* **122**, 872–884 (2013).
10. Lugo, T. G., Pendergast, A.-M., Muller, A. J. & Witte, O. N. Tyrosine kinase activity and transformation potency of bcr-abl oncogene products. *Science* **247**, 1079–1082 (1990).
11. Hernández, S. E., Krishnaswami, M., Miller, A. L. & Koleske, A. J. How do Abl family kinases regulate cell shape and movement? *Trends Cell Biol.* **14**, 36–44 (2004).
12. Nagar, B. *et al.* Structural basis for the autoinhibition of c-Abl tyrosine kinase. *Cell* **112**, 859–871 (2003).
13. Van Etten, R. A., Jackson, P. & Baltimore, D. The mouse type IV c-abl gene product is a nuclear protein, and activation of transforming ability is associated with cytoplasmic localization. *Cell* **58**, 669–678 (1989).
14. He, Y. *et al.* The coiled-coil domain and Tyr177 of bcr are required to induce a murine chronic myelogenous leukemia–like disease by bcr/abl. *Blood* **99**, 2957–2968 (2002).
15. Goss, V. L. *et al.* A common phosphotyrosine signature for the Bcr-Abl kinase. *Blood* **107**, 4888–4897 (2006).
16. Braun, T. P., Eide, C. A. & Druker, B. J. Response and resistance to BCR-ABL1-targeted therapies. *Cancer Cell* **37**, 530–542 (2020).
17. Gallipoli, P. *et al.* JAK2/STAT5 inhibition by nilotinib with ruxolitinib contributes to the elimination of CML CD34+ cells in vitro and in vivo. *Blood* **124**, 1492–1501 (2014).
18. Lin, H. *et al.* Selective JAK2/ABL dual inhibition therapy effectively eliminates TKI-insensitive CML stem/progenitor cells. *Oncotarget* **5**, 8637–8650 (2014).
19. Million, R. P. & Van Etten, R. A. The Grb2 binding site is required for the induction of chronic myeloid leukemia-like disease in mice by the Bcr/Abl tyrosine kinase. *Blood* **96**, 664–670 (2000).
20. Lowenstein, E. J. *et al.* The SH2 and SH3 domain-containing protein GRB2 links receptor tyrosine kinases to ras signaling. *Cell* **70**, 431–442 (1992).

21. Li, S., Ilaria, R. L., Million, R. P., Daley, G. Q. & Van Etten, R. A. The P190, P210, and P230 forms of the BCR/ABL oncogene induce a similar chronic myeloid leukemia–like syndrome in mice but have different lymphoid leukemogenic activity. *J. Exp. Med.* **189**, 1399–1412 (1999).
22. Hirsch-Ginsberg, C. *et al.* Phenotypic and molecular heterogeneity in Philadelphia chromosome- positive acute leukemia. *Blood* **71**, 186–195 (1988).
23. Kurzrock, R., Shtalrid, M., Talpaz, M., Kloetzer, W. S. & Gutterman, J. U. Expression of c-abl in Philadelphia-positive acute myelogenous leukemia. *Blood* **70**, 1584–1588 (1987).
24. Pane, F. *et al.* Neutrophilic-chronic myeloid leukemia: a distinct disease with a specific molecular marker (BCR/ABL with C3/A2 junction) [see comments]. *Blood* **88**, 2410–2414 (1996).
25. Goldman, J. M. Chronic myeloid leukemia: a historical perspective. in vol. 47 302–311 (Elsevier, 2010).
26. Silver, R. T. *et al.* An evidence-based analysis of the effect of busulfan, hydroxyurea, interferon, and allogeneic bone marrow transplantation in treating the chronic phase of chronic myeloid leukemia: Developed for the American Society of Hematology: Presented in part at the Education Session of the American Society of Hematology, December 5, 1998, Miami Beach, FL. *Blood* **94**, 1517–1536 (1999).
27. Fefer, A. *et al.* Disappearance of Ph1-positive cells in four patients with chronic granulocytic leukemia after chemotherapy, irradiation and marrow transplantation from an identical twin. *N. Engl. J. Med.* **300**, 333–337 (1979).
28. McGlave, P. B. *et al.* Autologous transplants for chronic myelogenous leukaemia: results from eight transplant groups. *The Lancet* **343**, 1486–1488 (1994).
29. Speck, B. *et al.* Allogeneic bone-marrow transplantation for chronic myelogenous leukaemia. *The Lancet* **323**, 665–668 (1984).
30. Hehlmann, R. *et al.* Randomized comparison of interferon-alpha with busulfan and hydroxyurea in chronic myelogenous leukemia. The German CML Study Group [see comments]. *Blood* **84**, 4064–4077 (1994).
31. Talpaz, M. *et al.* Hematologic remission and cytogenetic improvement induced by recombinant human interferon alphaA in chronic myelogenous leukemia. *N. Engl. J. Med.* **314**, 1065–1069 (1986).
32. Anafi, M., Gazit, A., Gilon, C., Ben-Neriah, Y. & Levitzki, A. Selective interactions of transforming and normal abl proteins with ATP, tyrosine-copolymer substrates, and tyrphostins. *J. Biol. Chem.* **267**, 4518–4523 (1992).
33. Druker, B. J. *et al.* Effects of a selective inhibitor of the Abl tyrosine kinase on the growth of Bcr–Abl positive cells. *Nat. Med.* **2**, 561–566 (1996).
34. Druker, B. J. *et al.* Efficacy and safety of a specific inhibitor of the BCR-ABL tyrosine kinase in chronic myeloid leukemia. *N. Engl. J. Med.* **344**, 1031–1037 (2001).
35. Baccarani, M. *et al.* Chronic myeloid leukemia: an update of concepts and management recommendations of European LeukemiaNet. *J. Clin. Oncol.* **27**, 6041 (2009).
36. O'Brien, S. G. *et al.* Imatinib compared with interferon and low-dose cytarabine for newly diagnosed chronic-phase chronic myeloid leukemia. *N. Engl. J. Med.* **348**, 994–1004 (2003).
37. Deininger, M. *et al.* International randomized study of interferon vs STI571 (IRIS) 8-year follow up: sustained survival and low risk for progression or events in patients with newly

diagnosed chronic myeloid leukemia in chronic phase (CML-CP) treated with imatinib. *Blood* **114**, 1126 (2009).
38. Jabbour, E. J., Cortes, J. E. & Kantarjian, H. M. Resistance to tyrosine kinase inhibition therapy for chronic myelogenous leukemia: A clinical perspective and emerging treatment options. *Clin. Lymphoma Myeloma Leuk.* **13**, 515–529 (2013).
39. Talpaz, M. *et al.* Imatinib induces durable hematologic and cytogenetic responses in patients with accelerated phase chronic myeloid leukemia: results of a phase 2 study. *Blood* **99**, 1928–1937 (2002).
40. Sawyers, C. L. *et al.* Imatinib induces hematologic and cytogenetic responses in patients with chronic myelogenous leukemia in myeloid blast crisis: results of a phase II study: Presented in part at the 43rd Annual Meeting of The American Society of Hematology, Orlando, FL, December 11, 2001. *Blood* **99**, 3530–3539 (2002).
41. Skorski, T. BCR/ABL regulates response to DNA damage: the role in resistance to genotoxic treatment and in genomic instability. *Oncogene* **21**, 8591–8604 (2002).
42. Jiang, X., Saw, K. M., Eaves, A. & Eaves, C. Instability of BCR–ABL gene in primary and cultured chronic myeloid leukemia stem cells. *JNCI J. Natl. Cancer Inst.* **99**, 680–693 (2007).
43. Schindler, T. *et al.* Structural mechanism for STI-571 inhibition of abelson tyrosine kinase. *Science* **289**, 1938–1942 (2000).
44. Shah, N. P. *et al.* Multiple BCR-ABL kinase domain mutations confer polyclonal resistance to the tyrosine kinase inhibitor imatinib (STI571) in chronic phase and blast crisis chronic myeloid leukemia. *Cancer Cell* **2**, 117–125 (2002).
45. Weisberg, E. *et al.* Characterization of AMN107, a selective inhibitor of native and mutant Bcr-Abl. *Cancer Cell* **7**, 129–141 (2005).
46. Tokarski, J. S. *et al.* The structure of dasatinib (BMS-354825) bound to activated ABL kinase domain elucidates its inhibitory activity against imatinib-resistant ABL mutants. *Cancer Res.* **66**, 5790–5797 (2006).
47. Weisberg, E., Manley, P. W., Cowan-Jacob, S. W., Hochhaus, A. & Griffin, J. D. Second generation inhibitors of BCR-ABL for the treatment of imatinib-resistant chronic myeloid leukaemia. *Nat. Rev. Cancer* **7**, 345–356 (2007).
48. Sara Redaelli *et al.* Activity of bosutinib, dasatinib, and nilotinib against 18 imatinib-resistant BCR/ABL mutants. *J. Clin. Oncol.* **27**, 469–471 (2009).
49. O'Hare, T. *et al.* AP24534, a pan-BCR-ABL inhibitor for chronic myeloid leukemia, potently inhibits the T315I mutant and overcomes mutation-based resistance. *Cancer Cell* **16**, 401–412 (2009).
50. Cortes, J. E. *et al.* Ponatinib efficacy and safety in Philadelphia chromosome–positive leukemia: final 5-year results of the phase 2 PACE trial. *Blood* **132**, 393–404 (2018).
51. Wylie, A. A. *et al.* The allosteric inhibitor ABL001 enables dual targeting of BCR–ABL1. *Nature* **543**, 733–737 (2017).
52. Holtz, M. S., Forman, S. J. & Bhatia, R. Nonproliferating CML CD34+ progenitors are resistant to apoptosis induced by a wide range of proapoptotic stimuli. *Leukemia* **19**, 1034–1041 (2005).
53. Graham, S. M. *et al.* Primitive, quiescent, Philadelphia-positive stem cells from patients with chronic myeloid leukemia are insensitive to STI571 in vitro. *Blood* **99**, 319–325 (2002).

54. Holyoake, T. L. *et al.* Primitive quiescent leukemic cells from patients with chronic myeloid leukemia spontaneously initiate factor-independent growth in vitro in association with up-regulation of expression of interleukin-3. *Blood* **97**, 720–728 (2001).
55. Bonnet, D. & Dick, J. E. Human acute myeloid leukemia is organized as a hierarchy that originates from a primitive hematopoietic cell. *Nat. Med.* **3**, 730–737 (1997).
56. Eisterer, W. *et al.* Different subsets of primary chronic myeloid leukemia stem cells engraft immunodeficient mice and produce a model of the human disease. *Leukemia* **19**, 435–441 (2005).
57. Majeti, R., Park, C. Y. & Weissman, I. L. Identification of a hierarchy of multipotent hematopoietic progenitors in human cord blood. *Cell Stem Cell* **1**, 635–645 (2007).
58. Kobayashi, C. I. *et al.* The IL-2/CD25 axis maintains distinct subsets of chronic myeloid leukemia-initiating cells. *Blood* **123**, 2540–2549 (2014).
59. Herrmann, H. *et al.* Dipeptidylpeptidase IV (CD26) defines leukemic stem cells (LSC) in chronic myeloid leukemia. *Blood* **123**, 3951–3962 (2014).
60. Herrmann, H. *et al.* CD34+/CD38− stem cells in chronic myeloid leukemia express Siglec-3 (CD33) and are responsive to the CD33-targeting drug gemtuzumab/ozogamicin. *Haematologica* **97**, 219 (2012).
61. Nievergall, E. *et al.* Monoclonal antibody targeting of IL-3 receptor α with CSL362 effectively depletes CML progenitor and stem cells. *Blood* **123**, 1218–1228 (2014).
62. Järås, M. *et al.* Isolation and killing of candidate chronic myeloid leukemia stem cells by antibody targeting of IL-1 receptor accessory protein. *Proc. Natl. Acad. Sci.* **107**, 16280–16285 (2010).
63. Jiang, X. *et al.* Chronic myeloid leukemia stem cells possess multiple unique features of resistance to BCR-ABL targeted therapies. *Leukemia* **21**, 926–935 (2007).
64. Corbin, A. S. *et al.* Human chronic myeloid leukemia stem cells are insensitive to imatinib despite inhibition of BCR-ABL activity. *J. Clin. Invest.* **121**, 396–409 (2011).
65. Hanahan, D. & Weinberg, R. A. Hallmarks of cancer: the next generation. *Cell* **144**, 646–674 (2011).
66. Popp, H. D. *et al.* DNA damage and DNA damage response in chronic myeloid leukemia. *Int. J. Mol. Sci.* **21**, 1177 (2020).
67. Koptyra, M. *et al.* BCR/ABL kinase induces self-mutagenesis via reactive oxygen species to encode imatinib resistance. *Blood* **108**, 319–327 (2006).
68. Bavaro, L., Martelli, M., Cavo, M. & Soverini, S. Mechanisms of disease progression and resistance to tyrosine kinase inhibitor therapy in chronic myeloid leukemia: An update. *Int. J. Mol. Sci.* **20**, 6141 (2019).
69. Warsch, W., Walz, C. & Sexl, V. JAK of all trades: JAK2-STAT5 as novel therapeutic targets in BCR-ABL1+ chronic myeloid leukemia. *Blood* **122**, 2167–2175 (2013).
70. Li, S. Src-family kinases in the development and therapy of Philadelphia chromosome-positive chronic myeloid leukemia and acute lymphoblastic leukemia. *Leuk. Lymphoma* **49**, 19–26 (2008).
71. Ma, L. *et al.* A therapeutically targetable mechanism of BCR-ABL–independent imatinib resistance in chronic myeloid leukemia. *Sci. Transl. Med.* **6**, 252ra121-252ra121 (2014).
72. Rothe, K. *et al.* Integrin-linked kinase mediates therapeutic resistance of quiescent CML stem cells to tyrosine kinase inhibitors. *Cell Stem Cell* **27**, 110-124.e9 (2020).

73. Arrigoni, E. *et al.* Concise review: Chronic myeloid leukemia: stem cell niche and response to pharmacologic treatment. *Stem Cells Transl. Med.* **7**, 305–314 (2018).
74. Chen, Y., Hu, Y., Zhang, H., Peng, C. & Li, S. Loss of the Alox5 gene impairs leukemia stem cells and prevents chronic myeloid leukemia. *Nat. Genet.* **41**, 783–792 (2009).
75. Chen, M. *et al.* Targeting primitive chronic myeloid leukemia cells by effective inhibition of a new AHI-1–BCR-ABL–JAK2 complex. *JNCI J. Natl. Cancer Inst.* **105**, 405–423 (2013).
76. Lai, D. *et al.* PP2A inhibition sensitizes cancer stem cells to ABL tyrosine kinase inhibitors in BCR-ABL$^+$ human leukemia. *Sci. Transl. Med.* **10**, eaan8735 (2018).
77. Chen, Y. *et al.* A tumor suppressor function of the Msr1 gene in leukemia stem cells of chronic myeloid leukemia. *Blood* **118**, 390–400 (2011).
78. Zhang, H. *et al.* The Blk pathway functions as a tumor suppressor in chronic myeloid leukemia stem cells. *Nat. Genet.* **44**, 861–871 (2012).
79. Dierks, C. *et al.* Expansion of Bcr-Abl-positive leukemic stem cells is dependent on Hedgehog pathway activation. *Cancer Cell* **14**, 238–249 (2008).
80. Rothe, K. *et al.* The core autophagy protein ATG4B is a potential biomarker and therapeutic target in CML stem/progenitor cells. *Blood* **123**, 3622–3634 (2014).
81. Illmer, T. *et al.* P-glycoprotein-mediated drug efflux is a resistance mechanism of chronic myelogenous leukemia cells to treatment with imatinib mesylate. *Leukemia* **18**, 401–408 (2004).
82. Takahashi, N. Biomarkers for determining the prognosis of CML. in *Molecular Pathogenesis and Treatment of Chronic Myelogenous Leukemia* (ed. Kizaki, M.) 69–80 (Springer Japan, 2016). doi:10.1007/978-4-431-55714-2_5.
83. Soverini, S. *et al.* BCR-ABL kinase domain mutation analysis in chronic myeloid leukemia patients treated with tyrosine kinase inhibitors: recommendations from an expert panel on behalf of European LeukemiaNet. *Blood* **118**, 1208–1215 (2011).
84. McWeeney, S. K. *et al.* A gene expression signature of CD34+ cells to predict major cytogenetic response in chronic-phase chronic myeloid leukemia patients treated with imatinib. *Blood* **115**, 315–325 (2010).
85. Radich, J. P. *et al.* Gene expression changes associated with progression and response in chronic myeloid leukemia. *Proc. Natl. Acad. Sci.* **103**, 2794–2799 (2006).
86. Yeung, K. Y. *et al.* Predicting relapse prior to transplantation in chronic myeloid leukemia by integrating expert knowledge and expression data. *Bioinformatics* **28**, 823–830 (2012).
87. Quintás-Cardama, A. *et al.* Reverse phase protein array profiling reveals distinct proteomic signatures associated with chronic myeloid leukemia progression and with chronic phase in the CD34-positive compartment. *Cancer* **118**, 5283–5292 (2012).
88. Pizzatti, L. *et al.* Label-free MSE proteomic analysis of chronic myeloid leukemia bone marrow plasma: disclosing new insights from therapy resistance. *Proteomics* **12**, 2618–2631 (2012).
89. Warfvinge, R. *et al.* Single-cell molecular analysis defines therapy response and immunophenotype of stem cell subpopulations in CML. *Blood* **129**, 2384–2394 (2017).
90. Li, H. & Yang, B. B. Friend or foe: the role of microRNA in chemotherapy resistance. *Acta Pharmacol. Sin.* **34**, 870–879 (2013).
91. Chipman, L. B. & Pasquinelli, A. E. miRNA targeting: Growing beyond the seed. *Trends Genet.* **35**, 215–222 (2019).

92. Gebert, L. F. R. & MacRae, I. J. Regulation of microRNA function in animals. *Nat. Rev. Mol. Cell Biol.* **20**, 21–37 (2019).
93. Calin, G. A. *et al.* Frequent deletions and down-regulation of micro- RNA genes miR15 and miR16 at 13q14 in chronic lymphocytic leukemia. *Proc. Natl. Acad. Sci.* **99**, 15524–15529 (2002).
94. Saito, Y. *et al.* Specific activation of microRNA-127 with downregulation of the proto-oncogene BCL6 by chromatin-modifying drugs in human cancer cells. *Cancer Cell* **9**, 435–443 (2006).
95. Zhu, X. *et al.* miR-126 enhances the sensitivity of non-small cell lung cancer cells to anticancer agents by targeting vascular endothelial growth factor A. *Acta Biochim. Biophys. Sin.* **44**, 519–526 (2012).
96. Lin, H. *et al.* The miR-185/PAK6 axis predicts therapy response and regulates survival of drug-resistant leukemic stem cells in CML. *Blood* **136**, 596–609 (2020).
97. Cimmino, A. *et al.* miR-15 and miR-16 induce apoptosis by targeting BCL2. *Proc. Natl. Acad. Sci.* **102**, 13944–13949 (2005).
98. Acunzo, M., Romano, G., Wernicke, D. & Croce, C. M. MicroRNA and cancer – A brief overview. *Adv. Biol. Regul.* **57**, 1–9 (2015).
99. Mardani, R. *et al.* MicroRNA in leukemia: Tumor suppressors and oncogenes with prognostic potential. *J. Cell. Physiol.* **234**, 8465–8486 (2019).
100. Litwińska, Z. & Machaliński, B. miRNAs in chronic myeloid leukemia: small molecules, essential function. *Leuk. Lymphoma* **58**, 1297–1305 (2017).
101. Venturini, L. *et al.* Expression of the miR-17-92 polycistron in chronic myeloid leukemia (CML) CD34+ cells. *Blood* **109**, 4399–4405 (2007).
102. Suresh, S. *et al.* MicroRNAs 130a/b are regulated by BCR-ABL and downregulate expression of CCN3 in CML. *J. Cell Commun. Signal.* **5**, 183–191 (2011).
103. Wang, W.-Z. *et al.* Silencing of miR-21 sensitizes CML CD34+ stem/progenitor cells to imatinib-induced apoptosis by blocking PI3K/AKT pathway. *Leuk. Res.* **39**, 1117–1124 (2015).
104. Machová Poláková, K. *et al.* Expression patterns of microRNAs associated with CML phases and their disease related targets. *Mol. Cancer* **10**, 41 (2011).
105. San José-Enériz, E. *et al.* MicroRNA expression profiling in imatinib-resistant chronic myeloid leukemia patients without clinically significant ABL1-mutations. *Mol. Cancer* **8**, 69 (2009).
106. Flamant, S. *et al.* Micro-RNA response to imatinib mesylate in patients with chronic myeloid leukemia. *Haematologica* **95**, 1325–1333 (2010).
107. Ferreira, A. F. *et al.* ApoptomiRs expression modulated by BCR–ABL is linked to CML progression and imatinib resistance. *Blood Cells. Mol. Dis.* **53**, 47–55 (2014).
108. Poirier, Y., Kozak, C. & Jolicoeur, P. Identification of a common helper provirus integration site in Abelson murine leukemia virus-induced lymphoma DNA. *J. Virol.* **62**, 3985–3992 (1988).
109. Scher, C. D. & Siegler, R. Direct transformation of 3T3 cells by Abelson murine leukaemia virus. *Nature* **253**, 729–731 (1975).
110. Savard, P., DesGroseillers, L., Rassart, E., Poirier, Y. & Jolicoeur, P. Important role of the long terminal repeat of the helper Moloney murine leukemia virus in Abelson virus-induced lymphoma. *J. Virol.* **61**, 3266–3275 (1987).

111. Jiang, X., Hanna, Z., Kaouass, M., Girard, L. & Jolicoeur, P. Ahi-1, a novel gene encoding a modular protein with WD40-repeat and SH3 domains, is targeted by the Ahi-1 and Mis-2 provirus integrations. *J. Virol.* **76**, 9046–9059 (2002).
112. Meng, X.-F., Luo, Y., Xiao, W., Li, M. & Shi, J. Cloning and characterization of the promoter of the human AHI1 gene. *Biochem. Genet.* **47**, 427–438 (2009).
113. Mason, J. M. & Arndt, K. M. Coiled coil domains: Stability, specificity, and biological implications. *Chembiochem* **5**, 170–176 (2004).
114. Jain, B. P. & Pandey, S. WD40 repeat proteins: signalling scaffold with diverse functions. *Protein J.* **37**, 391–406 (2018).
115. Musacchio, A., Wilmanns, M. & Saraster, M. Structure and function of the SH3 domain. *Prog. Biophys. Mol. Biol.* **61**, 283–297 (1994).
116. Liu, X. *et al.* Molecular and structural characterization of the SH3 domain of AHI-1 in regulation of cellular resistance of BCR-ABL+ chronic myeloid leukemia cells to tyrosine kinase inhibitors. *Proteomics* **12**, 2094–2106 (2012).
117. Rechsteiner, M. & Rogers, S. W. PEST sequences and regulation by proteolysis. *Trends Biochem. Sci.* **21**, 267–271 (1996).
118. Dixon-Salazar, T. *et al.* Mutations in the AHI1 gene, encoding Jouberin, cause Joubert Syndrome with cortical polymicrogyria. *Am. J. Hum. Genet.* **75**, 979–987 (2004).
119. Jiang, X. *et al.* Deregulated expression in Ph+ human leukemias of AHI-1, a gene activated by insertional mutagenesis in mouse models of leukemia. *Blood* **103**, 3897–3904 (2004).
120. Zhou, L. L. *et al.* AHI-1 interacts with BCR-ABL and modulates BCR-ABL transforming activity and imatinib response of CML stem/progenitor cells. *J. Exp. Med.* **205**, 2657–2671 (2008).
121. Xie, S. *et al.* Involvement of Jak2 tyrosine phosphorylation in Bcr–Abl transformation. *Oncogene* **20**, 6188–6195 (2001).
122. Liu, X. *et al.* A novel AHI-1–BCR-ABL–DNM2 complex regulates leukemic properties of primitive CML cells through enhanced cellular endocytosis and ROS-mediated autophagy. *Leukemia* **31**, 2376–2387 (2017).
123. Durieux, A.-C., Prudhon, B., Guicheney, P. & Bitoun, M. Dynamin 2 and human diseases. *J. Mol. Med.* **88**, 339–350 (2010).
124. Kennah, E. *et al.* Identification of tyrosine kinase, HCK, and tumor suppressor, BIN1, as potential mediators of AHI-1 oncogene in primary and transformed CTCL cells. *Blood* **113**, 4646–4655 (2009).
125. Esmailzadeh, S., Huang, Y., Su, M.-W., Zhou, Y. & Jiang, X. BIN1 tumor suppressor regulates Fas/Fas ligand–mediated apoptosis through c-FLIP in cutaneous T-cell lymphoma. *Leukemia* **29**, 1402–1413 (2015).
126. Valente, E. M. *et al.* AHI1 gene mutations cause specific forms of Joubert syndrome–related disorders. *Ann. Neurol.* **59**, 527–534 (2006).
127. Parisi, M. A. *et al.* AHI1 mutations cause both retinal dystrophy and renal cystic disease in Joubert syndrome. *J. Med. Genet.* **43**, 334–339 (2006).
128. Tory, K. *et al.* High NPHP1 and NPHP6 mutation rate in patients with Joubert syndrome and nephronophthisis: Potential epistatic effect of NPHP6 and AHI1 mutations in patients with NPHP1 mutations. *J. Am. Soc. Nephrol.* **18**, 1566 (2007).
129. Karamzade, A. *et al.* Identification of a novel truncating variant in AHI1 gene and a brief review on mutations spectrum. *Mol. Biol. Rep.* **48**, 5339–5345 (2021).

130. Hildebrandt, F., Attanasio, M. & Otto, E. Nephronophthisis: Disease mechanisms of a ciliopathy. *J. Am. Soc. Nephrol.* **20**, 23–35 (2009).
131. Lancaster, M. A. & Gleeson, J. G. The primary cilium as a cellular signaling center: lessons from disease. *Curr. Opin. Genet. Dev.* **19**, 220–229 (2009).
132. Sang, L. *et al.* Mapping the NPHP-JBTS-MKS protein network reveals ciliopathy disease genes and pathways. *Cell* **145**, 513–528 (2011).
133. Lee, Y. L. *et al.* Cby1 promotes Ahi1 recruitment to a ring-shaped domain at the centriole–cilium interface and facilitates proper cilium formation and function. *Mol. Biol. Cell* **25**, 2919–2933 (2014).
134. Hsiao, Y.-C. *et al.* Ahi1, whose human ortholog is mutated in Joubert syndrome, is required for Rab8a localization, ciliogenesis and vesicle trafficking. *Hum. Mol. Genet.* **18**, 3926–3941 (2009).
135. Kaskow, B. J. *et al.* MS AHI1 genetic risk promotes IFNγ+ CD4+ T cells. *Neurol. - Neuroimmunol. Neuroinflammation* **5**, (2018).
136. Ingason, A. *et al.* Support for involvement of the AHI1 locus in schizophrenia. *Eur. J. Hum. Genet.* **15**, 988–991 (2007).
137. Alvarez Retuerto, A. I. *et al.* Association of common variants in the Joubert syndrome gene (AHI1) with autism. *Hum. Mol. Genet.* **17**, 3887–3896 (2008).
138. Porcelli, S. *et al.* Abelson helper integration site-1 gene variants on major depressive disorder and bipolar disorder. *Psychiatry Investig.* **11**, 481–486 (2014).
139. Xu, X. *et al.* Neuronal Abelson helper integration site-1 (Ahi1) deficiency in mice alters TrkB signaling with a depressive phenotype. *Proc. Natl. Acad. Sci.* **107**, 19126–19131 (2010).
140. Ren, L. *et al.* Loss of Ahi1 impairs neurotransmitter release and causes depressive behaviors in mice. *PLOS ONE* **9**, e93640 (2014).
141. Wang, B. *et al.* Ahi1 regulates the nuclear translocation of glucocorticoid receptor to modulate stress response. *Transl. Psychiatry* **11**, 1–13 (2021).
142. Salonen, J. T. *et al.* Type 2 diabetes whole-genome association study in four populations: The DiaGen consortium. *Am. J. Hum. Genet.* **81**, 338–345 (2007).
143. Prior, M. J. *et al.* The characterization of Abelson helper integration site–1 in skeletal muscle and its links to the metabolic syndrome. *Metabolism* **59**, 1057–1064 (2010).
144. Wang, H. *et al.* Hypothalamic Ahi1 mediates feeding behavior through interaction with 5-HT2C receptor. *J. Biol. Chem.* **287**, 2237–2246 (2012).
145. Hershey, J. W. B., Sonenberg, N. & Mathews, M. B. Principles of translational control: An overview. *Cold Spring Harb. Perspect. Biol.* **4**, a011528 (2012).
146. Schuller, A. P. & Green, R. Roadblocks and resolutions in eukaryotic translation. *Nat. Rev. Mol. Cell Biol.* **19**, 526–541 (2018).
147. Parsyan, A. *et al.* mRNA helicases: the tacticians of translational control. *Nat. Rev. Mol. Cell Biol.* **12**, 235–245 (2011).
148. Hinnebusch, A. G. Molecular mechanism of scanning and start codon selection in eukaryotes. *Microbiol. Mol. Biol. Rev.* **75**, 434–467 (2011).
149. Shatkin, A. J. Capping of eucaryotic mRNAs. *Cell* **9**, 645–653 (1976).
150. Pelletier, J., Graff, J., Ruggero, D. & Sonenberg, N. Targeting the eIF4F translation initiation complex: A critical nexus for cancer development. *Cancer Res.* **75**, 250–263 (2015).

151. Duncan, R. & Hershey, J. W. Identification and quantitation of levels of protein synthesis initiation factors in crude HeLa cell lysates by two-dimensional polyacrylamide gel electrophoresis. *J. Biol. Chem.* **258**, 7228–7235 (1983).
152. Conroy, S. C., Dever, T. E., Owens, C. L. & Merrick, W. C. Characterization of the 46,000-Dalton subunit of eIF-4F. *Arch. Biochem. Biophys.* **282**, 363–371 (1990).
153. Gradi, A. *et al.* A novel functional human eukaryotic translation initiation factor 4G. *Mol. Cell. Biol.* **18**, 334–342 (1998).
154. Imataka, H. & Sonenberg, N. Human eukaryotic translation initiation factor 4G (eIF4G) possesses two separate and independent binding sites for eIF4A. *Mol. Cell. Biol.* **17**, 6940–6947 (1997).
155. Kapp, L. D. & Lorsch, J. R. The molecular mechanics of eukaryotic translation. *Annu. Rev. Biochem.* **73**, 657–704 (2004).
156. Rogers, G. W., Richter, N. J., Lima, W. F. & Merrick, W. C. Modulation of the helicase activity of eIF4A by eIF4B, eIF4H, and eIF4F. *J. Biol. Chem.* **276**, 30914–30922 (2001).
157. Bi, X., Ren, J. & Goss, D. J. Wheat germ translation initiation factor eIF4B affects eIF4A and eIFiso4F helicase activity by increasing the ATP binding affinity of eIF4A. *Biochemistry* **39**, 5758–5765 (2000).
158. Sarkar, G., Edery, I., Gallo, R. & Sonenberg, N. Preferential stimulation of rabbit α globin mRNA translation by a cap-binding protein complex. *Biochim. Biophys. Acta BBA - Gene Struct. Expr.* **783**, 122–129 (1984).
159. Edery, I., Lee, K. A. W. & Sonenberg, N. Functional characterization of eukaryotic mRNA cap binding protein complex: effects on translation of capped and naturally uncapped RNAs. *Biochemistry* **23**, 2456–2462 (1984).
160. Haghighat, A. & Sonenberg, N. eIF4G dramatically enhances the binding of eIF4E to the mRNA 5′-cap structure. *J. Biol. Chem.* **272**, 21677–21680 (1997).
161. De Benedetti, A. & Graff, J. R. eIF-4E expression and its role in malignancies and metastases. *Oncogene* **23**, 3189–3199 (2004).
162. Shantz, L. M. & Pegg, A. E. Overproduction of ornithine decarboxylase caused by relief of translational repression is associated with neoplastic transformation. *Cancer Res.* **54**, 2313–2316 (1994).
163. Graff, J. R. & Zimmer, S. G. Translational control and metastatic progression: Enhanced activity of the mRNA cap-binding protein eIF-4E selectively enhances translation of metastasis-related mRNAs. *Clin. Exp. Metastasis* **20**, 265–273 (2003).
164. Hsieh, A. C. *et al.* The translational landscape of mTOR signalling steers cancer initiation and metastasis. *Nature* **485**, 55–61 (2012).
165. Cunningham, J. T., Moreno, M. V., Lodi, A., Ronen, S. M. & Ruggero, D. Protein and nucleotide biosynthesis are coupled by a single rate-limiting enzyme, PRPS2, to drive cancer. *Cell* **157**, 1088–1103 (2014).
166. Wendel, H.-G. *et al.* Dissecting eIF4E action in tumorigenesis. *Genes Dev.* **21**, 3232–3237 (2007).
167. Robichaud, N. *et al.* Phosphorylation of eIF4E promotes EMT and metastasis via translational control of SNAIL and MMP-3. *Oncogene* **34**, 2032–2042 (2015).
168. Gwinn, D. M. *et al.* AMPK phosphorylation of raptor mediates a metabolic checkpoint. *Mol. Cell* **30**, 214–226 (2008).

169. Inoki, K., Zhu, T. & Guan, K.-L. TSC2 mediates cellular energy response to control cell growth and survival. *Cell* **115**, 577–590 (2003).
170. Hara, K. *et al.* Amino acid sufficiency and mTOR regulate p70 S6 kinase and eIF-4E BP1 through a common effector mechanism. *J. Biol. Chem.* **273**, 14484–14494 (1998).
171. Brugarolas, J. *et al.* Regulation of mTOR function in response to hypoxia by REDD1 and the TSC1/TSC2 tumor suppressor complex. *Genes Dev.* **18**, 2893–2904 (2004).
172. Gingras, A.-C. *et al.* Regulation of 4E-BP1 phosphorylation: a novel two-step mechanism. *Genes Dev.* **13**, 1422–1437 (1999).
173. Hara, K. *et al.* Regulation of eIF-4E BP1 Phosphorylation by mTOR. *J. Biol. Chem.* **272**, 26457–26463 (1997).
174. Burnett, P. E., Barrow, R. K., Cohen, N. A., Snyder, S. H. & Sabatini, D. M. RAFT1 phosphorylation of the translational regulators p70 S6 kinase and 4E-BP1. *Proc. Natl. Acad. Sci.* **95**, 1432–1437 (1998).
175. Pause, A. *et al.* Insulin-dependent stimulation of protein synthesis by phosphorylation of a regulator of 5'-cap function. *Nature* **371**, 762–767 (1994).
176. Gingras, A.-C. *et al.* Hierarchical phosphorylation of the translation inhibitor 4E-BP1. *Genes Dev.* **15**, 2852–2864 (2001).
177. Pearson, R. B. *et al.* The principal target of rapamycin-induced p70s6k inactivation is a novel phosphorylation site within a conserved hydrophobic domain. *EMBO J.* **14**, 5279–5287 (1995).
178. Dennis, P. B., Pullen, N., Kozma, S. C. & Thomas, G. The principal rapamycin-sensitive p70(s6k) phosphorylation sites, T-229 and T-389, are differentially regulated by rapamycin-insensitive kinase kinases. *Mol. Cell. Biol.* **16**, 6242–6251 (1996).
179. Holz, M. K., Ballif, B. A., Gygi, S. P. & Blenis, J. mTOR and S6K1 mediate assembly of the translation preinitiation complex through dynamic protein interchange and ordered phosphorylation events. *Cell* **123**, 569–580 (2005).
180. Shahbazian, D. *et al.* The mTOR/PI3K and MAPK pathways converge on eIF4B to control its phosphorylation and activity. *EMBO J.* **25**, 2781–2791 (2006).
181. Dorrello, N. V. *et al.* S6K1- and βTRCP-mediated degradation of PDCD4 promotes protein translation and cell growth. *Science* **314**, 467–471 (2006).
182. Loh, P. G. *et al.* Structural basis for translational inhibition by the tumour suppressor Pdcd4. *EMBO J.* **28**, 274–285 (2009).
183. Liu, F., Yang, X., Geng, M. & Huang, M. Targeting ERK, an achilles' heel of the MAPK pathway, in cancer therapy. *Acta Pharm. Sin. B* **8**, 552–562 (2018).
184. Waskiewicz, A. J., Flynn, A., Proud, C. G. & Cooper, J. A. Mitogen-activated protein kinases activate the serine/threonine kinases Mnk1 and Mnk2. *EMBO J.* **16**, 1909–1920 (1997).
185. Flynn, A. & Proud, C. G. Serine 209, not serine 53, is the major site of phosphorylation in initiation factor eIF-4E in serum-treated chinese hamster ovary cells. *J. Biol. Chem.* **270**, 21684–21688 (1995).
186. Furic, L. *et al.* eIF4E phosphorylation promotes tumorigenesis and is associated with prostate cancer progression. *Proc. Natl. Acad. Sci.* **107**, 14134–14139 (2010).
187. Rosenwald, I. B., Rhoads, D. B., Callanan, L. D., Isselbacher, K. J. & Schmidt, E. V. Increased expression of eukaryotic translation initiation factors eIF-4E and eIF-2 alpha in response to growth induction by c-myc. *Proc. Natl. Acad. Sci.* **90**, 6175–6178 (1993).

188. Lin, C.-J., Malina, A. & Pelletier, J. c-Myc and eIF4F constitute a feedforward loop that regulates cell growth: implications for anticancer therapy. *Cancer Res.* **69**, 7491–7494 (2009).
189. Miyagi, Y. *et al.* Elevated levels of eukaryotic translation initiation factor eIF-4E, mRNA in a broad spectrum of transformed cell lines. *Cancer Lett.* **91**, 247–252 (1995).
190. Anthony, B., Carter, P. & De Benedetti, A. Overexpression of the proto-oncogene/translation factor 4E in breast-carcinoma cell lines. *Int. J. Cancer* **65**, 858–863 (1996).
191. Lazaris-Karatzas, A., Montine, K. S. & Sonenberg, N. Malignant transformation by a eukaryotic initiation factor subunit that binds to mRNA 5' cap. *Nature* **345**, 544–547 (1990).
192. De Benedetti, A. & Rhoads, R. E. Overexpression of eukaryotic protein synthesis initiation factor 4E in HeLa cells results in aberrant growth and morphology. *Proc. Natl. Acad. Sci.* **87**, 8212–8216 (1990).
193. Ruggero, D. *et al.* The translation factor eIF-4E promotes tumor formation and cooperates with c-Myc in lymphomagenesis. *Nat. Med.* **10**, 484–486 (2004).
194. De Benedetti, A., Joshi-Barve, S., Rinker-Schaeffer, C. & Rhoads, R. E. Expression of antisense RNA against initiation factor eIF-4E mRNA in HeLa cells results in lengthened cell division times, diminished translation rates, and reduced levels of both eIF-4E and the p220 component of eIF-4F. *Mol. Cell. Biol.* **11**, 5435–5445 (1991).
195. Rinker-Schaeffer, C. W., Graff, J. R., De Benedetti, A., Zimmer, S. G. & Rhoads, R. E. Decreasing the level of translation initiation factor 4E with antisense rna causes reversal of ras-mediated transformation and tumorigenesis of cloned rat embryo fibroblasts. *Int. J. Cancer* **55**, 841–847 (1993).
196. Polunovsky, V. A. *et al.* Translational control of programmed cell death: eukaryotic translation initiation factor 4E blocks apoptosis in growth-factor-restricted fibroblasts with physiologically expressed or deregulated Myc. *Mol. Cell. Biol.* **16**, 6573–6581 (1996).
197. Li, S. *et al.* Translation factor eIF4E rescues cells from Myc-dependent apoptosis by inhibiting cytochrome C release. *J. Biol. Chem.* **278**, 3015–3022 (2003).
198. Worch, J. *et al.* The serine-threonine kinase MNK1 is post-translationally stabilized by PML-RARα and regulates differentiation of hematopoietic cells. *Oncogene* **23**, 9162–9172 (2004).
199. Wheater, M. J., Johnson, P. WM. & Blaydes, J. P. The role of MNK proteins and eIF4E phosphorylation in breast cancer cell proliferation and survival. *Cancer Biol. Ther.* **10**, 728–735 (2010).
200. Eberle, J., Krasagakis, K. & Orfanos, C. E. Translation initiation factor eIF-4A1 mRNA is consistently overexpressed in human melanoma cells in vitro. *Int. J. Cancer* **71**, 396–401 (1997).
201. Silvera, D., Formenti, S. C. & Schneider, R. J. Translational control in cancer. *Nat. Rev. Cancer* **10**, 254–266 (2010).
202. Modelska, A. *et al.* The malignant phenotype in breast cancer is driven by eIF4A1-mediated changes in the translational landscape. *Cell Death Dis.* **6**, e1603–e1603 (2015).
203. Ji, P. *et al.* MALAT-1, a novel noncoding RNA, and thymosin β4 predict metastasis and survival in early-stage non-small cell lung cancer. *Oncogene* **22**, 8031–8041 (2003).

204. Fukuchi-Shimogori, T. *et al.* Malignant transformation by overproduction of translation initiation factor eIF4G1. *Cancer Res.* **57**, 5041–5044 (1997).
205. Lu, Y. *et al.* Elevation of EIF4G1 promotes non-small cell lung cancer progression by activating mTOR signalling. *J. Cell. Mol. Med.* **25**, 2994–3005 (2021).
206. Jaiswal, P. K., Koul, S., Shanmugam, P. S. T. & Koul, H. K. Eukaryotic Translation Initiation Factor 4 Gamma 1 (eIF4G1) is upregulated during prostate cancer progression and modulates cell growth and metastasis. *Sci. Rep.* **8**, 7459 (2018).
207. Goh, T. S. *et al.* Prognostic significance of EIF4G1 in patients with pancreatic ductal adenocarcinoma. *OncoTargets Ther.* **12**, 2853–2859 (2019).
208. Jaiswal, P. K., Koul, S., Palanisamy, N. & Koul, H. K. Eukaryotic Translation Initiation Factor 4 Gamma 1 (EIF4G1): a target for cancer therapeutic intervention? *Cancer Cell Int.* **19**, 224 (2019).
209. Wu, S. & Wagner, G. Deep computational analysis details dysregulation of eukaryotic translation initiation complex eIF4F in human cancers. *Cell Syst.* **12**, 907-923.e6 (2021).
210. Ghosh, B. *et al.* Nontoxic chemical interdiction of the epithelial-to-mesenchymal transition by targeting cap-dependent translation. *ACS Chem. Biol.* **4**, 367–377 (2009).
211. Li, S. *et al.* Treatment of breast and lung cancer cells with a N-7 benzyl guanosine monophosphate tryptamine phosphoramidate pronucleotide (4Ei-1) results in chemosensitization to gemcitabine and induced eIF4E proteasomal degradation. *Mol. Pharm.* **10**, 523–531 (2013).
212. Graff, J. R. *et al.* Therapeutic suppression of translation initiation factor eIF4E expression reduces tumor growth without toxicity. *J. Clin. Invest.* **117**, 2638–2648 (2007).
213. Hong, D. S. *et al.* A phase 1 dose escalation, pharmacokinetic, and pharmacodynamic evaluation of eIF-4E antisense oligonucleotide LY2275796 in patients with advanced cancer. *Clin. Cancer Res.* **17**, 6582–6591 (2011).
214. Bordeleau, M.-E. *et al.* Functional characterization of IRESes by an inhibitor of the RNA helicase eIF4A. *Nat. Chem. Biol.* **2**, 213–220 (2006).
215. Bordeleau, M.-E. *et al.* Stimulation of mammalian translation initiation factor eIF4A activity by a small molecule inhibitor of eukaryotic translation. *Proc. Natl. Acad. Sci.* **102**, 10460–10465 (2005).
216. Bordeleau, M.-E. *et al.* Therapeutic suppression of translation initiation modulates chemosensitivity in a mouse lymphoma model. *J. Clin. Invest.* **118**, 2651–2660 (2008).
217. Sun, Y. *et al.* Single-molecule kinetics of the eukaryotic initiation factor 4AI upon RNA unwinding. *Structure* **22**, 941–948 (2014).
218. Bordeleau, M.-E. *et al.* RNA-mediated sequestration of the RNA helicase eIF4A by pateamine A inhibits translation initiation. *Chem. Biol.* **13**, 1287–1295 (2006).
219. Tsumuraya, T. *et al.* Effects of hippuristanol, an inhibitor of eIF4A, on adult T-cell leukemia. *Biochem. Pharmacol.* **81**, 713–722 (2011).
220. Kuznetsov, G. *et al.* Potent in vitro and in vivo anticancer activities of des-methyl, des-amino pateamine A, a synthetic analogue of marine natural product pateamine A. *Mol. Cancer Ther.* **8**, 1250–1260 (2009).
221. Lucas, D. M. *et al.* The novel plant-derived agent silvestrol has B-cell selective activity in chronic lymphocytic leukemia and acute lymphoblastic leukemia in vitro and in vivo. *Blood* **113**, 4656–4666 (2009).

222. Nilewski, C. *et al.* 1-Aminomethyl SAR in a novel series of flavagline-inspired eIF4A inhibitors: Effects of amine substitution on cell potency and in vitro PK properties. *Bioorg. Med. Chem. Lett.* **47**, 128111 (2021).
223. Gerson-Gurwitz, A. *et al.* Zotatifin, an eIF4A-selective inhibitor, blocks tumor growth in receptor tyrosine kinase driven tumors. *Front. Oncol.* **11**, (2021).
224. Thompson, P. A. *et al.* Targeting oncogene mRNA translation in B-cell malignancies with eFT226, a potent and selective inhibitor of eIF4A. *Mol. Cancer Ther.* **20**, 26–36 (2021).
225. Ernst, J. T. *et al.* Design of development candidate eFT226, a first in class inhibitor of eukaryotic initiation factor 4A RNA helicase. *J. Med. Chem.* **63**, 5879–5955 (2020).
226. Moerke, N. J. *et al.* Small-molecule inhibition of the interaction between the translation initiation factors eIF4E and eIF4G. *Cell* **128**, 257–267 (2007).
227. Descamps, G. *et al.* The cap-translation inhibitor 4EGI-1 induces apoptosis in multiple myeloma through Noxa induction. *Br. J. Cancer* **106**, 1660–1667 (2012).
228. Chen, L. *et al.* Tumor suppression by small molecule inhibitors of translation initiation. *Oncotarget* **3**, 869–881 (2012).
229. Cencic, R. *et al.* Reversing chemoresistance by small molecule inhibition of the translation initiation complex eIF4F. *Proc. Natl. Acad. Sci.* **108**, 1046–1051 (2011).
230. Feng, Y. *et al.* SBI-0640756 attenuates the growth of clinically unresponsive melanomas by disrupting the eIF4F translation initiation complex. *Cancer Res.* **75**, 5211–5218 (2015).
231. Herzog, L. *et al.* Targeting eIF4F translation initiation complex with SBI-756 sensitises B lymphoma cells to venetoclax. *Br. J. Cancer* **124**, 1098–1109 (2021).
232. Jiang, X. *et al.* Properties of CD34+ CML stem/progenitor cells that correlate with different clinical responses to imatinib mesylate. *Blood* **116**, 2112–2121 (2010).
233. Hochhaus, A. *et al.* Long-term benefits and risks of frontline nilotinib vs imatinib for chronic myeloid leukemia in chronic phase: 5-year update of the randomized ENESTnd trial. *Leukemia* **30**, 1044–1054 (2016).
234. Kantarjian, H. M. *et al.* Long-term outcomes with frontline nilotinib versus imatinib in newly diagnosed chronic myeloid leukemia in chronic phase: ENESTnd 10-year analysis. *Leukemia* **35**, 440–453 (2021).
235. Hochhaus, A. *et al.* European LeukemiaNet 2020 recommendations for treating chronic myeloid leukemia. *Leukemia* **34**, 966–984 (2020).
236. White, A. K. *et al.* High-throughput microfluidic single-cell RT-qPCR. *Proc. Natl. Acad. Sci.* **108**, 13999–14004 (2011).
237. Dvinge, H. & Bertone, P. HTqPCR: High - throughput analysis and visualization of quantitative real - time PCR data in R. *Bioinformatics* **25(24)**, 3325 (2009).
238. Hothorn, T. & Lausen, B. On the exact distribution of maximally selected rank statistics. *Comput. Stat. Data Anal.* **43**, 121–137 (2003).
239. Therneau, T. M., until 2009), T. L. (original S.->R port and R. maintainer, Elizabeth, A. & Cynthia, C. survival: Survival Analysis. (2022).
240. Kuhn, M. caret: Classification and Regression Training. (2022).
241. John, C. R. MLeval: Machine Learning Model Evaluation. (2020).
242. Wilkerson, D, M., Hayes & Neil, D. ConsensusClusterPlus: a class discovery tool with confidence assessments and item tracking. *Bioinformatics* **26**, 1572–1573 (2010).
243. Kolde, R. pheatmap: Pretty Heatmaps. (2019).

244. John, C. R. *et al.* M3C: A Monte Carlo reference-based consensus clustering algorithm. *bioRxiv* (2018) doi:https://doi.org/10.1101/377002.
245. Ritchie, M. E. *et al.* limma powers differential expression analyses for RNA-sequencing and microarray studies. *Nucleic Acids Res.* **43**, e47 (2015).
246. Blighe, K., Rana, S. & Lewis, M. EnhancedVolcano: Publication-ready volcano plots with enhanced colouring and labeling. (2019).
247. Raudvere, U. *et al.* g:Profiler: A web server for functional enrichment analysis and conversions of gene lists (2019 update). *Nucleic Acids Res.* **47**, W191–W198 (2019).
248. Rio, D. C., Ares, M., Hannon, G. J. & Nilsen, T. W. Purification of RNA using TRIzol (TRI reagent). *Cold Spring Harb. Protoc.* **2010**, pdb.prot5439 (2010).
249. Holyoake, T. L. & Vetrie, D. The chronic myeloid leukemia stem cell: stemming the tide of persistence. *Blood* **129**, 1595–1606 (2017).
250. Druker, B. J. *et al.* Five-year follow-up of patients receiving imatinib for chronic myeloid leukemia. *N. Engl. J. Med.* **355**, 2408–2417 (2006).
251. Shah, N. P. *et al.* Overriding imatinib resistance with a novel ABL kinase inhibitor. *Science* **305**, 399–401 (2004).
252. Ross, D. M. & Hughes, T. P. Treatment-free remission in patients with chronic myeloid leukaemia. *Nat. Rev. Clin. Oncol.* **17**, 493–503 (2020).
253. Shah, N. P. *et al.* Dasatinib discontinuation in patients with chronic-phase chronic myeloid leukemia and stable deep molecular response: the DASFREE study. *Leuk. Lymphoma* **61**, 650–659 (2020).
254. Rea, D. *et al.* Discontinuation of dasatinib or nilotinib in chronic myeloid leukemia: interim analysis of the STOP 2G-TKI study. *Blood* **129**, 846–854 (2017).
255. Caldemeyer, L. & Akard, L. P. Rationale and motivating factors for treatment-free remission in chronic myeloid leukemia. *Leuk. Lymphoma* **57**, 2739–2751 (2016).
256. Hughes, T. P. *et al.* Nilotinib dose-optimization in newly diagnosed chronic myeloid leukaemia in chronic phase: final results from ENESTxtnd. *Br. J. Haematol.* **179**, 219–228 (2017).
257. Vetrie, D., Helgason, G. V. & Copland, M. The leukaemia stem cell: similarities, differences and clinical prospects in CML and AML. *Nat. Rev. Cancer* **20**, 158–173 (2020).
258. Quintás-Cardama, A., Kantarjian, H. M. & Cortes, J. E. Mechanisms of primary and secondary resistance to imatinib in chronic myeloid leukemia. *Cancer Control* **16**, 122–131 (2009).
259. Rousselot, P. *et al.* Loss of major molecular response as a trigger for restarting tyrosine kinase inhibitor therapy in patients with chronic-phase chronic myelogenous leukemia who have stopped imatinib after durable undetectable disease. *J. Clin. Oncol.* **32**, 424–430 (2014).
260. Mahon, F.-X. *et al.* Discontinuation of imatinib in patients with chronic myeloid leukaemia who have maintained complete molecular remission for at least 2 years: the prospective, multicentre Stop Imatinib (STIM) trial. *Lancet Oncol.* **11**, 1029–1035 (2010).
261. Giustacchini, A. *et al.* Single-cell transcriptomics uncovers distinct molecular signatures of stem cells in chronic myeloid leukemia. *Nat. Med.* **23**, 692–702 (2017).
262. Chen, Y. & Li, S. Molecular signatures of chronic myeloid leukemia stem cells. *Biomark. Res.* **1**, 21 (2013).

263. Krishnan, V., Kim, D. D. H., Hughes, T. P., Branford, S. & Ong, S. T. Integrating genetic and epigenetic factors in chronic myeloid leukemia risk assessment: toward gene expression-based biomarkers. *Haematologica* **107**, 358–370 (2022).
264. Clark, R. E., Apperley, J. F., Copland, M. & Cicconi, S. Additional chromosomal abnormalities at chronic myeloid leukemia diagnosis predict an increased risk of progression. *Blood Adv.* **5**, 1102–1109 (2021).
265. Song, H. *et al.* BCR-ABL1 transcript levels at 4 weeks have prognostic significance for time-specific responses and for predicting survival in chronic-phase chronic myeloid leukemia patients treated with various tyrosine kinase inhibitors. *Cancer Med.* **7**, 5107–5117 (2018).
266. Glauche, I. *et al.* Quantitative prediction of long-term molecular response in TKI-treated CML – Lessons from an imatinib versus dasatinib comparison. *Sci. Rep.* **8**, 12330 (2018).
267. Kok, C. H. *et al.* Gene expression signature that predicts early molecular response failure in chronic-phase CML patients on frontline imatinib. *Blood Adv.* **3**, 1610–1621 (2019).
268. Si, W., Shen, J., Zheng, H. & Fan, W. The role and mechanisms of action of microRNAs in cancer drug resistance. *Clin. Epigenetics* **11**, 25 (2019).
269. Peng, Y. & Croce, C. M. The role of microRNAs in human cancer. *Signal Transduct. Target. Ther.* **1**, 1–9 (2016).
270. O'Brien, J., Hayder, H., Zayed, Y. & Peng, C. Overview of microRNA biogenesis, mechanisms of actions, and circulation. *Front. Endocrinol.* **9**, 402 (2018).
271. Bissels, U., Bosio, A. & Wagner, W. MicroRNAs are shaping the hematopoietic landscape. *Haematologica* **97**, 160–167 (2012).
272. Alves, R. *et al.* MicroRNA signature refine response prediction in CML. *Sci. Rep.* **9**, 9666 (2019).
273. Ciccone, M. & Adrian Calin, G. MicroRNAs in Myeloid Hematological Malignancies. *Curr. Genomics* **16**, 336–348 (2015).
274. Breiman, L. Random Forests. *Mach. Learn.* **45**, 5–32 (2001).
275. van der Heide, E. M. M. *et al.* Comparing regression, naive Bayes, and random forest methods in the prediction of individual survival to second lactation in Holstein cattle. *J. Dairy Sci.* **102**, 9409–9421 (2019).
276. Turhan, A. G. *et al.* Evidence of BCR-ABL1-positive progenitor spread in blood during molecular recurrence after TKI discontinuation in chronic myeloid leukemia (CML). *Leuk. Lymphoma* **61**, 1719–1723 (2020).
277. Abraham, S. A. *et al.* Dual targeting of p53 and c-MYC selectively eliminates leukaemic stem cells. *Nature* **534**, 341–346 (2016).
278. Jamieson, C. H. M. *et al.* Granulocyte–macrophage progenitors as candidate leukemic stem cells in blast-crisis CML. *N. Engl. J. Med.* **351**, 657–667 (2004).
279. Xu, W.-X. *et al.* MiR-145: a potential biomarker of cancer migration and invasion. *Am. J. Transl. Res.* **11**, 6739–6753 (2019).
280. Xu, W. *et al.* MiR-145 in cancer therapy resistance and sensitivity: A comprehensive review. *Cancer Sci.* **111**, 3122–3131 (2020).
281. Manvati, S. *et al.* miR-145 supports cancer cell survival and shows association with DDR genes, methylation pattern, and epithelial to mesenchymal transition. *Cancer Cell Int.* **19**, 230 (2019).

282. Monteleone, N. J. & Lutz, C. S. miR-708-5p: a microRNA with emerging roles in cancer. *Oncotarget* **8**, 71292–71316 (2017).
283. Srutova, K. *et al.* BCR-ABL1 mediated miR-150 downregulation through MYC contributed to myeloid differentiation block and drug resistance in chronic myeloid leukemia. *Haematologica* **103**, 2016–2025 (2018).
284. Habib, E. M. *et al.* Mir-150 expression in chronic myeloid leukemia: relation to imatinib response. *Lab. Med.* **53**, 58–64 (2022).
285. Di Stefano, C., Mirone, G., Perna, S. & Marfe, G. The roles of microRNAs in the pathogenesis and drug resistance of chronic myelogenous leukemia (Review). *Oncol. Rep.* **35**, 614–624 (2016).
286. Svoronos, A. A., Engelman, D. M. & Slack, F. J. OncomiR or tumor suppressor? The duplicity of microRNAs in cancer. *Cancer Res.* **76**, 3666–3670 (2016).
287. Kinexus Bioinformatics Corportation. Kinex KAM-1325 antibody microarray services information package. http://www.kinexus.ca/pdf/KAM-1325-Service_Information.pdf (2018).
288. Dobrikov, M. I., Dobrikova, E. Y. & Gromeier, M. Dynamic regulation of the translation initiation helicase complex by mitogenic signal transduction to eukaryotic translation initiation factor 4G. *Mol. Cell. Biol.* **33**, 937–946 (2013).
289. Dobrikov, M. I., Shveygert, M., Brown, M. C. & Gromeier, M. Mitotic phosphorylation of eukaryotic initiation factor 4G1 (eIF4G1) at Ser1232 by Cdk1:Cyclin B inhibits eIF4A helicase complex binding with RNA. *Mol. Cell. Biol.* **34**, 439–451 (2014).
290. Prabhu, S. *et al.* A novel mechanism for Bcr-Abl action: Bcr-Abl-mediated induction of the eIF4F translation initiation complex and mRNA translation. *Oncogene* **26**, 1188–1200 (2007).
291. Vo, T.-T. *et al.* Targeting eIF4F translation complex sensitizes B-ALL cells to tyrosine kinase inhibition. *Sci. Rep.* **11**, 21689 (2021).
292. Lai, A. C. *et al.* Modular PROTAC design for the degradation of oncogenic BCR-ABL. *Angew. Chem. Int. Ed.* **55**, 807–810 (2016).
293. Scherr, M. *et al.* Specific inhibition of bcr-abl gene expression by small interfering RNA. *Blood* **101**, 1566–1569 (2003).
294. Valencia-Serna, J. *et al.* siRNA-mediated BCR-ABL silencing in primary chronic myeloid leukemia cells using lipopolymers. *J. Controlled Release* **310**, 141–154 (2019).
295. Jiang, S. *et al.* Suppression of USP7 induces BCR-ABL degradation and chronic myelogenous leukemia cell apoptosis. *Cell Death Dis.* **12**, 1–12 (2021).
296. Li, S. *et al.* Homoharringtonine promotes BCR-ABL degradation through the p62-mediated autophagy pathway. *Oncol. Rep.* **43**, 113–120 (2020).
297. Chen, R., Gandhi, V. & Plunkett, W. A sequential blockade strategy for the design of combination therapies to overcome oncogene addiction in chronic myelogenous leukemia. *Cancer Res.* **66**, 10959–10966 (2006).
298. Nimmanapalli, R. *et al.* Arsenic trioxide inhibits translation of mRNA of bcr-abl, resulting in attenuation of Bcr-Abl levels and apoptosis of human leukemia cells. *Cancer Res.* **63**, 7950–7958 (2003).
299. Sokal, J. E. *et al.* Prognostic discrimination in “good-risk” chronic granulocytic leukemia. *Blood* **63**, 789–799 (1984).

300. Hasford, J. *et al.* Predicting complete cytogenetic response and subsequent progression-free survival in 2060 patients with CML on imatinib treatment: the EUTOS score. *Blood* **118**, 686–692 (2011).
301. Skorski, T. *et al.* Transformation of hematopoietic cells by BCR/ABL requires activation of a PI-3k/Akt-dependent pathway. *EMBO J.* **16**, 6151–6161 (1997).
302. Steelman, L. S. *et al.* JAK/STAT, Raf/MEK/ERK, PI3K/Akt and BCR-ABL in cell cycle progression and leukemogenesis. *Leukemia* **18**, 189–218 (2004).

Appendices

Appendix A

Overview of BCR-ABL1 Transcript Changes and Nilotinib Responses of CML Patients

Patient #	Baseline (BCR-ABL1 ratio)	12 month BCR-ABL1 (%)	Response status* (12 month)
1	144	0.31	NR
2	91	0.86	NR
3	126	0.01	R
4	112	0.02	R
5	176	0.009	R
6	201	0.002	R
7	142	0.02	R
8	206	0.07	R
9	150	0.1	R
10	173	0.3	NR
11	133	0.04	R
12	124	0	R
13	202	2.6	NR
14	30	0.03	R
15	98	0.8	NR
16	253	0.9	NR
17	93	0	R
18	341	0.007	R
19	306	0.02	R
20	258	0	R
21	80	0.01	R
22	122	0.01	R
23	76	0.4	NR
24	168	0.03	R
25	123	0.1	R
26	210	0.03	R
27	124	0.01	R
28	179	0.20	NR
29	258	0.009	R
30	123	0.04	R
31	85	81.5	NR
32	43	0.002	R
33	56	0.01	R
34	83	0	R
35	123	0.3	NR
36	62	0.005	R
37	124	0.014	R

38	101	0.009	R
39	126	0.003	R
40	148	0	R
41	91	0	R
42	60	0.05	R
43	206	0.3	NR
44	140	0.003	R
45	97	0	R
46	113	0.001	R
47	124	0.0022	R
48	117	0.6	NR
49	137	0.003	R
50	109	0.08	R
51	100	0	R
52	46	0	R
53	100	0.006	R
54	124	0.002	R
55	68	0.001	R
56	78	0.001	R
57	152	0.03	R
58	107	0	R

* Patient response statuses were classified into NL-responders (R) and NL-nonresponders (NR) based on the European Leukemia Net Treatment Guidelines. Responders achieved major molecular response, characterised as measured BCR-ABL1 transcript levels of < 0.1% (3 log reduction) at 12 months while NL-nonresponders did not achieve this threshold of response criteria. 0% for response = undetected BCR-ABL1, n/a= data not available.

Appendix B

Table 1: Table of Enriched Pathways for Targets with Decreased Signals for WT Ahi-1 Versus B/A Only

Pathway Name	*p*-value	Pathway Size	Targets
MAPK signaling pathway	6.9E-13	286	12
Protein autophosphorylation	3.3E-09	227	9
MAPK signaling pathway	4.7E-09	241	10
Angiopoietin-like protein 8 regulatory pathway	2.7E-08	127	8
Translation inhibitors in chronically activated PDGFRA cells (eIF4F complex)	7.5E-08	45	6
Insulin signaling	1.5E-07	157	8
Peptidyl-tyrosine phosphorylation	2.8E-07	373	9
Peptidyl-tyrosine modification	3.0E-07	376	9
Malignant pleural mesothelioma	1.5E-06	433	10
Glioblastoma signaling pathways	3.0E-06	82	6
Interleukin-1 (IL-1) structural pathway	1.1E-05	50	5
Cardiac hypertrophic response	2.1E-05	57	5
Positive regulation of kinase activity	7.4E-05	489	8
MAPK cascade	1.1E-04	33	4
EGFR tyrosine kinase inhibitor resistance	1.3E-04	81	5
TNF signaling pathway	1.4E-04	110	5
Host-pathogen interaction of human coronaviruses - MAPK signaling	1.6E-04	36	4
Central carbon metabolism in cancer	6.7E-04	69	4
Photodynamic therapy-induced AP-1 survival signaling	6.7E-04	51	4
Interferon type I signaling pathways	8.4E-04	54	4
IL-1 signaling pathway	8.4E-04	54	4
Hepatitis B	8.8E-04	159	5
EGFR tyrosine kinase inhibitor resistance	9.8E-04	76	4
4-hydroxytamoxifen, dexamethasone, and retinoic acids regulation of p27 expression	0.0011	18	3
ErbB signaling pathway	0.0013	81	4
MAP kinase activation	0.0018	63	4
GnRH signaling pathway	0.0021	92	4
Kaposi sarcoma-associated herpesvirus infection	0.0021	191	5
Hepatitis B infection	0.0027	151	5
Interleukin-17 signaling	0.0029	71	4
Cellular senescence	0.0040	83	4
ErbB signaling pathway	0.0056	87	4
MyD88 cascade initiated on plasma membrane	0.0057	84	4
Toll Like Receptor 10 (TLR10) cascade	0.0057	84	4
Toll Like Receptor 5 (TLR5) cascade	0.0057	84	4
Regulation of myeloid cell differentiation	0.0058	208	5
MAPK family signaling cascades	0.0061	308	6

Pathway Name	*p*-value	Pathway Size	Targets
TRAF6 mediated induction of NFkB and MAP kinases upon TLR7/8 or 9 activation	0.0072	89	4
MyD88 dependent cascade initiated on endosome	0.0076	90	4
Toll Like Receptor 7/8 (TLR7/8) cascade	0.0079	91	4
p38 MAPK signaling pathway	0.0081	34	3
Toll Like Receptor 3 (TLR3) cascade	0.0082	92	4
Yersinia infection	0.0086	132	4
Toll Like Receptor 9 (TLR9) cascade	0.0090	94	4
MicroRNAs in cardiomyocyte hypertrophy	0.0094	99	4
TRIF(TICAM1)-mediated TLR4 signaling	0.0097	96	4
MyD88-independent TLR4 cascade	0.0097	96	4
Stress-activated MAPK cascade	0.011	239	5
MyD88:MAL(TIRAP) cascade initiated on plasma membrane	0.011	100	4
Toll Like Receptor TLR6:TLR2 cascade	0.011	100	4
Toll Like Receptor TLR1:TLR2 cascade	0.013	103	4
Toll Like Receptor 2 (TLR2) cascade	0.013	103	4
Stress-activated protein kinase signaling cascade	0.013	246	5
Positive regulation of telomerase activity	0.013	34	3
Cellular senescence	0.015	152	4
Regulation of myeloid leukocyte differentiation	0.017	119	4
JAK-STAT signaling pathway	0.018	159	4
Fc epsilon RI signaling pathway	0.019	64	3
MicroRNAs in cancer	0.020	306	5
Positive regulation of apoptotic signaling pathway	0.022	128	4
Melanoma	0.025	70	3
TGF-beta signaling pathway	0.026	129	4
Wnt signaling pathway	0.029	52	3
RANKL/RANK signaling pathway	0.032	54	3
Diseases of signal transduction by growth factor receptors and second messengers	0.033	417	6
Toll Like Receptor 4 (TLR4) Cascade	0.034	132	4
Epstein-Barr virus infection	0.036	191	4
VEGFA-VEGFR2 signaling pathway	0.037	415	6
RAF/MAP kinase cascade	0.039	264	5
Peptidyl-serine phosphorylation	0.042	313	5
MAPK1/MAPK3 signaling	0.042	269	5
Regulation of telomerase activity	0.044	50	3
Positive regulation of neuron apoptotic process	0.044	50	3
Positive regulation of extrinsic apoptotic signaling pathway	0.044	50	3
PD-L1 expression and PD-1 checkpoint pathway in cancer	0.048	88	3
Human immunodeficiency virus 1 infection	0.048	207	4
Lipid and atherosclerosis	0.050	209	4

Table 2: Table of Enriched Pathways for Targets with Increased Signals for WT Ahi-1 Versus B/A Only

Pathway Name	*p*-value	Pathway Size	Targets
Small cell lung cancer	0.0061	95	2
Small cell lung cancer	0.020	90	2
Regulation of cell-matrix adhesion	0.048	119	2

Table 3: Table of Enriched Pathways for Targets with Decreased Signals for WT Ahi-1 Versus Ahi-1 SH3$^{\Delta}$

Pathway Name	*p*-value	Pathway Size	Targets
Protein autophosphorylation	1.4E-11	227	12
Peptidyl-tyrosine phosphorylation	1.2E-07	373	11
Peptidyl-tyrosine modification	1.3E-07	376	11
Signaling by phosphorylated juxtamembrane, extracellular and kinase domain KIT mutants	5.9E-07	17	5
Signaling by KIT in disease	5.9E-07	17	5
Thymic stromal lymphopoietin (TSLP) signaling pathway	4.8E-06	47	6
Regulation of myeloid cell differentiation	8.2E-06	208	8
Malignant pleural mesothelioma	1.4E-05	433	12
Diseases of signal transduction by growth factor receptors and second messengers	2.0E-05	417	11
Insulin signaling	3.0E-05	157	8
Signaling by SCF-KIT	5.2E-05	39	5
MAPK signaling pathway	9.2E-05	286	9
Angiopoietin-like protein 8 regulatory pathway	1.1E-04	127	7
Regulation of myeloid leukocyte differentiation	1.7E-04	119	6
Peptidyl-serine phosphorylation	1.9E-04	313	8
Peptidyl-serine modification	3.4E-04	336	8
Central carbon metabolism in cancer	5.2E-04	69	5
Kit receptor signaling pathway	5.9E-04	59	5
Kaposi sarcoma-associated herpesvirus infection	6.3E-04	191	7
Regulation of hemopoiesis	7.6E-04	374	8
Response to insulin	7.8E-04	253	7
EGFR tyrosine kinase inhibitor resistance	8.4E-04	76	5
CD28 co-stimulation	9.7E-04	31	4
Fc-gamma receptor signaling pathway	9.9E-04	35	4
Myeloid cell differentiation	0.0012	396	8
Response to peptide hormone	0.0012	398	8
Hippo-Merlin signaling dysregulation	0.0013	120	6
PECAM1 interactions	0.0017	11	3
FLT3 Signaling	0.0018	36	4
Head and neck squamous cell carcinoma	0.0018	74	5
EGFR tyrosine kinase inhibitor resistance	0.0028	81	5
Regulation of KIT signaling	0.0030	13	3
Response to heat	0.0031	107	5

Pathway Name	*p*-value	Pathway Size	Targets
PI3K-Akt signaling pathway	0.0035	342	8
PI3K/AKT signaling in cancer	0.0039	92	5
Peptidyl-threonine phosphorylation	0.0043	114	5
Response to peptide	0.0047	477	8
Myeloid leukocyte differentiation	0.0052	214	6
Positive regulation of kinase activity	0.0056	489	8
Peptidyl-threonine modification	0.0062	123	5
Aryl hydrocarbon receptor pathway	0.0062	48	4
Immune response-regulating signaling pathway	0.0063	497	8
Hippo signaling regulation pathways	0.0074	99	5
MAPK signaling pathway	0.0076	241	7
PI3K-Akt signaling pathway	0.0081	333	8
Interferon type I signaling pathways	0.010	54	4
RANKL/RANK signaling pathway	0.010	54	4
CTLA4 inhibitory signaling	0.012	20	3
Melanoma	0.012	70	4
Regulation of protein serine/threonine kinase activity	0.012	383	7
Cellular response to heat	0.012	65	4
Transcriptional regulation by RUNX2	0.013	118	5
Regulation of signaling by CBL	0.014	21	3
Regulation of osteoclast differentiation	0.014	67	4
Regulation of lipid kinase activity	0.016	69	4
Regulation of protein-containing complex assembly	0.017	402	7
Costimulation by the CD28 family	0.022	67	4
AMP-activated protein kinase (AMPK) signaling	0.022	66	4
Thyroid stimulating hormone (TSH) signaling pathway	0.022	66	4
Melanoma	0.023	67	4
Inactivation of CSF3 (G-CSF) signaling	0.023	25	3
Receptor signaling pathway via JAK-STAT	0.027	166	5
Fc receptor signaling pathway	0.027	79	4
Focal adhesion: PI3K-Akt-mTOR-signaling pathway	0.027	295	7
Regulation of leukocyte differentiation	0.028	288	6
Cellular response to peptide hormone stimulus	0.028	288	6
JAK-STAT signaling pathway	0.029	159	5
PD-L1 expression and PD-1 checkpoint pathway in cancer	0.029	88	4
Extracellular vesicle-mediated signaling in recipient cells	0.031	29	3
Receptor signaling pathway via STAT	0.032	172	5
Fc-gamma receptor signaling pathway involved in phagocytosis	0.032	27	3
Immune response-regulating cell surface receptor signaling pathway involved in phagocytosis	0.032	27	3
Leptin signaling pathway	0.036	75	4
Energy reserve metabolic process	0.036	85	4

Pathway Name	*p*-value	Pathway Size	Targets
Brain-derived neurotrophic factor (BDNF) signaling pathway	0.038	140	5
Response to temperature stimulus	0.039	180	5
Bladder cancer	0.041	41	3
Signaling by CSF3 (G-CSF)	0.041	30	3
Regulation of MAP kinase activity	0.042	182	5
Immune response-activating cell surface receptor signaling pathway	0.046	314	6
Immune response-activating signal transduction	0.046	314	6
Positive regulation of peptidyl-tyrosine phosphorylation	0.049	188	5
Cellular response to external stimulus	0.049	317	6
Chemokine signaling pathway	0.049	179	5

Table 4: Table of Enriched Pathways for Targets with Increased Signals for WT Ahi-1 Versus Ahi-1 SH3$^{\Delta}$

Pathway Name	*p*-value	Pathway Size	Targets
Hepatocyte growth factor receptor signaling	7.0E-05	34	3
Androgen receptor signaling pathway	0.0012	87	3
MFAP5-mediated ovarian cancer cell motility and invasiveness	0.0022	13	2
Focal adhesion	0.0033	192	3
Quercetin and Nf-kB / AP-1 induced apoptosis	0.0034	16	2
Chemical carcinogenesis - reactive oxygen species	0.0041	206	3
MFAP5 effect on permeability and motility of endothelial cells via cytoskeleton rearrangement	0.0044	18	2
EGF/EGFR signaling pathway	0.0074	159	3
Focal adhesion	0.013	190	3
Response to muscle stretch	0.018	25	2
Regulation of epithelial cell migration	0.021	225	3
Protein autophosphorylation	0.022	227	3
Signaling by nuclear receptors	0.034	291	3
ErbB signaling pathway	0.035	81	2
Netrin-UNC5B signaling pathway	0.036	51	2
Copper homeostasis	0.036	51	2
RANKL/RANK signaling pathway	0.040	54	2
PD-L1 expression and PD-1 checkpoint pathway in cancer	0.041	88	2
Small cell lung cancer	0.043	90	2
Endocrine resistance	0.043	90	2
MET in type 1 papillary renal cell carcinoma	0.044	56	2
Epithelial cell migration	0.047	293	3
Epithelium migration	0.048	296	3

Table 5: Table of Enriched Pathways for Targets with Decreased Signals in WT Ahi-1 Cells after IM Treatment

Pathway Name	*p*-value	Pathway Size	Targets
Protein autophosphorylation	2.5E-15	227	15
Peptidyl-tyrosine phosphorylation	4.8E-15	373	17
Peptidyl-tyrosine modification	5.5E-15	376	17
Positive regulation of kinase activity	1.0E-11	489	16
Peptidyl-serine phosphorylation	6.6E-09	313	12
Peptidyl-serine modification	1.5E-08	336	12
Axon development	1.0E-06	484	12
Regulation of cell growth	3.8E-06	425	11
Cellular response to chemical stress	4.0E-06	323	10
Gland development	4.8E-06	435	11
Axonogenesis	5.1E-06	438	11
Aell growth	1.6E-05	490	11
G1/S transition of mitotic cell cycle	3.1E-05	205	8
Cellular response to reactive oxygen species	4.8E-05	140	7
Positive regulation of neuron death	6.8E-05	86	6
Leukocyte proliferation	8.4E-05	331	9
Cell cycle G1/S phase transition	9.0E-05	235	8
Axon guidance	9.6E-05	237	8
Neuron projection guidance	9.9E-05	238	8
Ephrin signaling	1.8E-04	17	4
Ephrin receptor signaling pathway	2.0E-04	52	5
Actin cytoskeleton reorganization	2.8E-04	109	6
Cellular response to oxidative stress	2.9E-04	274	8
Leukocyte apoptotic process	3.2E-04	111	6
MAPK signaling pathway	3.2E-04	286	9
Response to reactive oxygen species	4.3E-04	193	7
Lymphocyte proliferation	5.6E-04	298	8
Mononuclear cell proliferation	6.1E-04	302	8
Response to oxidative stress	6.3E-04	420	9
Glioblastoma signaling pathways	7.4E-04	82	6
Wound healing	7.6E-04	429	9
Regulation of neuron death	7.9E-04	312	8
Regulation of neuron projection development	7.9E-04	431	9
Mitotic cell cycle phase transition	9.3E-04	440	9
Regulation of G1/S transition of mitotic cell cycle	0.0012	140	6
Regulation of tissue remodeling	0.0013	75	5
Lymphocyte apoptotic process	0.0013	76	5
Response to X-ray	0.0013	32	4
Regulation of fibroblast proliferation	0.0017	80	5
Hematopoietic progenitor cell differentiation	0.0019	150	6
Fibroblast proliferation	0.0020	82	5
Neuron death	0.0020	353	8
Positive regulation of production of miRNAs involved	0.0022	10	3

Pathway Name	*p*-value	Pathway Size	Targets
in gene silencing by miRNA			
Regulation of leukocyte apoptotic process	0.0023	85	5
Regulation of axonogenesis	0.0023	156	6
Positive regulation of cellular component biogenesis	0.0026	497	9
Telencephalon development	0.0026	252	7
Regulation of leukocyte proliferation	0.0027	254	7
Positive regulation of cell growth	0.0030	163	6
Regulation of miRNA-mediated gene silencing	0.0030	39	4
Tissue remodeling	0.0034	166	6
Regulation of cell cycle G1/S phase transition	0.0036	168	6
Regulation of post-transcriptional gene silencing by RNA	0.0037	41	4
Regulation of gene silencing by RNA	0.0041	42	4
Regulation of post-transcriptional gene silencing	0.0041	42	4
Positive regulation of G1/S transition of mitotic cell cycle	0.0045	43	4
Positive regulation of protein kinase activity	0.0059	409	8
EPHB-mediated forward signaling	0.0065	40	4
NF-kappa B signaling pathway	0.0073	102	5
Positive regulation of fibroblast proliferation	0.0077	49	4
Cell junction assembly	0.0077	424	8
Neural crest cell migration during development	0.0079	39	4
Corpus callosum development	0.0082	15	3
Axon guidance	0.0097	174	6
EPH-Ephrin signaling	0.0099	90	5
Peptidyl-threonine phosphorylation	0.010	114	5
Mononuclear cell differentiation	0.010	440	8
VEGFA-VEGFR2 signaling pathway	0.010	415	10
Neural crest cell migration in cancer	0.011	42	4
Regulation of mitotic cell cycle phase transition	0.012	320	7
Embryonic organ development	0.013	455	8
Positive regulation of protein localization	0.013	457	8
Negative regulation of cell activation	0.013	211	6
Integrated cancer pathway	0.014	45	4
Regulation of lymphocyte apoptotic process	0.014	57	4
Necrotic cell death	0.014	57	4
Peptidyl-threonine modification	0.014	123	5
Malignant pleural mesothelioma	0.015	433	10
EPH-ephrin mediated repulsion of cells	0.015	49	4
Negative regulation of B cell proliferation	0.015	18	3
Positive regulation of cell cycle G1/S phase transition	0.015	58	4
Regulation of protein localization to cell periphery	0.016	125	5
Gland morphogenesis	0.016	126	5
Regulation of mitotic cell cycle	0.018	475	8
Response to peptide	0.018	477	8

Pathway Name	*p*-value	Pathway Size	Targets
Positive regulation of MAPK cascade	0.019	479	8
Imatinib and chronic myeloid leukemia	0.019	19	3
Regulation of production of miRNAs involved in gene silencing by miRNA	0.020	20	3
Regulation of production of small RNA involved in gene silencing by RNA	0.020	20	3
Melanoma	0.022	70	4
Regulation of lymphocyte proliferation	0.022	231	6
Photodynamic therapy-induced AP-1 survival signaling	0.023	51	4
Non-small cell lung cancer	0.023	71	4
Glioma	0.023	71	4
Regulation of B cell proliferation	0.024	65	4
Regulation of mononuclear cell proliferation	0.024	234	6
Mammary gland development	0.025	138	5
Positive regulation of miRNA-mediated gene silencing	0.028	22	3
Hippo signaling regulation pathways	0.028	99	5
Human cytomegalovirus infection	0.031	215	6
EGF/EGFR signaling pathway	0.031	159	6
Positive regulation of post-transcriptional gene silencing by RNA	0.032	23	3
Positive regulation of post-transcriptional gene silencing	0.032	23	3
Mammary gland epithelium development	0.034	71	4
Peptidyl-tyrosine autophosphorylation	0.036	24	3
Positive regulation of growth	0.039	255	6
Regulation of protein serine/threonine kinase activity	0.040	383	7
Forebrain development	0.040	384	7
TP53 regulates transcription of DNA repair genes	0.042	64	4
Negative regulation of cell cycle	0.043	388	7
Negative regulation of transferase activity	0.049	265	6

Table 6: Table of Enriched Pathways for Targets with Increased Signals in WT Ahi-1 Cells after IM Treatment

Pathway Name	*p*-value	Pathway Size	Targets
Translation inhibitors in chronically activated PDGFRA cells (eIF4F complex)	4.1E-06	45	4
MAPK signaling pathway	7.4E-05	286	5
Angiopoietin-like protein 8 regulatory pathway	2.8E-04	127	4
Regulation of epithelial cell migration	4.4E-04	225	4
Insulin signaling	6.5E-04	157	4
Interferon type I signaling pathways	0.0013	54	3
Epithelial cell migration	0.0013	293	4
Epithelium migration	0.0013	296	4
Tissue migration	0.0014	302	4

Pathway Name	*p*-value	Pathway Size	Targets
EGFR tyrosine kinase inhibitor resistance	0.0017	76	3
Thyroid stimulating hormone (TSH) signaling pathway	0.0023	66	3
EGFR tyrosine kinase inhibitor resistance	0.0043	81	3
Glioblastoma signaling pathways	0.0044	82	3
Ameboidal-type cell migration	0.0052	418	4
Liver development	0.0088	134	3
Thermogenesis	0.0088	103	3
Hepaticobiliary system development	0.0094	137	3
4-hydroxytamoxifen, dexamethasone, and retinoic acids regulation of p27 expression	0.012	18	2
Positive regulation of epithelial cell migration	0.012	147	3
Regulation of endothelial cell migration	0.017	167	3
Extracellular vesicle-mediated signaling in recipient cells	0.031	29	2
Regulation of myeloid cell differentiation	0.033	208	3
Thermogenesis	0.033	207	3
Malignant pleural mesothelioma	0.035	433	4
Endothelial cell migration	0.036	215	3
BDNF-TrkB signaling	0.040	33	2
Host-pathogen interaction of human coronaviruses - MAPK signaling	0.047	36	2